Université d'Ottawa · University of Ottawa

Université d'Ottawa · University of Ottawa

FACULTÉ DES ÉTUDES SUPÉRIEURES ET POSTDOCTORALES

FACULTY OF GRADUATE AND POSTDOCTORAL STUDIES

Li PAN

AUTEUR DE LA THÈSE - AUTHOR OF THESIS

M. A. Sc. (Electrical Engineering)

GRADE - DEGREE

Department of Electrical Engineering

FACULTÉ, ÉCOLE, DÉPARTEMENT - FACULTY, SCHOOL, DEPARTMENT

TITRE DE LA THÈSE - TITLE OF THE THESIS

Selective Multistage Detection Algorithm in Flat Rayleigh Fading Channel

C. D'Amours

DIRECTEUR DE LA THÈSE - THESIS SUPERVISOR

CO-DIRECTEUR DE LA THÈSE - THESIS CO-SUPERVISOR

EXAMINATEURS DE LA THÈSE - THESIS EXAMINERS

I. Marsland

A. Yougacoglod

J.-M. De Koninck, Ph.D.

LE DOYEN DE LA FACULTÉ DES ÉTUDES SUPÉRIEURES ET POSTDOCTORALES

DEAN OF THE FACULTY OF GRADUATE AND POSTDOCTORAL STUDIES

Selective Multistage Detection Algorithm in Flat Rayleigh Fading Channel

Li Pan

a thesis
Submitted to the Faculty of Graduate Studies and Research
of University of Ottawa
in partial fulfillment of the requirements for the degree of
Master of Applied Science
Under the supervision of Prof. C.D'Amours

Ottawa-Carleton Institute for Electrical and Computer Engineering
School of Information Technology and Engineering
University of Ottawa

Your file Votre référence
ISBN: 0-494-01570-5
Our file Notre référence
ISBN: 0-494-01570-5

Abstract

Selective multistage detection algorithm applied in AWGN channel is first proposed in [1]. It is shown that the BER performance of this detector is slightly better than conventional multistage detector if the threshold level is properly selected. At the same time, the number of computations performed by the receiver is greatly reduced since MAI cancellation is only applied to those decision variables whose magnitudes are less than a threshold value. In this thesis, we will investigate the performance of selective multistage detection algorithm for the frequency nonselective Rayleigh fading channel which is more common in the wireless communications. The performance will be determined by computer simulation. First, we will consider the performance of selective multistage detection and nonselective multistage detection when the receiver perfectly estimates the channel gains of all of the users. Then we will employ pilots based estimation with optimum interpolator to estimate the channel gains. Receiver will make use of the estimated channel gain to detect the data of every user. Finally we will compare the performances of selective and nonselective multistage detectors under the imperfect channel estimation case.

We also propose a modified selective multistage algorithm in order to improve the performance of selective multistage detector further without a large increase in the amount of computation. It applies partial MAI cancellation, instead of full cancellation, to those decision variables whose magnitudes are less than a threshold value.

By employing the modified selective multistage algorithm, we will achieve the performance that is close to that of conventional multistage with perfect channel estimation.

Acknowledgements

First, and most importantly, I should thank my supervisor, Prof. Claude D'Amours, for his relentless support for my work, both intellectually and financially. I am grateful for his help comments, suggestions and constructive criticism throughout the entire project. My thesis has benefited substantially from his insightful recommendations. His suggestions helped me manage difficult problems. Without his support, my thesis would not have been possible.

Next, I would like to thank Prof. Abbas Yongacoglu and Prof. Ian D. Marsland. Both professors have taught me and given me a very deep understanding due to their expertise in digital communications and coding theory. Also, they were very kind to agree to be my committee, to take time to read my thesis and examine my research work.

I would also like to thank my colleagues: Naser Salem, Wei Zhang, Gunes Karabulut, Qi Hong, Azar Mouzari. They have had fruitful discussions with me and given me some helpful suggestions.

I would like to thank School of Information Technology and Engineering for providing computer facilities and financial supports that permitted me to complete my thesis.

I am grateful to my parents for their never ending encouragements and always being there with me.

Finally, I would like to express my sincere gratitude toward my husband for his constant love and huge support. He always backs me up, encourages me to solve all of the difficult problems that appeared in the research. Without him, I wouldnot have had the confidence to overcome these difficulties and complete the thesis. Thanks a lot!

Contents

List of Tables

List of Figures

List of Acronyms

AR	:	Autoregressive
AWGN	:	Additive White Gaussian Noise
BER	:	Bit Error Rate
BPSK	:	Binary Phase Shift Keying
DF	:	Decision Feedback
DS-CDMA	:	Direct Sequence Code Division Multiple Access
FFT	:	Fast Fourier Transform
IFFT	:	Inverse Fast Fourier Transform
LMS	:	Least Mean Squares
LOS	:	Line-Of-Sight
MAI	:	Multiple Access Interference
MFB	:	Matched Filter Bank
MIMO	:	Multiple Input Multiple Output
MLS	:	Maximum Likelihood Sequence
MMSE	:	Minimum Mean Square
PDF	:	Probability Density Function

PE : Polynomial Expansion

PSAM : Pilot Symbol Assisted Modulation

PSD : Power Spectrum Density

PIC : Parallel Interference Cancellation

RF : Radio Frequency

RLS : Recursive Least Squares

SIC : Successive Interference Cancellation

SNR : Signal Noise Ratio

VOD : Video On Demand

List of Symbols

$a(t)$: Magnitude of complex fading process

A_k : Amplitude of the k-th user

$b_k(i)$: Transmitting data of the k-th user on the i-th signal interval

$c_k(t)$: Complex fading process for k-th user

$c_k^I(t)$: The inphase component of fading process

$c_k^Q(t)$: The quadrature component of fading process

E_b : Bit energy

f_c : Carrier frequency

f_d : Doppler frequency

f_m : Maximum Doppler frequency

$g(t)$: Channel gain

$h(t, \tau)$: Channel impulse response

i : Index of the signal interval

$J_0(\cdot)$: Zero-th order Bessel function of first kind

k : User index

$n_k(i)$: The filtered noise for k-th user on i-th signal interval at the output of matched filter

$n(t)$: Complex Gaussian white noise

N_0 : Double sided noise spectral density

$r(t)$: The received signal arriving at the base station

$s_k(t)$: Normalized signature waveform for the k-th user

$S(f)$: The power spectrum density function of fading process

T : Symbol interval

Th : The threshold value used in selective multistage algorithm

v : The velocity of the mobile

$v_k^{(p)}(i)$: The output of p-th stage for k-th user on i-th signal interval

τ_k : Delay of the k-th user

$y_k(i)$: The output of matched filter for k-th user on i-th signal interval

ρ_{jk} : Cross-correlation between the j-th user's signature waveform and the k-th user's signature waveform

$\phi(t)$: Phase shift of complex fading process

λ : The wavelength of the incident wave

$\hat{g}(t)$: Estimated channel gain

σ_e^2 : The Variance of estimation error

σ_g^2 : The variance of channel gain

$\mathbf{b}$: Transmitting data sequence

$\mathbf{G}$: Diagonal amplitude matrix

$\mathbf{H}(i)$: Coefficient vector of the transversal filter (interpolator)

$\mathbf{P}$: The pilot symbol vector

$\mathbf{R}$: Normalized crosscorrelation matrix of the user' signature waveforms

$\mathbf{Y}$: The vector of the output of matched filter

$\mathbf{\Phi}_{yy}$: The autocorrelation matrix for the noisy channel gain estimates from the received pilot symbols

$\mathbf{\Phi}_{gy}$: The crosscorrelation vector between actual channel gain and estimated channel gain of pilots

Chapter 1

Introduction

1.1 Problem Statement

Code-Division Multiple Access (CDMA) is one of several methods by which multiple users may access a common transmission channel. In a DS-CDMA system as shown in Figure 1.1, each user is assigned a unique "signature waveform", which is used to modulate its associated data stream as in a single user communication system [2]. All users employ the same carrier frequency without time division. The received signal is the superposition of all users' signals plus noise. If their signature waveforms are mutually orthogonal and received signals are time-aligned, the ouput of the receiver would be free from the interference caused by other users. However, In practice due to the multi-path effect, the signals of different users usually arrive at the receiver with random time delays, therefore, there exists a non-zero cross-correlation between the signature waveforms which result in an interference component in each user's matched filter's output. This is called multiple access interference (MAI). Although the portion of MAI caused by one user is generally small, the total effect becomes substantial as the number of simultaneous transmitting users as well as their received powers increase. As a result, the existence of MAI degrades the performance of the

receivers and limits the capacity of the CDMA systems.

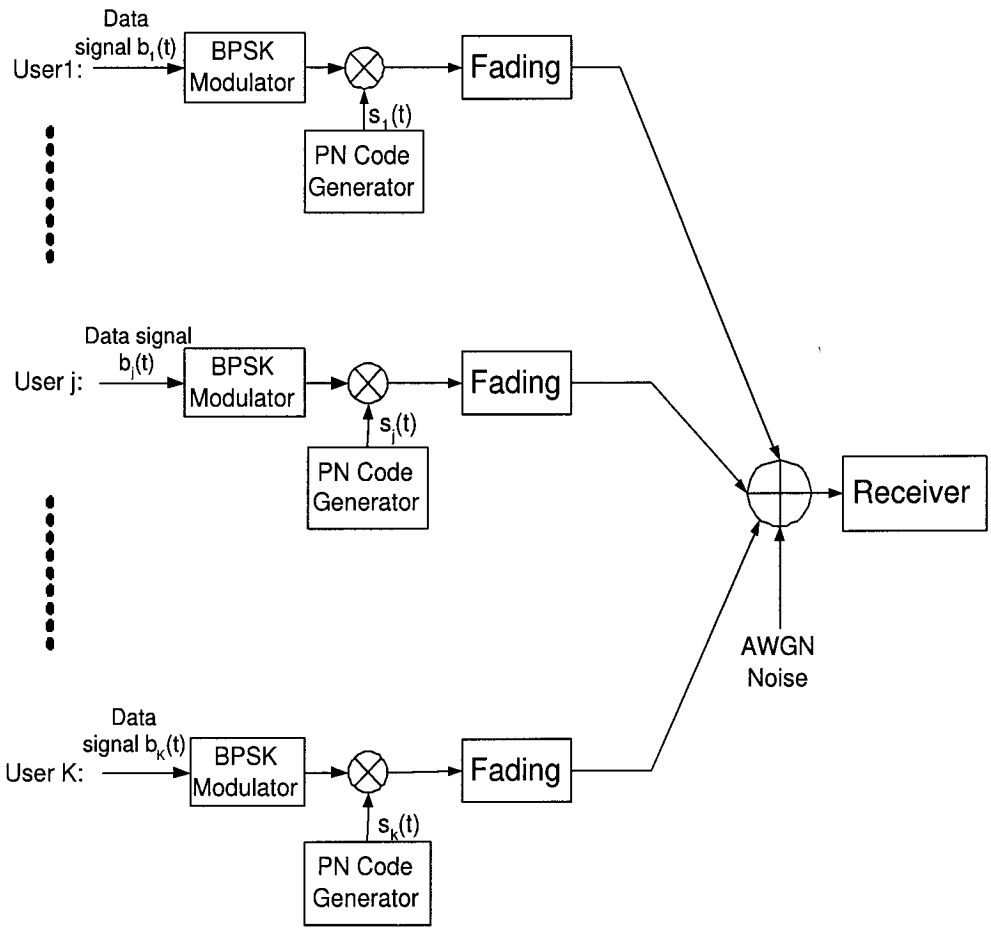

Figure 1.1: Direct Sequence Code Division Multiple Access

In order to reduce the effect of MAI and increase the capacity of a DS-CDMA system, there are four factors that we need to consider [2]: they are the received Signal-to-Noise Ratio (SNR), signature waveforms' cross-correlation properties, channel coding and receiver structure. For the first factor, the transmitter power has to be increased in order to increase SNR, which in turn increases the interference to other users as well. For the second factor, due to the fact that different time delays exist

within different users, the MAI can not be completely avoided even when the signature waveforms have been designed with good auto-correlation and cross-correlation properties. As for the third factor, channel coding can improve the performance of the system at the cost of decreased information rate. However, this is unbearable for high-speed services, such as Video On Demand (VOD) etc. For the last factor, as we know, a conventional DS-CDMA receiver only correlates the entire received signal with each user's signature waveform individually, and this may lead to serious near-far problem and error floor caused by excessive interference. The reason for this is that the conventional receiver ignores the existence of interference. A multi-user receiver may provide much improvement by taking into account the structure of MAI. This brings us to the objective of this thesis: the design and analysis of a multiuser detector in the presence of MAI in the flat fading channel.

1.2 Past Research on Multiuser Detectors

In this section we will briefly review the conventional DS-CDMA detector, as well as some common multiuser detectors.

1.2.1 Conventional DS-CDMA Detector

As shown in Figure 1.2, the conventional DS-CDMA detector is a bank of K correlators [3]. Each signature waveform is regenerated and correlated with the entire received signal in a seperate detector branch. Here, the correlator is equivalent to a matched filter. Thus we also refer to a bank of correlators as a matched filter bank. The output of each correlator is sampled at the bit times, and the decisions are made according to the sign of the sampled output (assuming Binary Phase Shift Keying-BPSK). The conventional detector treats MAI as if it were noise and follows the

same strategy as single-user detection. Therefore, it may lead to significant near-far problem.

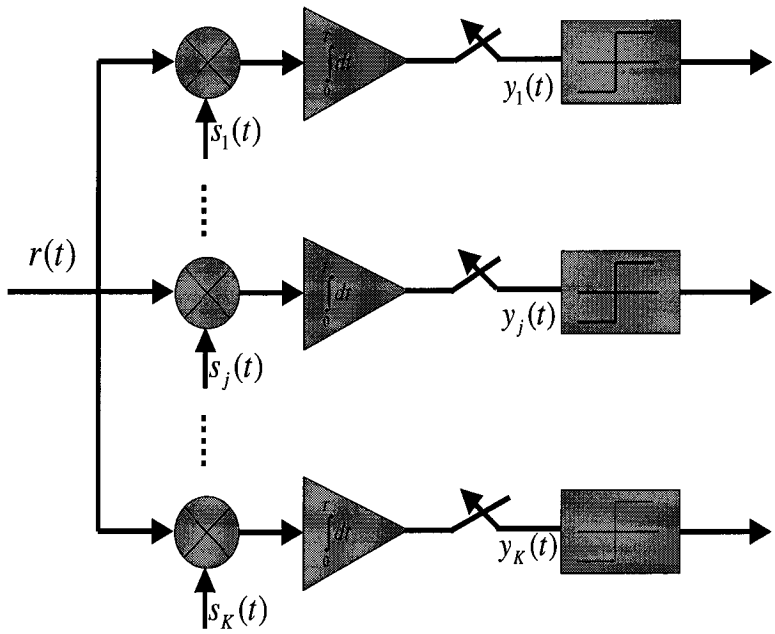

Figure 1.2: Conventional Detector Structure

1.2.2 Maximum Likelihood Sequence (MLS) Detector or Optimal Detector

Proposed by Sergio Verdú in 1986, the MLS multiuser detector is based on the principle of maximum likelihood [2, 3]. It is also refered as "optimal multiuser detector" in the literature because it can achieve minimum probability of error, optimum asymptotic multiuser efficiency and optimum near-far resistance. This detector enumerates all the possible combinations of data based on the message size and calculates the probability of each combination $\mathbf{d}$ being transmitted given a received signal $r(t)$, $P[\mathbf{d}|r(t)]$. The combination with the hightest probability $P[\mathbf{d}|r(t)]$ is chosen as the

estimated data sequence. However, since there are totally 2^{MK} possible data combinations, where M represents the size of the message and K represents the total number of users, this exhaustive search method is obviously impractical when M and K are large. Although it turns out the MLS detector can be implemented by Viterbi algorithm, the computational complexity of Viterbi algorithm is still exponential in the number of users. Another problem of MLS detector is that it requires the knowledge of the signal's amplitude and phase for every user, which have to be estimated at the receiver. An improper estimate may be catastrophic to the performance of the entire system. In summary, although the MLS multi-user detector provides significant improvement on the performance of DS-CDMA system compared to the conventional detector, its high complexity makes it impractical for real time implementation. Therefore, a lot of research has been done to develop sub-optimal multi-user detector [4] that can provide improved performance compared to the conventional CDMA receiver without an overwhelming amount of computations. In the rest of this section, we look at several major sub-optimal multi-user detectors and compare their advantages and disadvantages.

Figure 1.3 depicts the tree of multi-user detectors. As shown, they can be divided into two classes of sub-optimal multi-user detectors proposed in the literature: linear multi-user detectors and decision driven multi-user detectors. Common linear multi-user detectors are the decorrelating detector, MMSE detector and polynomial expansion detector while common decision-driven detectors include the multistage detector, decision feedback detector and successive interference canceller. In the following sections, we will briefly review these detectors.

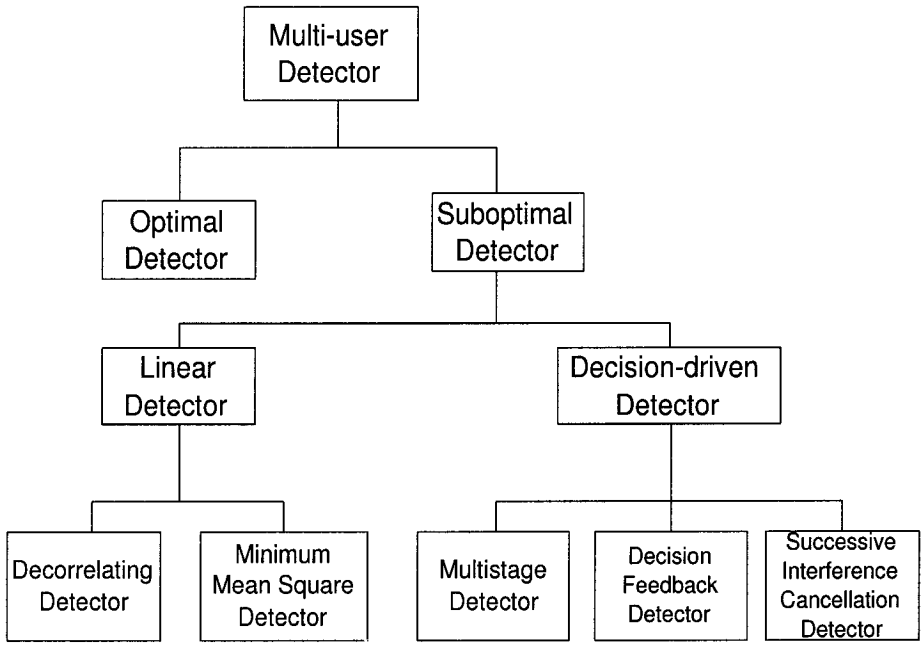

Figure 1.3: The Block Diagram for Class of Multi-user Detectors

1.2.3 Linear Detector

The main property of linear multiuser detector is applying a linear mapping $\mathbf{L}$ to the output of the matched filter in order to reduce the MAI. The linear detector type depends on the mapping matrix $\mathbf{L}$ and realization of the mapping matrix. Decorrelator, minimum mean square and polynomial expansion detectors [2, 3, 5] are examples of linear detectors.

Decorrelating Detector

Compared to the conventional detector, decorrelating detector can provide some advantages by applying the inverse of the correlation matrix $\mathbf{R}$ to the output of the matched filters [2, 3, 6]. Here, $\mathbf{R}$ is the normalized crosscorrelation matrix of the users' signature waveforms. The estimated data sequence $\hat{\mathbf{d}}$ can then be written in

the following form assuming BPSK modulation:

$$\hat{\mathbf{d}} = sgn\{\mathbf{R}^{-1}\mathbf{Y}\} \tag{1.1}$$

where

$$sgn\{x\} = \begin{cases} 1 & x > 0 \\ -1 & x < 0 \end{cases}$$

and $\mathbf{Y}$ represents the output vector of the matched filter. It is convenient to express $\mathbf{Y}$ in the matrix form:

$$\mathbf{Y} = \mathbf{RGb} + \mathbf{N}_c \tag{1.2}$$

where $\mathbf{N}_c$ is a zero-mean colored Gaussian random vector with covariance matrix equal to

$$E[\mathbf{N}_c\mathbf{N}_c^T] = \mathbf{R}$$

$\mathbf{G}$ is a diagonal amplitude matrix, and $\mathbf{b}$ represents the transmitting data vector. Thus, by substituting Equation (1.2) into (1.1), $\hat{\mathbf{d}}$ can be rewritten as:

$$\hat{\mathbf{d}} = sgn\{\mathbf{Gb} + \mathbf{R}^{-1}\mathbf{N}_c\} \tag{1.3}$$

Such a transformation can provide two main advantages. First, it completely eliminates MAI from the different users. Therefore the detection of each user can be implemented independent of other users. Second, it simplifies the complexity of the detector because no estimation of different users' power levels is required. However, this detector cause noise enhancement, which in turn leads to a higher bit error rate (BER). Also, matrix inversion is a computationally intensive task. It becomes even more serious for asynchronous systems where the dimension of crosscorrelation matrix $\mathbf{R}$ is very large (can be done adaptively).

Minimum Mean Square Error (MMSE) Detector

MMSE detector tries to minimize the mean squared error between the transmitted data and the data after applying linear mapping to the matched filter output, i.e.,

$$\min E[|\mathbf{d} - \mathbf{LY}|^2] \tag{1.4}$$

Where $E[\cdot]$ denotes the expectation function. Starting from Equation (1.4), the estimated data sequence $\hat{\mathbf{d}}$ can be written in the following form after taking into account the background noise and making use of the knowledge of the received signal power:

$$\hat{\mathbf{d}} = sgn\{\mathbf{LY}\} = sgn\{(\mathbf{R} + \frac{N_0}{2}\mathbf{G}^{-2})^{-1}\mathbf{Y}\} \tag{1.5}$$

where: $\mathbf{L} = \mathbf{R} + \frac{N_0}{2}\mathbf{G}^{-2}$, and $\frac{N_0}{2}$ represents double sided noise spectral density.

Compared to the decorrelating detector, MMSE detector implements a modified inverse of a correlation matrix. The amount of modification is directly proportional to the background noise. Thus, the MMSE detector balances decoupling the users with enhancing the noise level. As the background noise goes to zero, the performance of the decorrelator approaches the performance of the MMSE detector. Thus, this detector ovecomes the noise enhancement problem faced by the decorrelating detector and provides some improvement in BER performance. However, the received amplitudes of users have to be estimated. Erroneous estimations can lead to degradation of performance.

Polynomial Expansion (PE) Detector

The polynomial expansion detector is based on the well-known Cayley-Hamilton theorem in linear algebra. The detector does not actually perform matrix inversion, but implements a linear combination of $\mathbf{R}$ [3]. Based on Cayley-Hamilton theorem, the

inverse of $\mathbf{R}$ can be restated in Equation (1.6):

$$\mathbf{R}^{-1} \approx \sum_{i=0}^{p} W_i \cdot \mathbf{R}^i \tag{1.6}$$

Where W_i is the weight of $\mathbf{R}_i$. By substituting Equation (1.6) into (1.1), the estimated data $\hat{\mathbf{d}}$ can be computed as follow:

$$\hat{\mathbf{d}} = sgn\{\sum_{i=0}^{p} W_i \mathbf{R}^i \mathbf{Y}\}$$

Thus, it greatly reduces the computational complexity greatly. At the same time, it is also able to achieve the same performance level as decorrelating detector. This technique can also be applied to MMSE detector.

1.2.4 Decision-driven Detector

Decision driven detector is another important class of multi-user detector. It makes use of feedback to reduce the MAI in the received signal. Such detectors are often implemented with multiple stages, where the expectation is that the decisions will improve at the output of the successive stages. We will briefly review three main decision-driven detectors in the following:

Successive Interference Cancellation (SIC) Detector

The SIC detector takes a serial approach to interference cancellation. This approach is based on a simple idea: if a decision has been made about an interfering user's bit, then that interfering signal can be recreated at the receiver and subtracted from the received signal. This will cancel the interfering signal provided that the decision was correct; otherwise it will quadruple the interference power. The receiver begins by selecting the strongest signal and making a decision. Its interference estimates are then

subtracted from all other signals. This is then repeated for the next strongest signal and all signals have been detected. The SIC detector requires only a minimal amount of additional hardware and has the potential to provide significant improvement over the conventional detector. However, there exist several implementation difficulties. First, additional bit delay is required per stage of cancellation. Thus, a trade off must be made between the number of users that are cancelled and the amount of delay that can be tolerated. Second, there is a need to reorder the signals whenever the power profile changes. So, a tradeoff must be made between the precision of the power ordering and the acceptable processing complexity. Thirdly, a potential problem with the SIC detector occurs when phase estimates are not perfect [2, 3, 7]. The MAI will not be cancelled and may actually increase. Thus, the performance is extremely sensitive to initial bit estimate and power level.

Multistage Parallel Interference Cancellation (PIC) Detector

In contrast to SIC, the PIC detector estimates and subtracts out all of the MAI for each users in parallel [3]. Like SIC, the performance of this detector is severely affected by incorrect initial bit estimates and erroneous amplitude estimation. Too many incorrect initial data estimates may cause performance to degrade. Compared to SIC, PIC is found to outperform SIC in power controlled channel. On the contrary, SIC outperforms PIC in non-power controlled channels since it cancels MAI in order of signal strength [8, 9].

Decision Feedback (DF) Detector

This detector performs two operations: linear preprocessing followed by a SIC detection [3, 6, 10]. The linear operation partially decorrelates the users without enhancing

the noise. The DF detector is based on a white noise channel model. A noise-whiteening filter is obtained by factoring the correlation matrix $\mathbf{R}$ using Cholesky factorization, ($\mathbf{R} = \mathbf{F}^T\mathbf{F}$), where $\mathbf{F}$ is a low triangular matrix. Applying $(\mathbf{F}^T)^{-1}$to the output of matched filter bank yields the white noise model.

$$\begin{aligned} \mathbf{W} &= (\mathbf{F}^T)^{-1}\mathbf{Y} = (\mathbf{F}^T)^{-1}(\mathbf{RGb} + \mathbf{N}_c) \\ &= (\mathbf{F}^T)^{-1} \cdot (\mathbf{F}^T\mathbf{FGb} + \mathbf{N}_c) = \mathbf{FGb} + \mathbf{N}_w \end{aligned} \tag{1.7}$$

where $\mathbf{N}_w$ is a white noise. The linear operation partially decorrelates the users since $\mathbf{F}$ is a low triangular matrix. The SIC operation makes decision and subtracts out the interference from one additional user at a time, in descending order of strength. The performance of DF detector is similar to the decorrelating detector. However, the workload for computing the Cholesky factorization and noise whitening filter $(\mathbf{F}^T)^{-1}$ is very large. Furthmore, like the other nonlinear detectors, DF detector needs to estimate the received signal amplitude [3].

1.2.5 Adaptive Multi-user Detector

Several linear multi-user detection techniques discussed earlier have significant computational workloads. Adaptive techniques have thus been suggested in literature to realize these linear transforms. MMSE detection is very attractive from an implementation standpoint because of its natural link to adaptive filtering techniques which are very well understood. In such implementations, the received signal is passed through a transversal filter, which outputs the sufficient statistic for making bit decisions. The filter coefficients are adapted based on feedback from the output. The coefficients can be updated may be based on training sequences. Least Mean Squares (LMS) and Recursive Least Squares (RLS) are two popular training sequence based

algorithms for coefficient adaptation. Both of these two detectors converge to MMSE detector described earlier if the step size is properly chosen.

1.3 Objective of This Thesis

The purpose of this thesis is to develop a modified low-complexity multistage detector, named Selective Multistage Detector (SMD), and investigate the performance of this detector in the slow flat Rayleigh fading channel by computer simulation. Selective multistage detector is first proposed in [1] for the additive white Gaussian noise (AWGN) channel. The results in [1] show that the selective multistage detector greatly reduces the number of computations and provides slight improvement in the BER performance compared to the conventional multistage detection algorithm [11]. In this thesis, we extend the selective multistage detection algorithm in AWGN channel to the slow flat Rayleigh fading channel, which is more common in wireless communication. The efficiency of this detection scheme is explored. First, we consider the performance of selective multistage detection and nonselective multistage detection when the receiver perfectly estimates the channel gains of all users. Then we employ pilot-based optimum Wiener interpolator filter to estimate the channel gains. We will make use of the channel gain estimation to get more reliable MAI estimates and obtain results close to the ideal channel estimation case.

1.4 Content of Thesis

This thesis is organized as follows: the system model of the selective multistage multiuser detector in the asynchronous DS-CDMA system in the presence of flat Rayleigh fading is briefly described in Chapter 2. The system model is comprised of fading channel generation, channel estimation and multiuser detection. Also in Chapter 2,

three kinds of fading channel generation models are introduced in detail. Channel estimation is described in Chapter 3 for the single user case and multi-user channel case respectively, the simulation results for both cases are presented as well. The selective multistage algorithm in flat fading channel is presented in Chapter 4 and the comparison between the selective multistage algorithm with conventional multistage algorithm is conducted based on the computer simulation results. In Chapter 5, we present our conclusions based on the results in Chapter 4 and discuss future work to be done on this topic.

Chapter 2

System Design

2.1 System Description

In this thesis, we investigate the performance of selective multistage multi-user detector in asynchronous DS-CDMA systems in the presence of slow flat Rayleigh fading, which is applicable to both narrowband systems where the maximum delay spread is very small compared to the symbol duration or wideband systems where there exists only one fading path, for instance in suburban mobile radio channel or indoor wireless channel [12]. The entire system model is presented in Figure 2.1, which consists of the channel model, receiver matched filter bank, channel estimator and selective multistage multi-user detector.

In this system, signals from K mobile users arrive at the base station through slow flat frequency-nonselective fading channel, the received signal $r(t)$ can be written as:

$$r(t) = \sum_{k=1}^{K} \left(c_k(t) \cdot A_k(\sum_{i=0}^{M} b_k(i) \cdot s_k(t - iT - \tau_k)) \right) + n(t) \tag{2.1}$$

where:

T : symbol interval

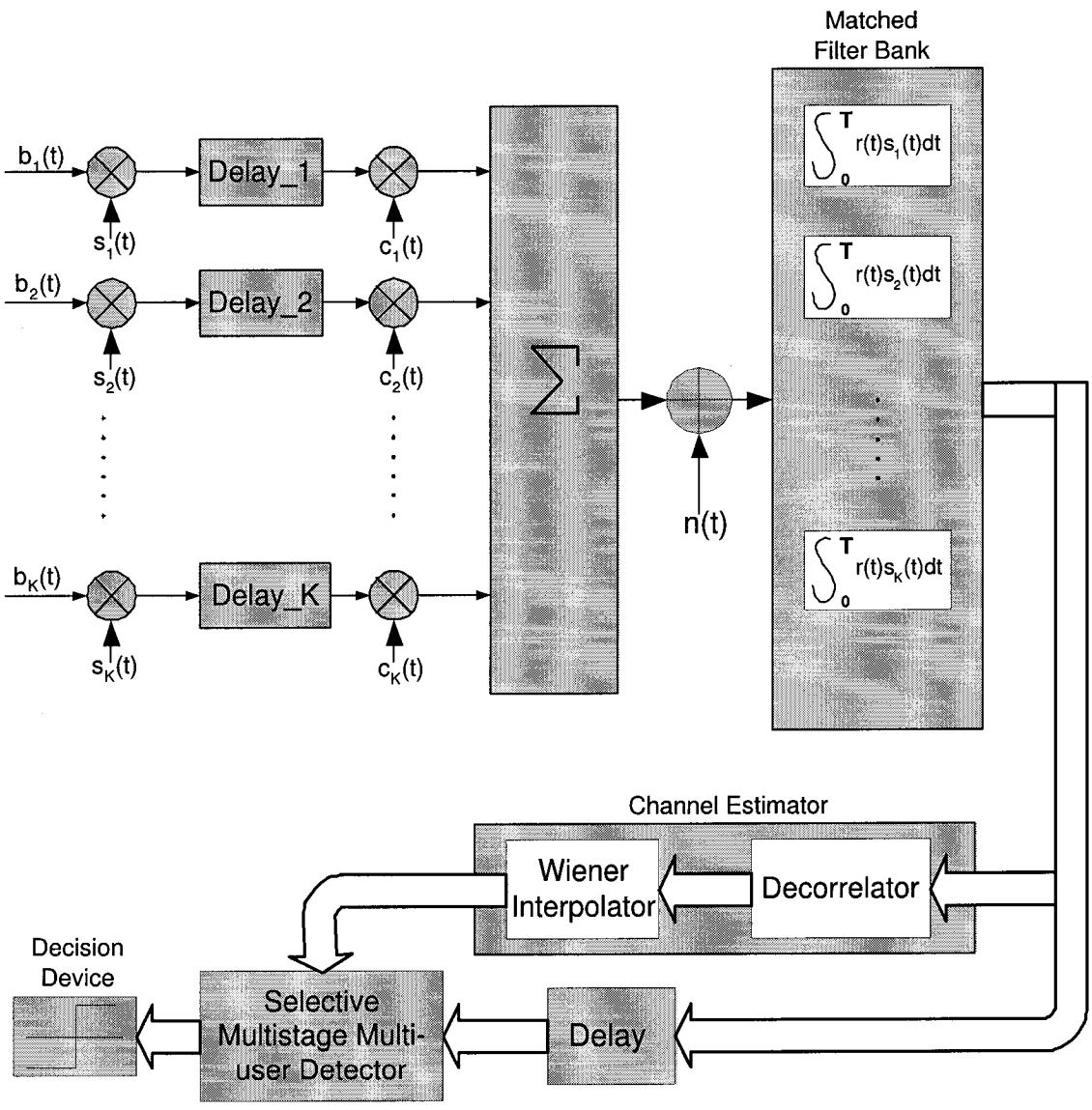

Figure 2.1: System Block Diagram

i : index of the signal interval, i= 0, 1, ..., M

k : user index, k =0, 1, ..., K, the total number of users is K

A_k : amplitude of the k^{th} user

$b_k(i)$: data bit of the k^{th} user on the i^{th} signal interval, $b_k(i) \in [+1, -1]$

$s_k(t)$: normalized signature waveform for the k^{th} user, i.e., $\int_0^T s_k(t)^2 dt = 1$

τ_k : delay of the k^{th} user, $0 \leq \tau_k \leq T$

$n(t)$: complex Gaussian white noise with double-sided spectral density $N_0/2$

$c_k(t)$: complex fading coefficient of k^{th} slow flat fading channel.

$c_k(t)$ is a time-varing Gaussian random process with zero mean and unity variance. It has the following properties:

$$\begin{aligned} E[c_k(t)] &= E[c_k^I(t)] = E[c_k^Q(t)] = 0 \\ VAR(c_k^I(t)) &= VAR(c_k^Q(t)) = \frac{1}{2} \\ VAR[(c_k(t))^2] &= E[(c_k(t))^2] = E[(c_k^I(t))^2] + E[(c_k^Q(t))^2] = 1 \end{aligned}$$

where $c_k^I(t)$ and $c_k^Q(t)$ are in-phase and quadrature components of fading process respectively [13]. We will discuss the generation of the flat Rayleigh fading process $c_k(t)$ in the following sections.

Since the channel is slow flat fading, we can assume that $c_k(t)$ is constant during one symbol interval T, i.e., $c_k(t) = c_k(iT)$ for $t \in [iT, iT + T]$. As a result, Equation (2.1) can be rewritten as follows:

$$r(t) = \sum_{k=1}^{K} \left(A_k \cdot \sum_{i=0}^{M} b_k(i) c_k(i) \cdot s_k(t - iT - \tau_k) \right) + n(t) \tag{2.2}$$

where we replace $c_k(iT)$ with $c_k(i)$ for simplicity.

2.2 Matched Filter Bank

At the receiver, the received signal $r(t)$ is fed into a Matched Filter Bank (MFB) which is comprised of K matched filters, of which each is matched to the signature waveform of a specific user. So, the output of MFB is the correlation of the received signal with each user's signature waveform individually:

$$\begin{aligned} y_1(i) &= \int_{iT+\tau_1}^{iT+T+\tau_1} r(t) \cdot s_1(t - iT - \tau_1)dt \\ &\vdots \\ y_k(i) &= \int_{iT+\tau_k}^{iT+T+\tau_k} r(t) \cdot s_k(t - iT - \tau_k)dt \\ &\vdots \\ y_K(i) &= \int_{iT+\tau_K}^{iT+T+\tau_K} r(t) \cdot s_K(t - iT - \tau_K)dt \end{aligned} \tag{2.3}$$

Without loss of generality, we assume that $\tau_K > \tau_{K-1} > \cdots > \tau_2 > \tau_1$. By substituting Equation (2.2) into (2.3), the output of the k^{th} matched filter in MFB at the i^{th} time interval can be expressed as [2]:

$$\begin{aligned} y_k(i) = {} & A_k b_k(i) c_k(i) + \textstyle\sum_{j=1}^{k-1} A_j b_j(i+1) c_j(i+1) \rho_{kj} + \sum_{j=1}^{k-1} A_j b_j(i) c_j(i) \rho_{jk} \\ & + \textstyle\sum_{j=k+1}^{K} A_j b_j(i) c_j(i) \rho_{kj} + \sum_{j=k+1}^{K} A_j b_j(i-1) c_j(i-1) \rho_{jk} + n_k(i) \end{aligned} \tag{2.4}$$

where $n_k(i)$ is the filtered noise,

$$n_k(i) = \int_{iT+\tau_k}^{iT+T+\tau_k} n(t) s_k(t - iT - \tau_k)dt$$

ρ_{jk} is the cross-correlation between the j-th user's signature waveform and the k-th user's signature waveform.

$$\rho_{jk} = \begin{cases} \int_{\tau_j}^{\tau_k} s_k(t - \tau_k) s_j(t + T - \tau_j)dt & j > k \\ \int_{\tau_k}^{\tau_j + T} s_k(t - \tau_k) s_j(t - \tau_j)dt & j < k \end{cases}$$

Based on Equation (2.4), Equation (2.3) can be rewritten in the matrix form:

$$\mathbf{Y} = \mathbf{RGb} + \mathbf{N_c} \tag{2.5}$$

where: $\mathbf{Y}$ is the matched filters' output vector which is defined as:

$$\mathbf{Y} = \left[\, y_1(0),\ \cdots,\ y_K(0),\ y_1(1),\ \cdots,\ y_K(1),\ \ldots,\ y_1(M),\ \cdots,\ y_K(M) \,\right]^T$$

$\mathbf{b}$ is the tansmitting data vector and is defined as:

$$\mathbf{b} = \left[\, b_1(0),\ \cdots,\ b_K(0),\ b_1(1),\ \cdots,\ b_K(1),\ \ldots,\ b_1(M),\ \cdots,\ b_K(M) \,\right]^T$$

$\mathbf{N_c}$ is a noise vector and is defiend as:

$$\mathbf{N_c} = \left[\, n_1(0),\ \cdots,\ n_K(0),\ n_1(1),\ \cdots,\ n_K(1),\ \ldots,\ n_1(M),\ \cdots,\ n_K(M) \,\right]^T$$

$\mathbf{R}$ is a $MK \times MK$ crosscorrelation matrix, which is defined as:

$$\mathbf{R} = \begin{bmatrix} \mathbf{R}[0] & \mathbf{R}^T[1] & 0 & \ldots & 0 & 0 \\ \mathbf{R}[1] & \mathbf{R}[0] & \mathbf{R}^T[1] & \ldots & 0 & 0 \\ 0 & \mathbf{R}[1] & \mathbf{R}[0] & \ldots & 0 & 0 \\ \ldots & \ldots & \ldots & \ldots & \ldots & \ldots \\ 0 & 0 & 0 & \ldots & \mathbf{R}[1] & \mathbf{R}[0] \end{bmatrix}_{MK \times MK}$$

$$\mathbf{R}[0] = \begin{bmatrix} 1 & \rho_{12} & \cdots & \rho_{1K} \\ \rho_{12} & 1 & & \vdots \\ \vdots & & \ddots & \\ \rho_{1K} & \cdots & & 1 \end{bmatrix}_{K \times K} \qquad \mathbf{R}[1] = \begin{bmatrix} 0 & \rho_{21} & \cdots & \rho_{K1} \\ 0 & 0 & & \vdots \\ \vdots & & \ddots & \rho_{K,K-1} \\ 0 & 0 & \ldots & 0 \end{bmatrix}_{K \times K}$$

G is a diagonal amplitude matrix which is defined as:

$$\mathbf{G} = \begin{bmatrix} \mathbf{A}(0) & & & \\ & \ddots & & \\ & & \mathbf{A}(i) & \\ & & & \ddots \\ & & & & \mathbf{A}(M) \end{bmatrix}_{MK \times MK}$$

$$\mathbf{A}(i) = \begin{bmatrix} A_1 c_1(i) & & & \\ & \ddots & & \\ & & A_k c_k(i) & \\ & & & \ddots \\ & & & & A_K c_K(i) \end{bmatrix}_{K \times K}$$

As shown in Figure 2.1, the output of matched filter bank **Y** is split into two paths: one path is fed into a estimator for channel estimation, which is made up of a decorrelator and Wiener interpolator filter. This part of content will be introduced in Chapter 3. The other path is multiplied by the conjugate of estimated fading gain. The compensated signal is then fed into a selective multistage multi-user detector to detect the transmitted data. Selective multistage multi-user detection will be introduced in Chapter 4. Finally, the detected data is compared with the transmitted data and the number of errors are counted to compute the bit error rate.

2.3 Fading Channel Model

2.3.1 Multipath Propagation - Small Scale Fading

In an ideal radio channel, the received signal would consist of only a single direct path signal, which would be a perfect reconstruction of the transmitted signal [14]. However, in a practical wireless channel, since the height of mobile antennas are well

below the height of surrounding structures, there is rarely a single line-of-sight (LOS) path to the base station. Even if a LOS exists, multipath effect that is caused by reflections, scatter, or diffraction from the ground and surrounding structures still occurs as shown in Figure 2.2. Moreover, the incoming radio waves arrive from different directions with different propagation delays. These multipath components combine vectorially at the receiver antenna, and can cause received signal to fade. In summary, fading is caused by interference between two or more versions of the transmitted signal which arrive at the receiver at slightly different times. These signals, called multipath signals, are displaced with respect to one another in time and spatial orientation and combined at the receiver antenna to give a resultant signal which has fluctuation in the amplitude and phase [15]. This is calld small scale fading. In this thesis, we only consider the effect of small scale fading.

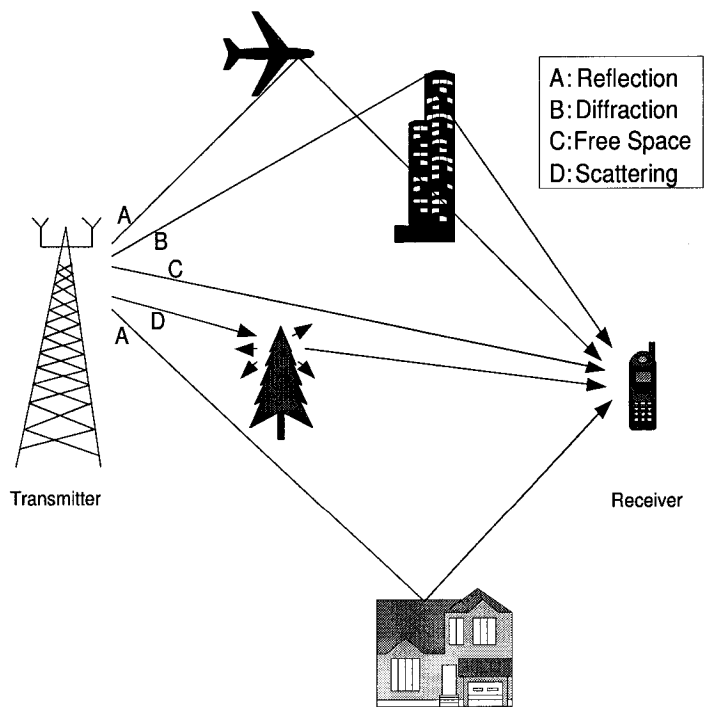

Figure 2.2: Propagation Mechanisms

2.3.2 Types of Fading

Depending on the relationship between the signal parameters (such as bandwidth, symbol period, etc) and channel parameters (such as rms delay spread and Doppler spread), different transmitted signals will undergo different types of fading [15]. Time dispersion due to multipath causes the transmitted signal undergo either flat or frequency selective fading. Frequency dispersion due to multipath causes slow fading or fast fading.

Flat Fading

For flat fading, bandwidth of signal is much less than coherence bandwidth of channel, which means that the delay spread τ is much less than symbol period T.

Frequency Selective Fading

For frequency-selective fading, bandwidth of signal is larger than the coherence bandwidth of channel, that is, delay spread is greater than symbol period.

Fast Fading

Fast fading has high Doppler spread, so coherence time is less than symbol period. Thus, channel variations are faster than baseband signal variations.

Slow Fading

Slow fading has low Doppler spread, its coherence time is much greater than symbol period T, the channel variations are slower than baseband signal variations.

In summary, the types of small-scale fading can be depicted in Figure 2.3.

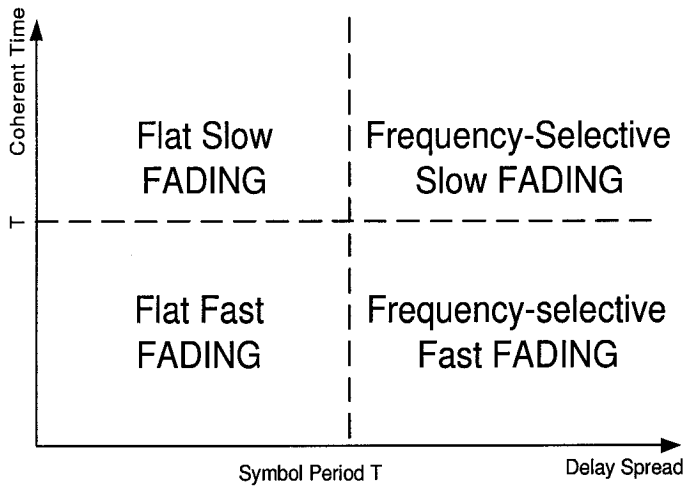

Figure 2.3: Types of Small-Scale Fading

2.3.3 Impulse Response of Multipath Channel

Fading can be directly described by the impulse response of the mobile radio channel. The impulse response contains all information necessary to simulate or analyze any type of radio transmission through the channel [15]. This originates from the fact that a mobile radio channel can be modeled as a linear filter with a time varying impulse response. Assuming transmitted signal is

$$m(t) = \sum_{i=0}^{i=\infty} b(i)p(t - iT) \tag{2.6}$$

where $b(i)$ is the lowpass equivalent of transmitted complex symbol, $p(t)$ is pulse waveform. The channel impulse response of multipath channel consists of L resolvable propagation path:

$$h(t, \tau) = \sum_{l=1}^{L} a_l(t) e^{j\phi_l(t)} \delta(t - \tau_l) \tag{2.7}$$

Here $a_l(t)$ is time-variant path attenuation, $\phi_l(t)$ is time-variant path phase shift, τ_l is path delay. Thus, the received multipath signal is equal to the time domain

convolution of $h(t,\tau)$ with $m(t)$.

$$r(t) = h(t,\tau) * m(t) = \int_{-\infty}^{\infty} h(t,\tau)m(t-\tau)d\tau = \sum_{l=1}^{L} a_l(t)e^{j\phi_l(t)}m(t-\tau_l) \qquad (2.8)$$

So, the received multipath signal is the sum of the L attenuated, phase shifted and delayed replicas of the transmitted siganl $m(t)$.

In a flat fading channel, the delay τ_l is much less than the symbol period T, so the channel impulse response reduces to a sum of L complex channel coefficients.

$$h(t) = \sum_{i=1}^{L} a_l(t)e^{j\phi_l(t)} = a(t)e^{j\phi(t)} = c_I(t) + jc_Q(t) \qquad (2.9)$$

Here, $c_I(t)$ and $c_Q(t)$ are the inphase and quadrature components of the fading process respectively. Both of them are independent Gaussian random process with zero mean and $\frac{1}{2}$ variance. The envelope $a(t)$ is Rayleigh distributed and the phase $\phi(t)$ is uniformly distributed in the interval $[0, 2\pi]$.

2.3.4 Clarke's Statistical Model for Flat Rayleigh Fading

Several mathematical models for the multipath channel have been proposed to model the observed statistical nature of a mobile channel. The first model presented by Ossana was based on interference of waves incident and reflected from the flat sides of randomly located buildings. Although Ossana's model predicts that flat fading power spectra were in agreement with measurements in suburban areas, it assumes the existence of a direct path between the transmitter and receiver, and is limited to a restricted range of reflection angles. Ossana's model is therefore rather inflexible and impratical for urban areas where the direct path is almost always blocked by buildings or other obstacles. Here, Clarke's model is based on scattering and is widely used [15, 16, 17].

Clarke developed a model where the statistical characteristics of the electromagnetic fields of the received signal at the mobile are deduced from scattering. The model assumes a fixed transmitter with a vertically polarized antenna. The field incident on the mobile antenna is assumed to be comprised of N azimuthal plane waves with arbitrary carrier phases, arbitrary azimuthal angles of arrival, and each wave having equal average amplitude. Every wave that is incident on the mobile undergoes a Doppler shift due to the motion of the receiver and arrives at the receiver at the same time. That is, no excess delay due to multipath is assumed for any of the waves (flat fading assumption). For the n-th wave arriving at an angle α_n, the Doppler shift is given by

$$f_d = \frac{v}{\lambda} \cos \alpha_n = f_m \cos \alpha_n \tag{2.10}$$

Here f_m is the maximum Doppler shift, λ is the wavelength of the incident wave, v is the velocity of the mobile. In Clarke's model, time-variant fading coefficient $c(t)$ can be modeled as inphase and quadrature components:

$$\begin{aligned} c(t) &= c_I(t) + jc_Q(t) \\ c_I(t) &= \sqrt{\frac{2}{N}} \sum_{n=1}^{N} \cos\left(2\pi f_d t \cos \alpha_n + \phi_n\right) \\ c_Q(t) &= \sqrt{\frac{2}{N}} \sum_{n=1}^{N} \sin\left(2\pi f_d t \cos \alpha_n + \phi_n\right) \end{aligned} \tag{2.11}$$

When $N \rightarrow \infty$, $c_I(t)$ and $c_Q(t)$ become uncorrelated Gaussian random process with zero mean and variance $\frac{1}{2}$. The envelope of $c(t)$, $a(t) = \sqrt{c_I^2(t) + c_Q^2(t)}$, has a Rayleigh distribution given by

$$f(a) = \begin{cases} \frac{a}{\sigma^2} \cdot e^{-\frac{a^2}{2\sigma^2}} & 0 \leq a \leq \infty \\ 0 & a < 0 \end{cases}$$

Where σ^2 is the time-average power of the received signal.

The desired second-order statistics given by the autocorrelation and cross-correlation function are presented as follows:

$$\begin{aligned} R_{c_I c_I}(\tau) &= E[c_I(t) \cdot c_I(t+\tau)] = \frac{1}{2} J_0(2\pi f_d \tau) \\ R_{c_Q c_Q}(\tau) &= E[c_Q(t) \cdot c_Q(t+\tau)] = \frac{1}{2} J_0(2\pi f_d \tau) \\ R_{c_I c_Q}(\tau) &= E[c_I(t) \cdot c_Q(t+\tau)] = 0 \\ R_{c_Q c_I}(\tau) &= E[c_Q(t) \cdot c_I(t+\tau)] = 0 \\ R_{cc}(\tau) &= E[c(t) \cdot c^*(t+\tau)] = J_0(2\pi f_d \tau) \end{aligned} \tag{2.12}$$

where $J_0(\cdot)$ is the 0-th order Bessel function of the first kind. Its shape is shown in Figure 2.4. As $|t_1 - t_2|$ increases, the correlation between $c(t_1)$ and $c(t_2)$ decreases. It approaches zero as $|t_1 - t_2|$ increases forwards ∞. Conversely, the correlation increases as $|t_1 - t_2|$ is decreased until $t_1 = t_2$, when the correlation becomes 1.

2.4 Three Types of Simulation Model for Fading Channel

In the last 30 years, there are many different methods for the simulation of mobile radio channels. Among them, Jakes model, FFT model and Autoregressive model are three main simulation models. These models are based on Clarke's statistical model. Many other models have been derived from these models [18]. We review them in the following sections:

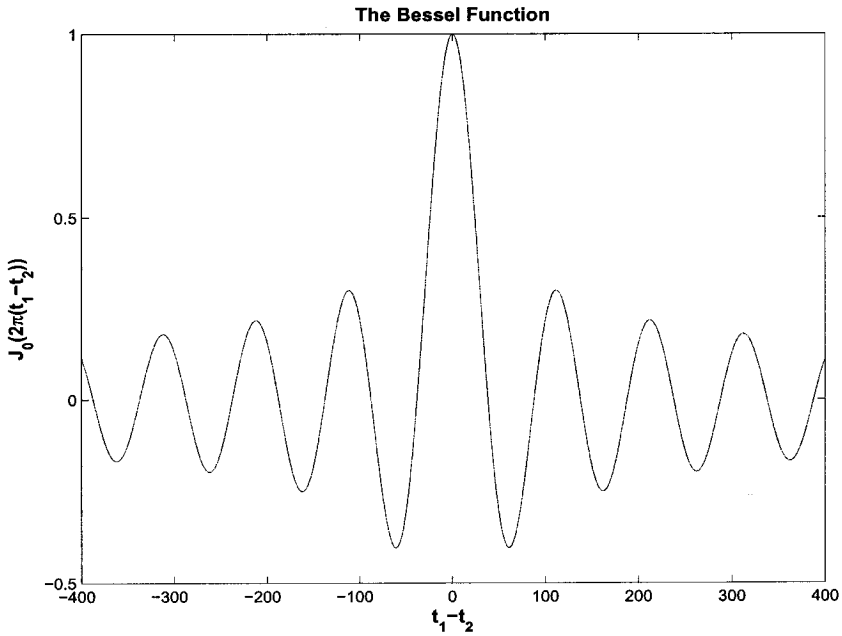

Figure 2.4: 0-th Order Bessel Function of the First Kind

2.4.1 Jakes Model

In Jakes model, a flat fading process is considered to be comprised of N propagation paths, so the normalized low-pass fading process is given as follow [17, 19]:

$$\begin{aligned} c(t) &= c_I(t) + jc_Q(t) \\ c_I(t) &= \frac{2}{\sqrt{N}} \sum_{n=1}^{M+1} a_n \cos(\omega_n t + \phi_n) \\ c_Q(t) &= \frac{2}{\sqrt{N}} \sum_{n=1}^{M+1} b_n \cos(\omega_n t + \phi_n) \end{aligned} \tag{2.13}$$

where $c_I(t)$ and $c_Q(t)$ are respectively the inphase and quadrature components of fading process $c(t)$, $N = 4M + 2$, ϕ_n are independent random variables uniformly

distributed over $[-\pi, \pi]$ for all n, and

$$
\begin{aligned}
a_n &= \begin{cases} 2\cos\beta_n & n = 1, 2 \ldots M \\ \sqrt{2}\cos\beta_n & n = M+1 \end{cases} \\
b_n &= \begin{cases} 2\sin\beta_n & n = 1, 2 \ldots M \\ \sqrt{2}\sin\beta_n & n = M+1 \end{cases} \\
\beta_n &= \begin{cases} \pi n/M & n = 1, 2 \ldots M \\ \pi/4 & n = M+1 \end{cases} \\
\omega_n &= \begin{cases} \omega_d \cos\frac{2\pi n}{N} & n = 1, 2 \ldots M \\ \omega_d & n = M+1 \end{cases} \\
\omega_d &= 2\pi f_d
\end{aligned}
$$

Although Jakes model has been widely used for a long time, some drawbacks still exist: First of all, it is difficult for Jakes model to generate multiple uncorrelated fading waveforms. Secondly, the fading process generated by Jakes model is deterministic and Wide-sense non-stationary, which is impractical in the real world. Thirdly, the autocorrelation and cross-correlation of the quadrature components generated by Jakes model fail to match the desired correlation statistics even when $M \to \infty$. In order to eliminate these drawbacks, many modifications have been made based on Jakes model. For instance, a random phase is added to overcome deterministic problem.

2.4.2 Autoregressive (AR) Model

AR model is a model that can generate the desired correlation without much computation. In AR model, Rayleigh fading process can be modeled as an autoregressive process of order p [18, 20]:

$$c[n] = -\sum_{k=1}^{p} u_k c[n-k] + w[n] \tag{2.14}$$

where $w[n]$ is a complex white Gaussian noise process with zero mean and variance σ_p^2. $\{u_1, u_2, \cdots, u_p\}$ are filter coefficients. Thus, the corresponding power spectrum density (PSD) of the AR process can be written as:

$$S_{AR}(f) = \frac{\sigma_p^2}{|1 + \sum_{k=1}^{p} u_k e^{-j2\pi kf}|^2} \tag{2.15}$$

As we known, arbitrary spectrum can be closely approximated by an AR model of sufficiently large order. Thus, if we let Doppler spectrum of fading process equal to the AR model spectrum, the basic relationship between the desired model autocorrelation function $R_{cc}[k]$ and the filter coefficients u_pi s given by

$$R_{cc}[k] = \begin{cases} -\sum_{m=1}^{p} u_m R_{cc}[k-m] & k \geq 1 \\ -\sum_{m=1}^{p} u_m R_{cc}[-m] + \sigma_p^2 & k = 0 \end{cases} \tag{2.16}$$

It is more convenient to write Equation (2.16) into matrix form.

$$\mathbf{R}_{cc} u = -V \tag{2.17}$$

where

$$\mathbf{R}_{cc} = \begin{bmatrix} R_{cc}[0] & R_{cc}[-1] & \cdots & R_{cc}[-p+1] \\ R_{cc}[1] & R_{cc}[0] & \cdots & R_{cc}[-p+2] \\ \vdots & \vdots & \vdots & \vdots \\ R_{cc}[p-1] & R_{cc}[p-2] & \cdots & R_{cc}[0] \end{bmatrix}$$

$$u = [u_1, u_2, \cdots, u_p]^T$$

$$V = [R_{cc}[1], R_{cc}[2], \cdots, R_{cc}[p]]^T$$

Therefore, We can calculate "u" by multiplying Equation (2.17) by $\mathbf{R}_{cc}^{-1}$.

$$u = -\mathbf{R}_{cc}^{-1} \cdot V \tag{2.18}$$

Once we get the filter coefficients u, the fading process can be generated by Equation (2.14).

2.4.3 FFT Simulation Model

In fading channel, the PSD of the resulting RF signal due to Doppler fading is given by:

$$S(f) = \frac{1.5}{\pi f_m \sqrt{1 - (\frac{f - f_c}{f_m})^2}} \tag{2.19}$$

where f_c is carrier frequency, f_m is maximum Doppler frequency. Figure 2.5 shows the shape of the PSD, which determines the time domain fading waveform and dictates the temporal correlation. FFT model makes use of this spectrum to produce realistic fading waveforms that have proper time correlation [15]. It uses the concept of inphase and quadrature modulation paths to produce a simulated signal representing Equation (2.19) with spectral and temporal characteristics very close to measured data [21, 15, 22]. As shown in Figure 2.6, two independent Gaussian low pass noise sources are used to produce inphase and quadrature fading branches. By using the spectral filter defined by Equation (2.19) to shape the random signals in the frequency domain, accurate time domain waveforms of Doppler fading can be produced by using an inverse fast Fourier transform (IFFT).

Smith came up with a simple computer program [22], of which the flowchart is shown in Figure 2.7. He uses a complex Gaussian number generator (noise source) to produce a baseband line spectrum with complex weights in the positive frequency band. The maximum frequency component of the line spectrum is f_m. Using the

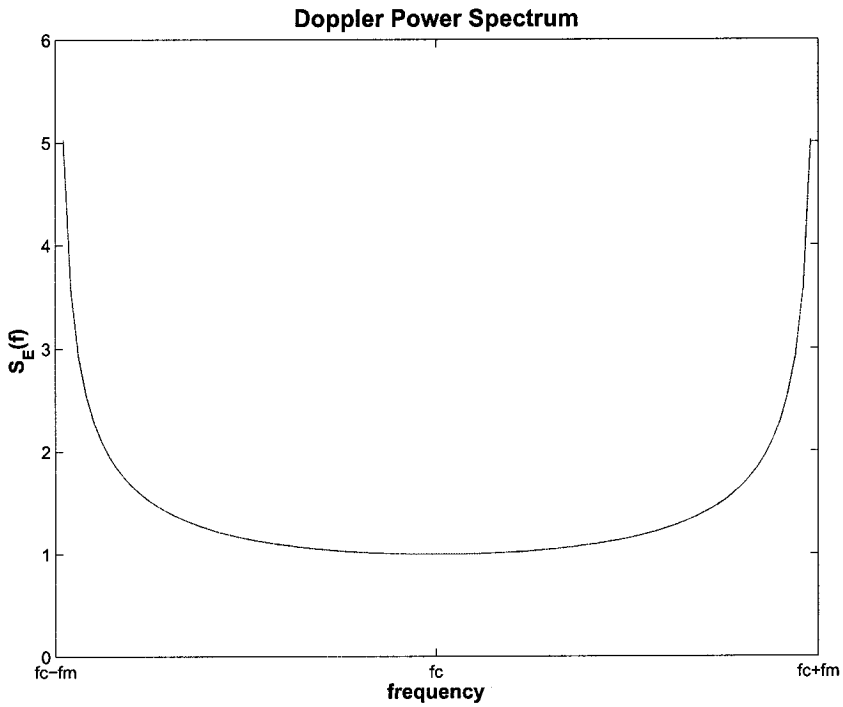

Figure 2.5: Power Spectrum of Fading Process

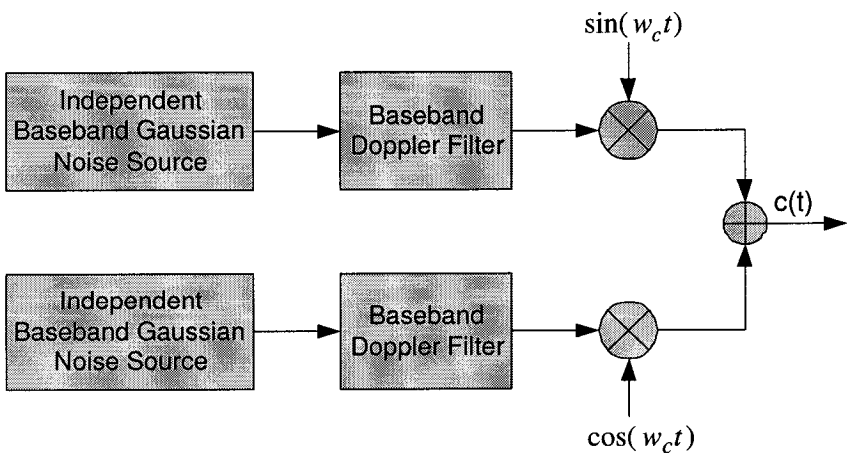

Figure 2.6: FFT Model

property of complex signals, the negative frequency components are constructed by simply conjugating the complex Gaussian values obtained for positive frequencies [15].

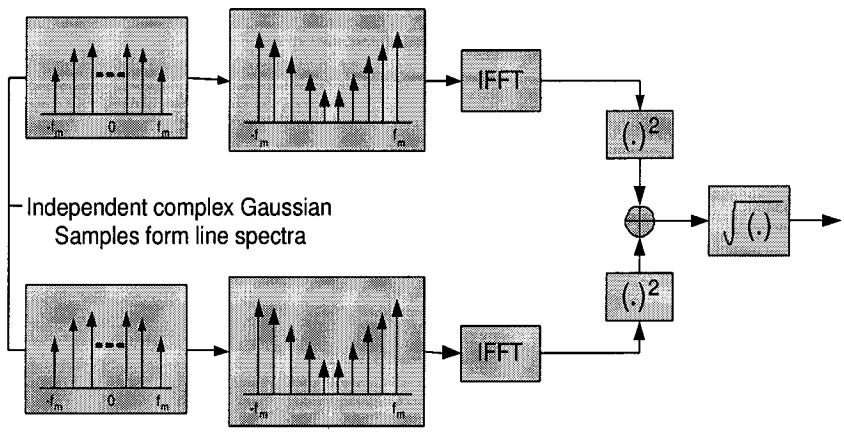

Figure 2.7: The Flow Chart for FFT Model

The detailed algorithm is listed as follows [15]:

1. Specify the number of frequency domain points (N) used to represent $\sqrt{S(f)}$ and the maximum Doppler frequency shift f_m. The value used for N is usually a power of two.

2. Compute the frequency spacing between adjacent spectral lines as $\Delta f = 2f_m/(N-1)$. This defines the time duration of a fading waveform, $T = 1/\Delta f$.

3. Generate complex Gaussian random variables for each of the $\frac{N}{2}$ positive frequency components of the noise source

4. Construct the negative frequency components of the noise source by conjugating positive frequency values and assigning these at negative frequency values.

5. Multiply the in-phase and quadrature noise sources by the fading spctrum $\sqrt{S(f)}$.

6. Perform an IFFT on the resulting frequency domain signals from the in-phase and quadrature arms to get two N-length time series, and add the squares of each signal point in time to create an N-point time series. Note that each quadrature arm should be a real signal after the IFFT.

7. Take the square root of the sum obtained in step 6 to obtain an N-point time series of a simulated Rayleigh fading signal with the proper Doppler spread and time correlation.

2.5 Implementation of Fading Channel

In this thesis, FFT model is employed to simulate the slow flat Rayleigh fading channel since it is a high quality and efficient fading generator.

The simulated complex channel gain magnitudes when Doppler frequency is 1Hz, 10Hz and 100Hz respectively are shown in Figure 2.8, 2.9 and 2.10. For all simulations in this thesis, 1ms symbol period is assumed, i.e., T=1ms. It is shown that Doppler frequency determines the changing speed of fading waveform: the bigger the Doppler frequency is, the faster the fading varies.

The simulated histogram for the amplitude of fading when the Doppler frequency is respectively 1Hz, 10Hz, and 100Hz are presented in Figure 2.11, 2.12 and 2.13. We can see that the amplitude is Rayleigh distributed. In Figure 2.14, the theoretical probability density function (PDF) of the envelope is compared with the simulated one. The result shows they fit very well.

The simulated histogram for the in-phase component when the Doppler frequency is respectively 1Hz, 10Hz, and 100Hz are presented in Figure 2.15, 2.16, 2.17 and 2.18. We can see that the simulated in-phase component is Gaussian distributed and its PDF fits well with the theoretical PDF.

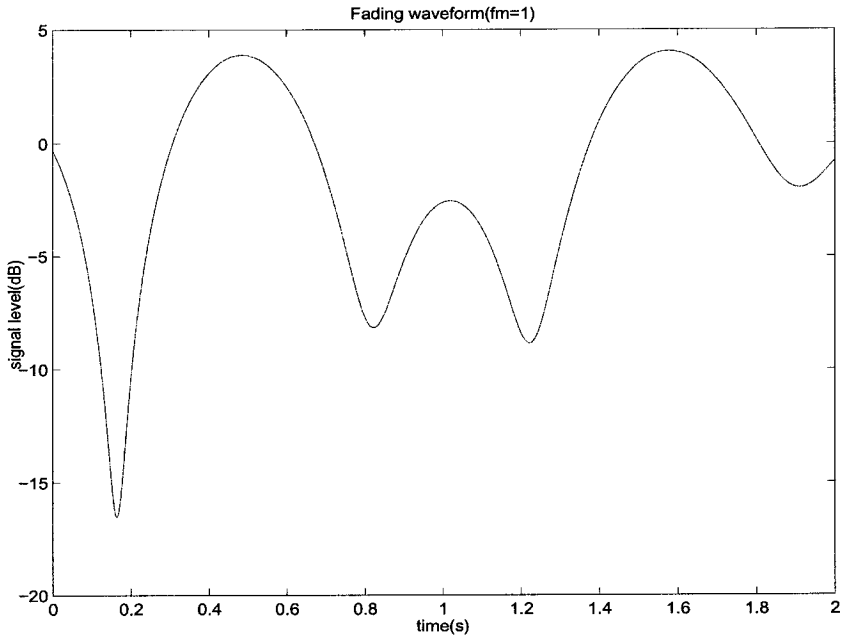

Figure 2.8: Magnitude of Fading when Doppler Frequency is 1Hz

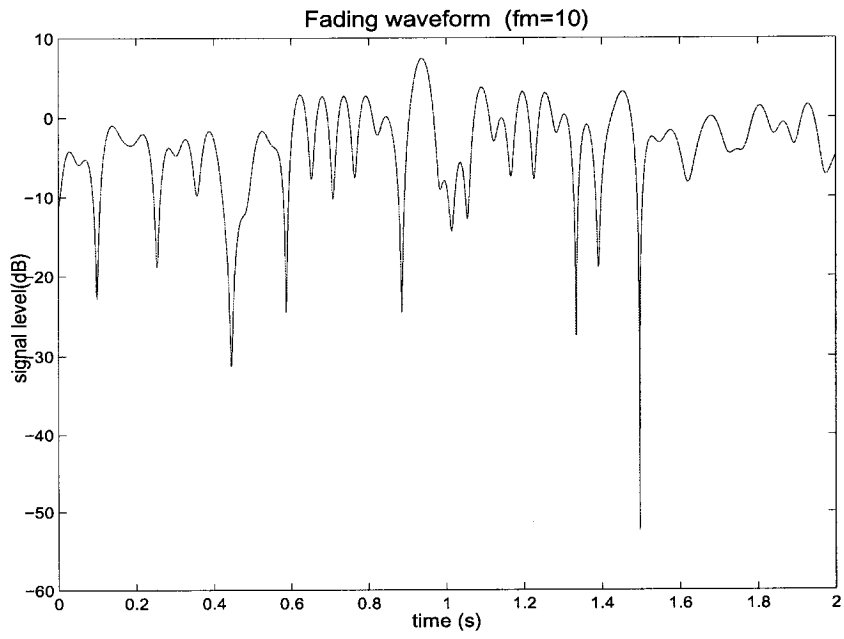

Figure 2.9: Magnitude of Fading when Doppler Frequency is 10Hz

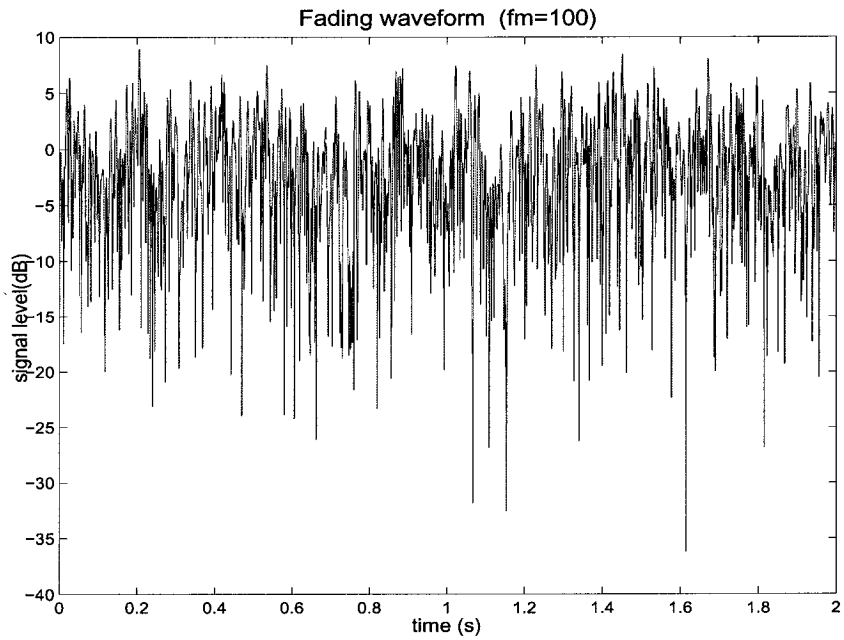

Figure 2.10: Magnitude of Fading when Doppler Frequency is 100Hz

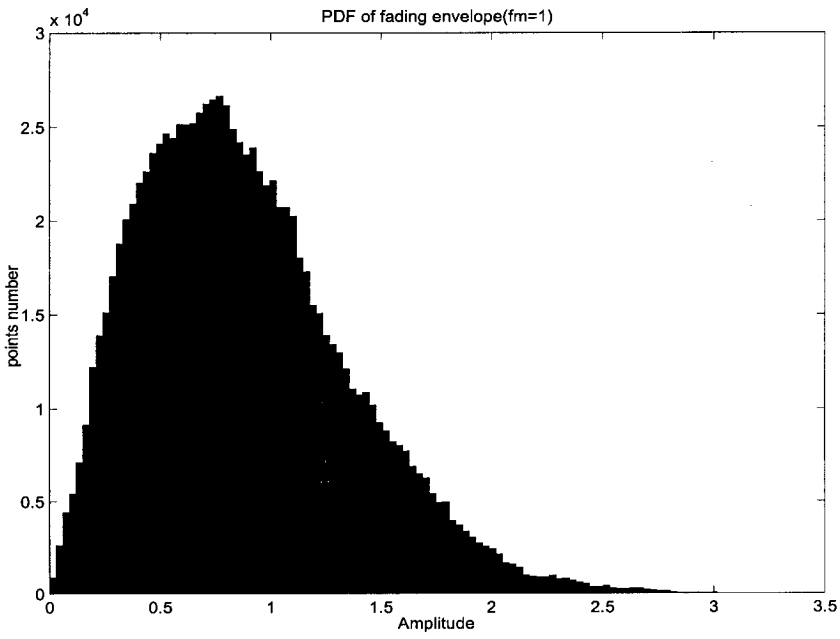

Figure 2.11: Histogram of Envelope when Doppler Frequency is 1Hz

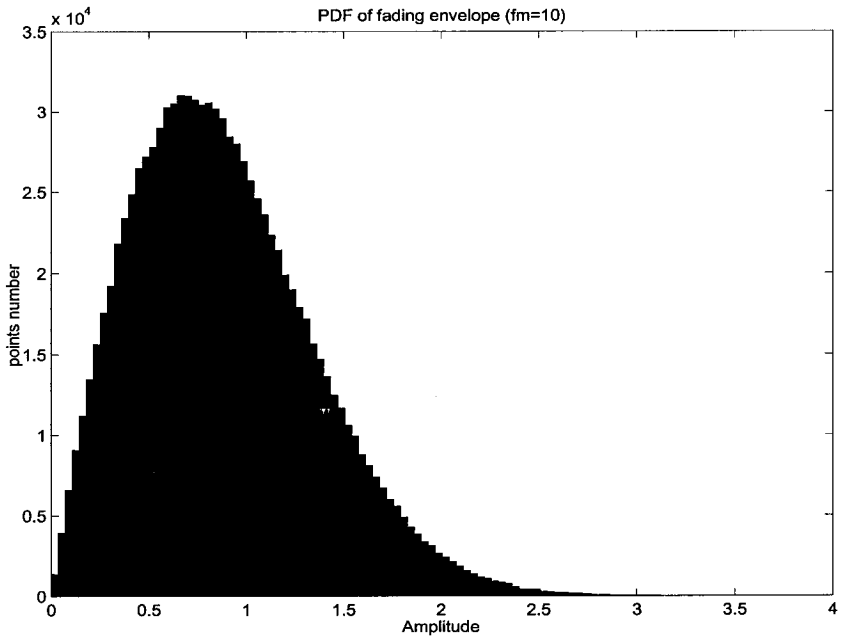

Figure 2.12: Histogram of Envelope when Doppler Frequency is 10Hz

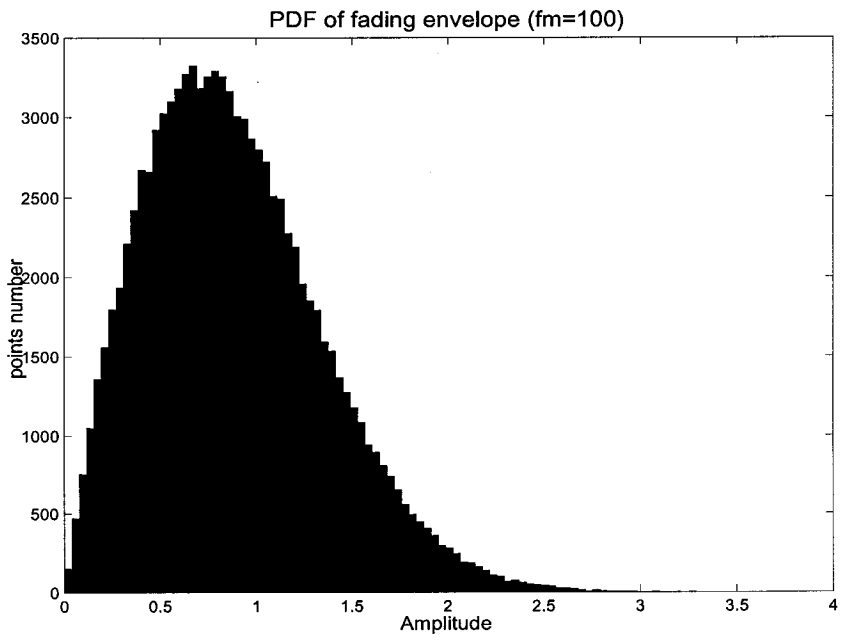

Figure 2.13: Histogram of Envelope when Doppler Frequency is 100Hz

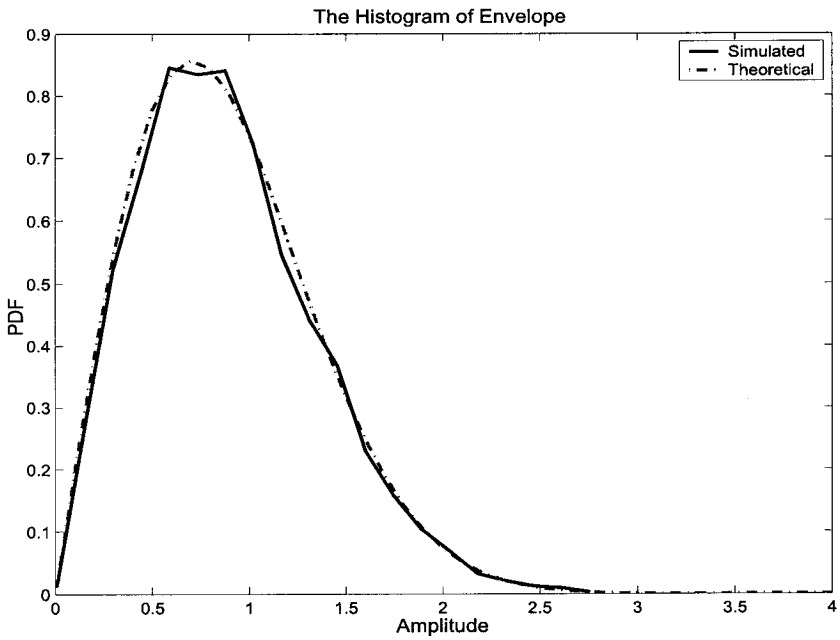

Figure 2.14: Comparision the Theoretical PDF Function with Simulated PDF Function of the Envelope

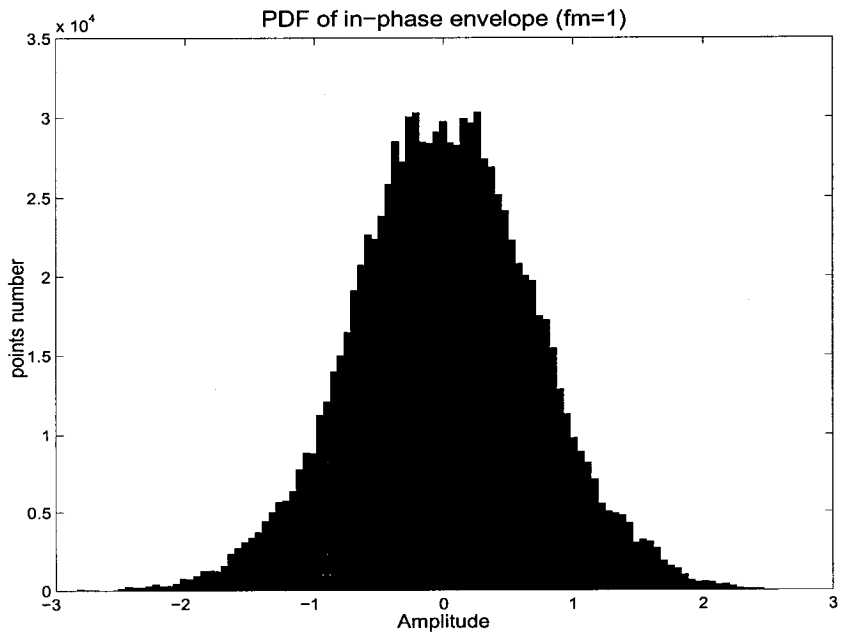

Figure 2.15: Histogram of Inphase Component when Doppler Frequency is 1Hz

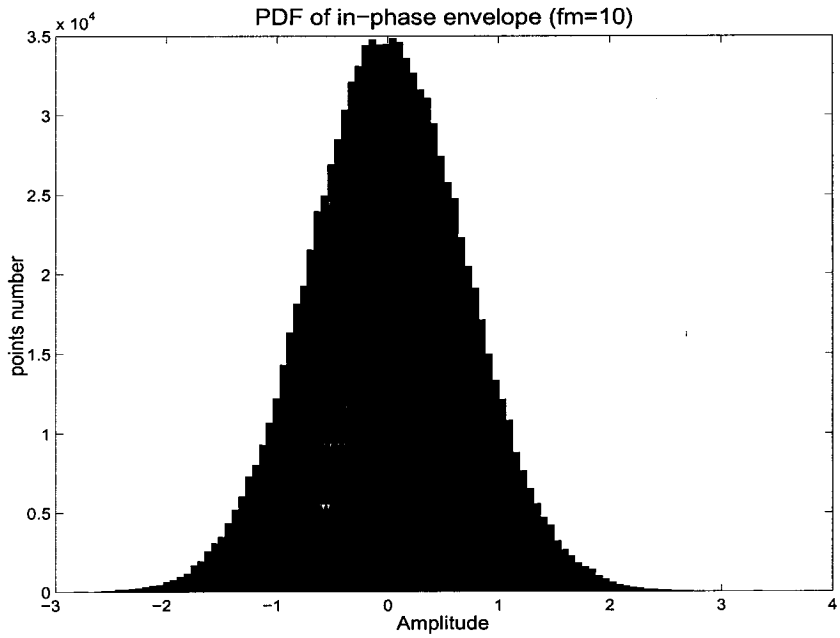

Figure 2.16: Histogram of Inphase Component when Doppler Frequency is 10Hz

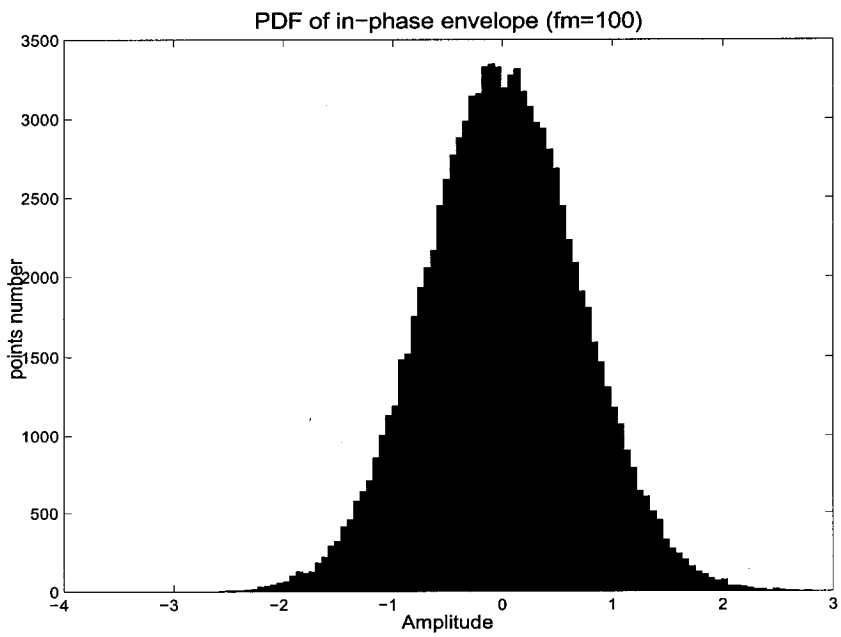

Figure 2.17: Histogram of Inphase Component when Doppler Frequency is 100Hz

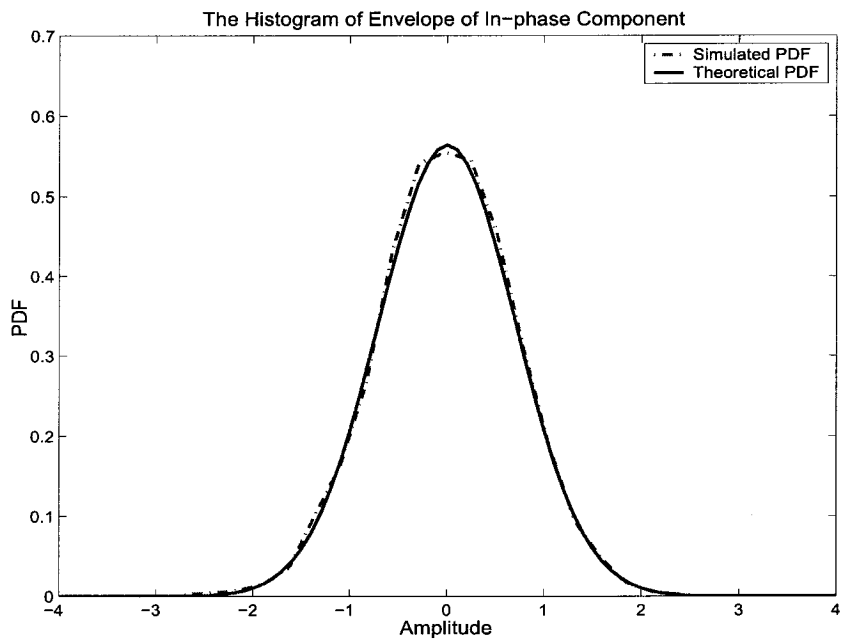

Figure 2.18: Comparison the Theoretical PDF Function with Simulated PDF Function of the Inphase Component

The simulated histograms for the quadrature component when the Doppler frequency are respectively 1Hz, 10Hz, and 100Hz are presented in Figure 2.19, 2.20 and 2.21. We can see the quadrature components are Gaussian distributed too.

Figure 2.23, 2.24 and 2.25 present the simulated autocorrelations of fading process, we can see from the figures that the simulated autocorrelation is very close to the theoretical value which is determined by Equation (2.12). It is also shown that autocorrelation generated by FFT model can match the desired autocorrelation statistics very well.

The BPSK BER performance in the flat Rayleigh fading channel when normalized Doppler frequency is 0.01 is presented in Figure 2.26, as well as the theoretical BER performance. They match very well as shown.

In summary, The above simulation results indicate the efficiency of FFT model

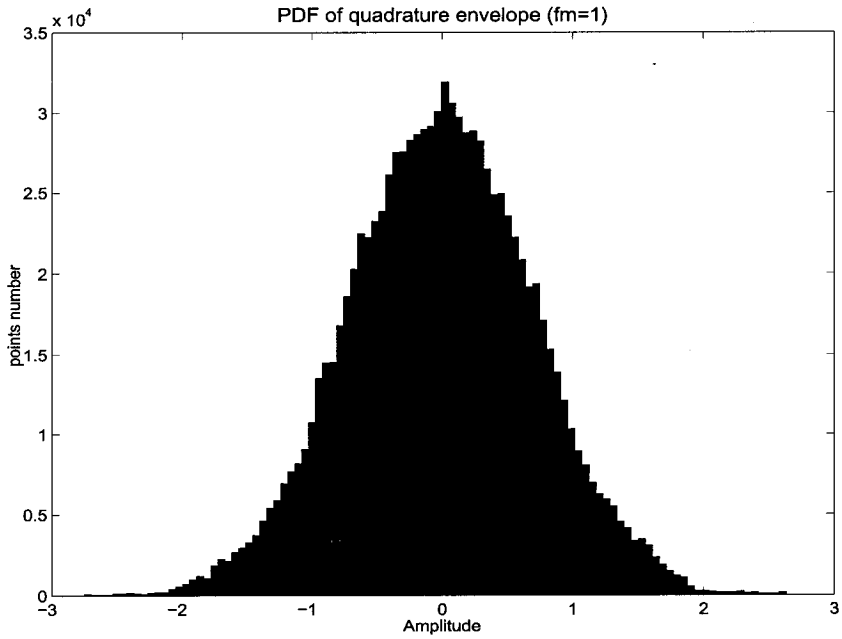

Figure 2.19: Histogram of Quadrature Component when Doppler Frequency is 1Hz

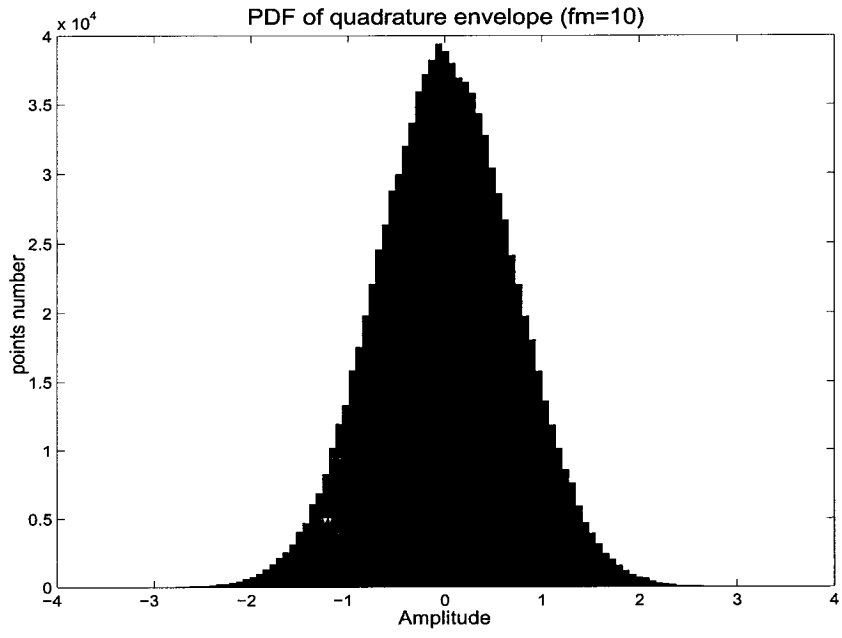

Figure 2.20: Histogram of Quadrature Component when Doppler Frequency is 10Hz

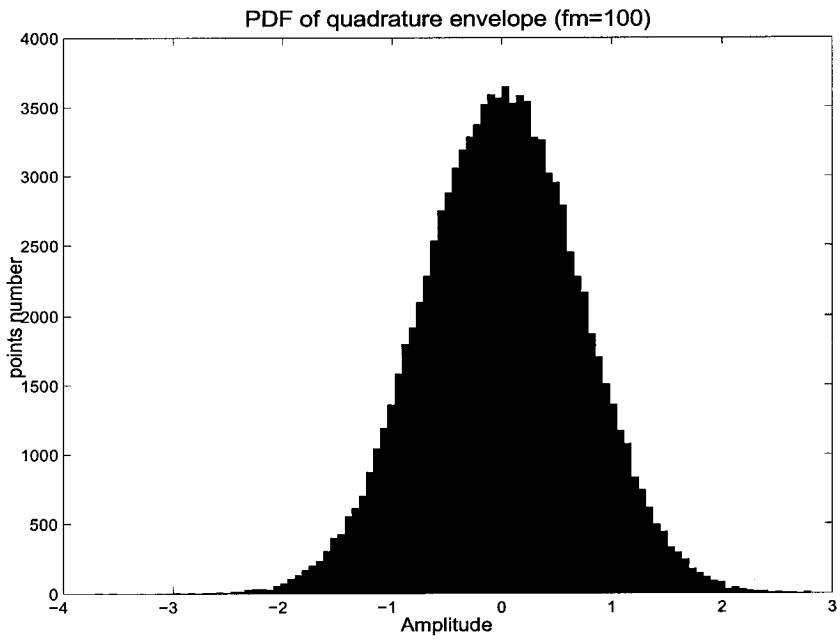

Figure 2.21: Histogram of Quadrature Component when Doppler Frequency is 100Hz

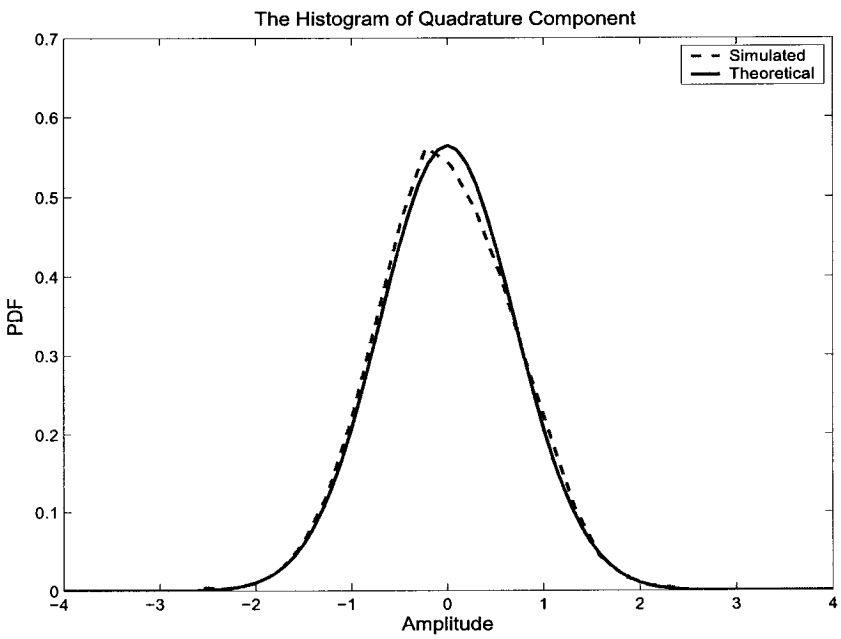

Figure 2.22: Comparison the Theoretical PDF Function with Simulated PDF Function of the Quadrature Component

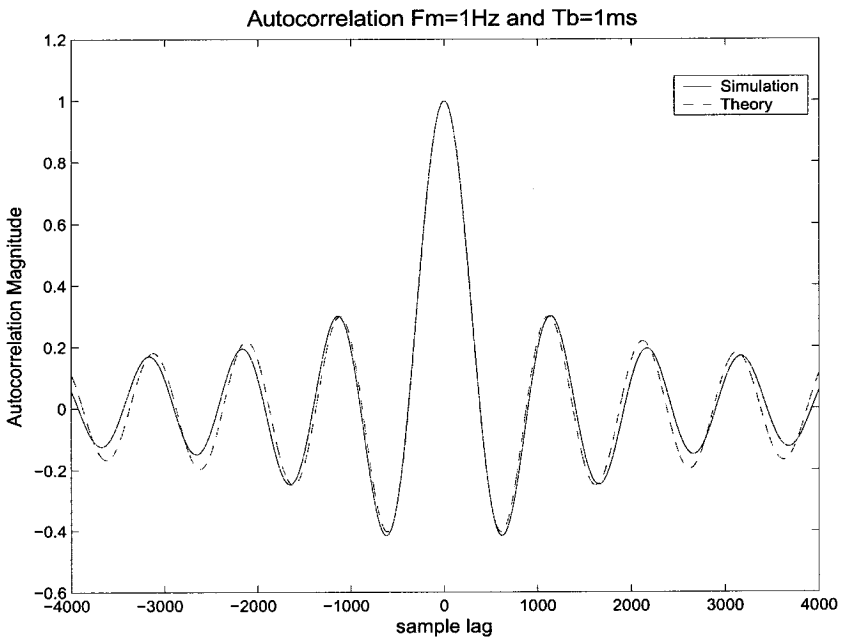

Figure 2.23: Autocorrelation of Fading Process when Doppler Frequency is 1Hz

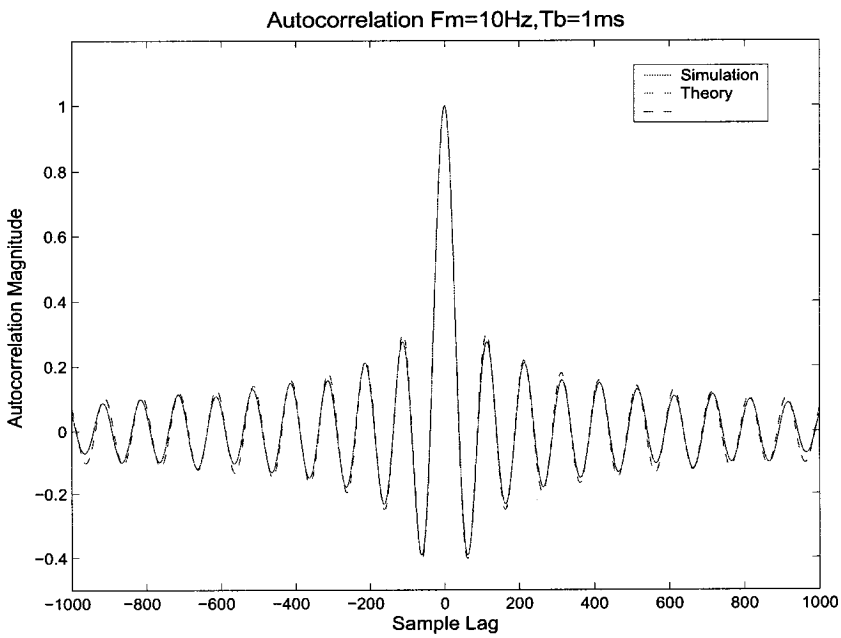

Figure 2.24: Autocorrelation of Fading Process when Doppler Frequency is 10Hz

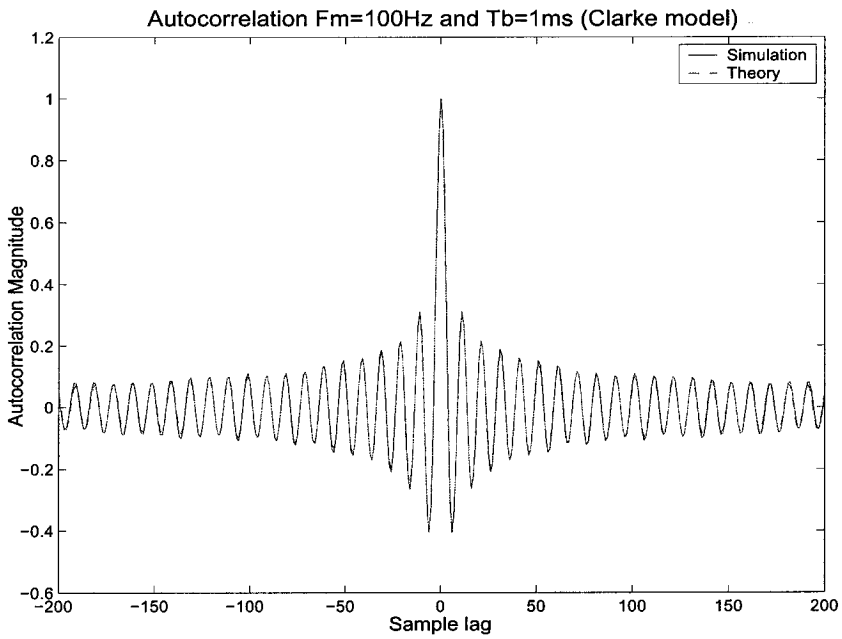

Figure 2.25: Autocorrelation of Fading Process when Doppler Frequency is 100Hz for generating the fading channel.

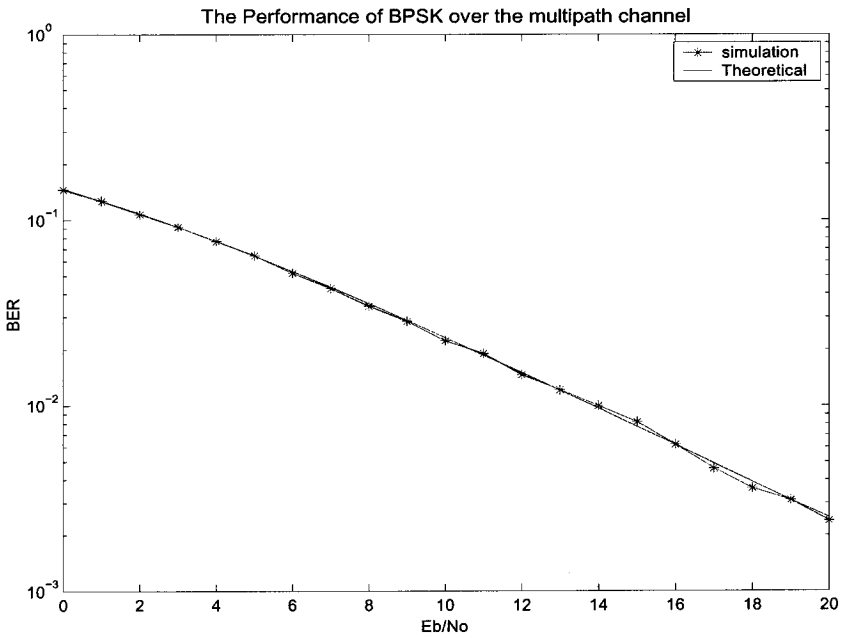

Figure 2.26: The BER Performance of BPSK in Flat Rayleigh Fading Channel when Normalized Doppler Frequency is 0.01

Chapter 3

Channel Estimation

3.1 PSAM for Single User Systems

When transmitting over a fading channel, a good estimate for complex channel gain allows us to perform coherent detection. Employing channel estimation with coherent detection improves BER performance over systems employing noncoherent detection or differential methods [23]. However, poor estimates will lead to poor BER performance of system. Therefore, it is important to obtain accurate channel estimates for coherent detection. In fading channel, using the conventional devices, such as "squaring loop" is not feasible since it is difficult to track the channel accurately since the channel varies too quickly. Thus, one of the solutions is to use the pilot symbol assisted modulation (PSAM) system [24, 25, 26]. This system doesn't change the transmitted pulse shape or peak-to-average power ratio and its implementation is very straightforward, hence it is popularly used. The block diagram of PSAM system is depicted in Figure 3.1. For the sake of simplicity, the single-user system is assumed; the multi-user system will be introduced in the next section based on single user system. In the PSAM system, the known symbols (pilots) are inserted periodically into random data sequence $b(i)$ [26]. The newly formed sequence $d(i)$ is shown in Figure

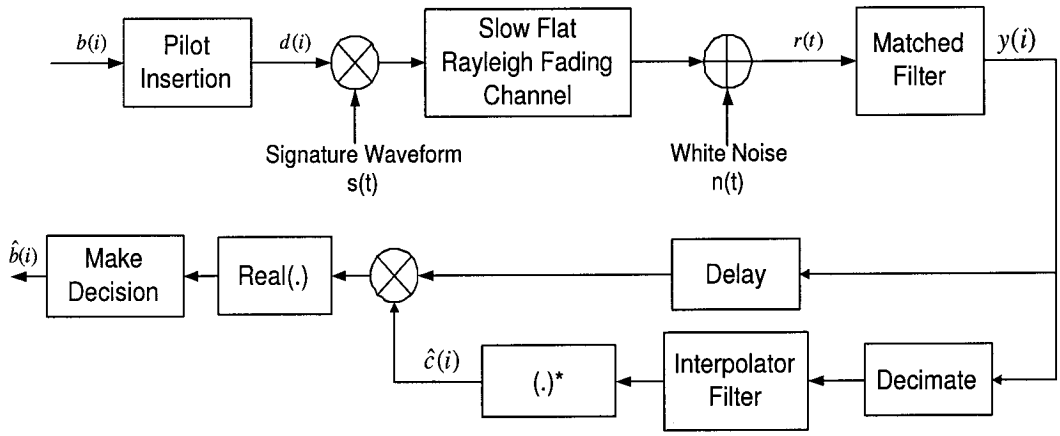

Figure 3.1: Block Diagram of a Single-user PSAM System

3.2. This sequence is formatted into frames of M symbol length. The first symbol of the frame is a pilot symbol followed by $(M-1)$ data. When the index is a multiple of M, the symbol is a pilot symbol. Otherwise, it is a data symbol. i.e.,

$$d(i) = \begin{cases} \text{data} & i \neq kM, k = 0, 1, \cdots, M \\ \text{pilot} & i = kM, k = 0, 1, \cdots, M \end{cases}$$

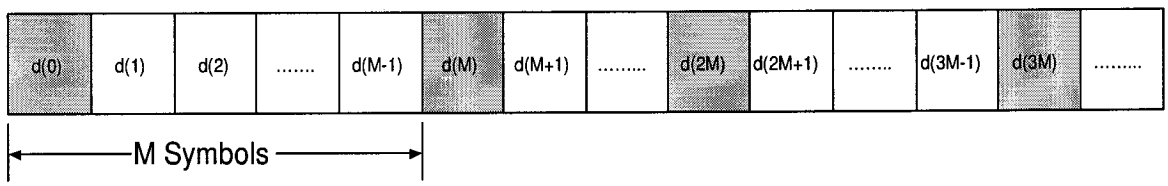

Figure 3.2: Frame Structure

The new sequence $d(i)$ is multiplied by a signature waveform $s(t)$ for spectrum spreading and the spread signal is transmitted through a slow flat Rayleigh fading channel. Hence, the received signal can be written as:

$$r(t) = A \cdot c(t) \cdot \left(\sum_{i=0}^{\infty} s(t - iT) \cdot d(i) \right) + n(t) \tag{3.1}$$

where A is the amplitude of $r(t)$, $c(t)$ is the complex fading coefficient of the channel. Its statistical properties have been described in Chapter 2. Since the channel is slow fading, we can assume $c(t) = c(iT)$. For the sake of simplicity, $c(iT)$ can be expressed as $c(i)$.

The received signal $r(t)$, is fed into a matched filter which is matched to the signature waveform $s(t)$. From Equation (2.3) in Chapter 2, the output of matched filter at iT sampling instance can be written as:

$$\begin{aligned} y(i) &= \int_{iT}^{iT+T} r(t)s(t-iT)dt \\ &= Ac(i)d(i) + n(i) \\ &= g(i)d(i) + n(i) \end{aligned} \tag{3.2}$$

Where $g(i) = Ac(i)$ is called the channel gain and $n(i)$ is the filtered noise which is defined as:

$$n(i) = \int_{iT}^{iT+T} n(t)s(t-iT)dt \tag{3.3}$$

The detected signal $y(i)$ is split into two paths as seen in Figure 3.1. The set of pilot symbols can be extracted by downsampling filter using a decimation factor of M. The extracted sequence of pilot symbols must be interpolated in order to derive a channel gain estimate $\hat{g}(i)$ for every received data symbol. Once the fading gain $\hat{g}(i)$ is obtained, the receiver forms a decision variable $z(i)$ can be obtained as follows:

$$z(i) = y(i) \cdot \hat{g}^*(i) \tag{3.4}$$

Assuming the channel estimate is perfect, that is, $\hat{g}(i) = g(i) = A \cdot c(i)$. Equation

(3.4) becomes:

$$z(i) = y(i) \cdot g^*(i) = (A \cdot c(i)d(i) + n(i)) \cdot (A \cdot c^*(i)) = A^2|c(i)|^2 d(i) + A \cdot n(i)c^*(i) \quad (3.5)$$

By ignoring the existence of $n(i)$, the real part of $z(i)$ should be greater than zero when $d(i)$ is "+1"; conversely, it should be less than zero when $d(i)$ is "-1". Hence, the decision rule is made as follow: If the real part of $z(i)$ is positive, the hard decision of $\hat{b}(i)$ is made as 1, otherwise, $\hat{b}(i)$ is made as -1, i.e.,

$$\hat{b}(i) = \begin{cases} 1 & \text{if } Re\{z(i)\} = 1 \\ -1 & \text{if } Re\{z(i)\} = -1 \end{cases}$$

In terms of the above analysis, one of the key problems of the system is how to obtain an accurate channel gain estimate $\hat{g}(i)$ from the received pilot symbols. It has been well documented that most of the estimators use linear interpolators. That is, the channel gain estimate can be obtained by the weighted sum of a few nearest pilot symbols [27]. Also, the interpolator can be illustrated as a transversal FIR filter, as shown in Figure 3.3. The inputs to the filter are pilots and the outputs are the estimated channel gains on the data signaling intervals. According to the figure, the channel gain estimate can be written as:

$$\hat{g}(i) = h_{-a}(i) \cdot y(-aM + xM) + h_{-a+1}(i) \cdot y(-aM + xM + M) + \cdots + h_b(i) \cdot y(bM + xM) \quad (3.6)$$

where $x = \lfloor \frac{i}{M} \rfloor$ denotes the integral part of $\frac{i}{M}$. The weighting coefficients: $h_{-a}(i)$, $h_{-a+1}(i), \cdots, h_b(i)$, are the coefficients of the transversal filter with a size of $(a+b+1)$.

It is more convenient to write Equation (3.6) in the matrix form:

$$\hat{g}(i) = \mathbf{H}(i) \cdot \mathbf{P} \quad (3.7)$$

where $\mathbf{H}(i)$ is the coefficient vector of the transversal filter.

$$\mathbf{H}(i) = [h_{-a}(i), h_{-a+1}(i), \cdots, h_b(i)]$$

$\mathbf{P}$ is a column vector representing the $(a + b + 1)$ pilot symbols that closest to the i position.

$$\mathbf{P} = [y(-aM + xM), y(-aM + xM + M), \cdots, y(bM + xM)]^T$$

where $[\cdot]^T$ denotes matrix transposition.

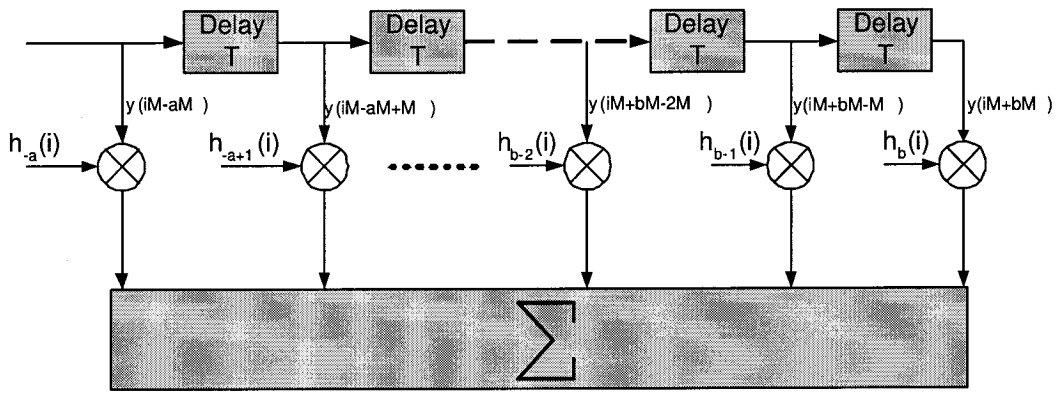

Figure 3.3: Interpolator Filter

In the previous PSAM system, $\mathbf{H}(i)$ is often obtained by either a low pass interpolator filter or an approximate Gaussian filter [25, 24]. If the temporal correlation of the fading process is known, Wiener interpolator filter is the optimal filter. Further, since the fading process can be modelled by an Autoregressive (AR) model, a Kalman filter can carry out the estimation recursively, which is computational efficient. If the statistical properties of fading channel are unknown, an adaptive filter can be used to calculate the fading gain. A popular adaptive algorithm is Least Mean Square (LMS) or Recursively Least Squares (RLS), which is used to minimize the prediction error.

In this thesis, we employ the optimal Wiener filter to estimate the channel gain, since it performs better than other low pass filters. In the following, the theory of optimal Wiener filter will be introduced:

Optimal Wiener filter is designed to minimize the variance of estimation error σ_e^2 and it can be formulated as follows [27]:

$$\begin{aligned}
\sigma_e^2 &= E[(g(i) - \hat{g}(i))^2] \\
&= E[|g(i) - \mathbf{H}(i)\mathbf{P}|^2] \\
&= E[(g(i) - \mathbf{H}(i)\mathbf{P})(g^*(i) - \mathbf{P}^H\mathbf{H}(i)^H)] \\
&= E[g(i)g^*(i) - \mathbf{H}(i)\mathbf{P}g^*(i) - g(i)\mathbf{P}^H\mathbf{H}(i)^H + \mathbf{H}(i)\mathbf{P}\mathbf{P}^H\mathbf{H}(i)^H] \\
&= \sigma_g^2 - \mathbf{H}(i)\mathbf{\Phi}_{yg}(i) - \mathbf{\Phi}_{gy}(i)\mathbf{H}(i)^H + \mathbf{H}(i)\mathbf{\Phi}_{yy}\mathbf{H}(i)^H \qquad (3.8)
\end{aligned}$$

where σ_g^2 is the variance of $g(i)$, $\mathbf{\Phi}_{yy}$ is the autocorrelation matrix for the noisy channel gain estimates from the received pilot symbols, $[\cdot]^H$ denotes Hermitan transposition of the matrix.

$$\mathbf{\Phi}_{yy} = E[\mathbf{P}\mathbf{P}^{\mathbf{H}}] =$$

$$\begin{bmatrix}
E[y(-aM+xM)y^*(-aM+xM)] & \cdots & E[y(-aM+xM)y^*(bM+xM)] \\
E[y(-aM+xM+M)y^*(-aM+xM) & \cdots & E[y(-aM+xM+M)y^*(bM+xM)] \\
\vdots & \ddots & \vdots \\
E[y(bM+xM)y^*(-aM+xM)] & \cdots & E[y(bM+xM)y^*(bM+xM)]
\end{bmatrix}$$

Where, the (p,q)-th component in $\mathbf{\Phi}_{yy}$ is:

$$\begin{aligned}
\mathbf{\Phi}_{yy}(p,q) &= E[y(xM - aM + (p-1)M) \cdot y^*(xM - aM + (q-1)M)] \\
&= E[(g(xM - aM + (p-1)M) + n(xM - aM + (p-1)M)) \\
&\quad \cdot (g^*(xM - aM + (q-1)M) + n^*(xM - aM + (q-1)M))]
\end{aligned}$$

$$= \sigma_g^2 J_0(2\pi f_d(p-q)M) + N_0\delta((p-q)M) \tag{3.9}$$

When $p = q$, Equation (3.9) becomes:

$$\mathbf{\Phi}_{yy}(p,p) = \sigma_g^2 + N_0$$

$\mathbf{\Phi}_{gy}$ is the crosscorrelation vector between channel gain $g(i)$ and channel gain of pilots $\mathbf{P}$. The w-th component in $\mathbf{\Phi}_{gy}$ can be written as

$$\begin{aligned}
\mathbf{\Phi}_{gy}(w) &= E[g(i)y^*(-aM + xM + (w-1)M)] \\
&= E[g(i)(g^*(-aM + xM + (w-1)M) + n^*(-aM + xM + (w-1)M))] \\
&= E[g(i)g^*(-aM + xM + (w-1)M)] + E[g(i)n^*(-aM + xM + (w-1)M))] \\
&= J_0(2\pi f_d(i + aM - xM - (w-1)M))
\end{aligned} \tag{3.10}$$

$\mathbf{H}(i)$ can be obtained by solving the following which is used to minimize σ_e^2:

$$\frac{\partial \sigma_e^2}{\partial h_n(i)} = 0 \qquad\qquad n = -a, -a+1, \ldots, b \tag{3.11}$$

Leading to

$$\mathbf{H}(i)\mathbf{\Phi}_{yy} = \mathbf{\Phi}_{gy}(i) \tag{3.12}$$

which is the well known normal equation.

Assuming $\mathbf{\Phi}_{yy}$ is nonsingular, $\mathbf{H}(i)$ can be obtained by multiplying $\mathbf{\Phi}_{yy}^{-1}$ on both sides, thus:

$$\mathbf{H}(i) = \mathbf{\Phi}_{yy}^{-1}\mathbf{\Phi}_{gy}(i) \tag{3.13}$$

By inserting the Equation (3.13) into (3.7), $\hat{g}(i)$ is obtained as:

$$\hat{g}(i) = \mathbf{\Phi}_{yy}^{-1}\mathbf{\Phi}_{gy}(i)\mathbf{P} \tag{3.14}$$

Also, the corresponding mean square error is:

$$\sigma_e^2(i) = \sigma_g^2 - \mathbf{\Phi}_{gy}(i)\mathbf{\Phi}_{yy}^{-1}\mathbf{\Phi}_{yg}(i) \tag{3.15}$$

3.2 The Performance of PSAM in Single User System

Employing the Wiener interpolator filter, the simulation results for the single-user channel estimation are presented in this section using a frame size of 5 and a filter size of 11.

Figure 3.4 is the comparison of the estimated in-phase component of channel gain with actual in-phase component.

Figure 3.5 is the comparison of the estimated quadrature component of channel gain with actual quardrature component.

Figure 3.6 is the comparison of the estimated envelope of channel gain with actual channel amplitude.

Figure 3.7 is the comparison of the estimated phase of channel gain with actual phase.

We can see from these figures that the estimates curves are very close to the actual values. However, most of errors occur in the peak points since they are the turning points from one tendency to another tendency.

The BER performance with estimated channel gain in flat Rayleigh fading channel is presented in Figure 3.8. We can see from figure that there is around 1dB difference between the performance of the system with ideal channel gain estimates and pilot based estimated channel gain. This is due mainly to the fact that some of the signal power is allocated to the pilots, therefore, there is energy loss to the symbols. In the

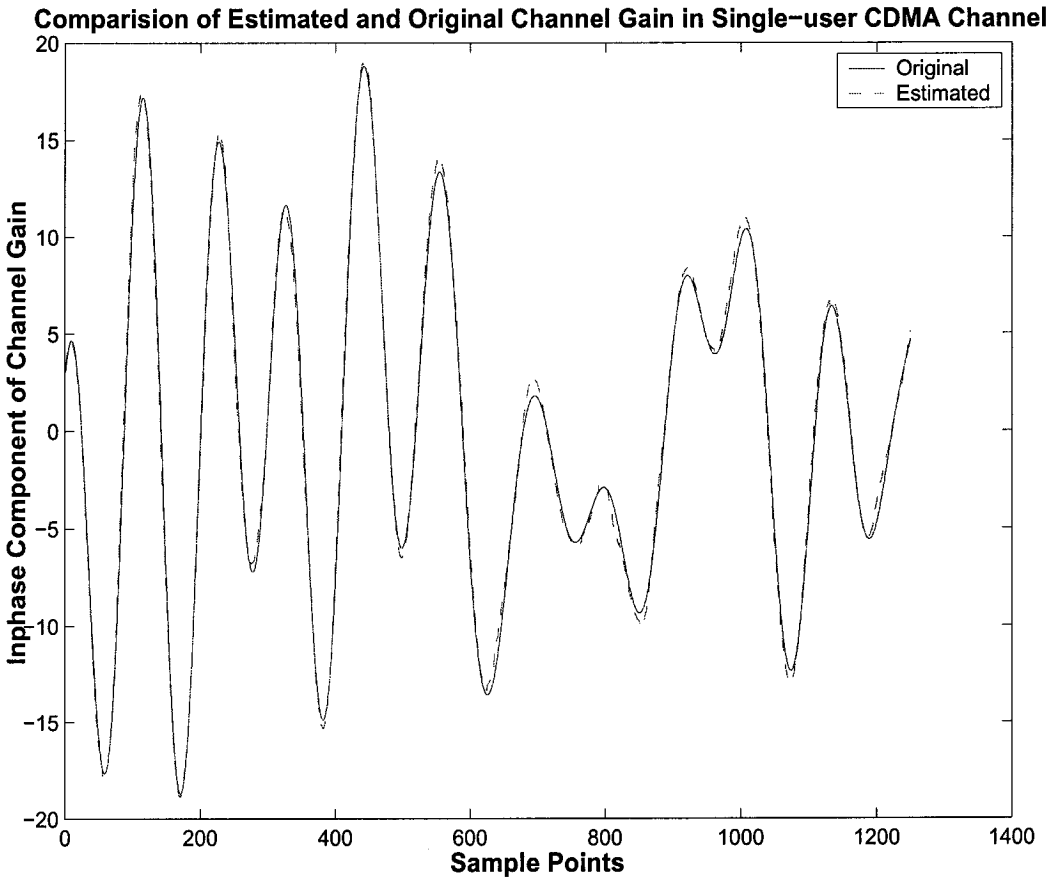

Figure 3.4: Comparison of Original and Estimated Inphase Component of Channel Gain in a Single-user CDMA System with a signal to noise ratio of 20dB (Frame size = 5, Interpolator size = 11 and Normalized Doppler Frequency = 0.01)

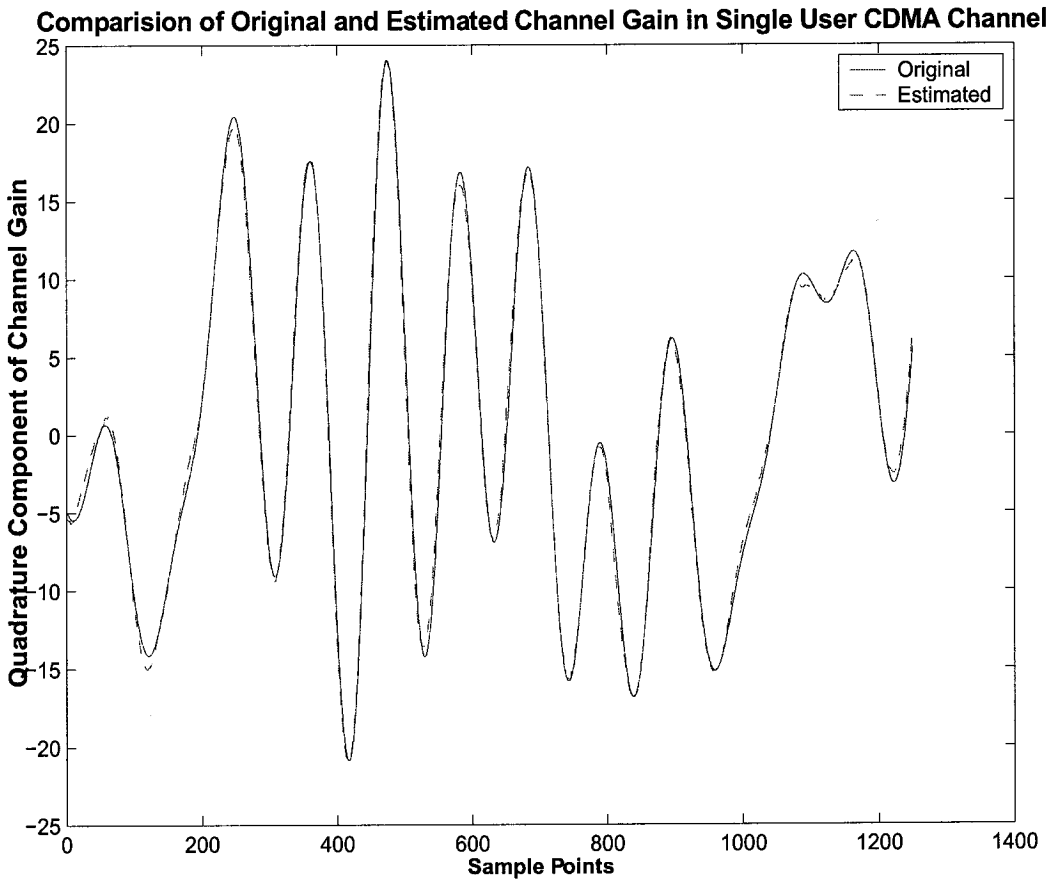

Figure 3.5: Comparison of Original and Estimated Quadrature Component of Channel Gain in a Single-user CDMA System with a signal to noise ratio of 20dB (Frame size = 5, Interpolator size = 11 and Normalized Doppler Frequency = 0.01)

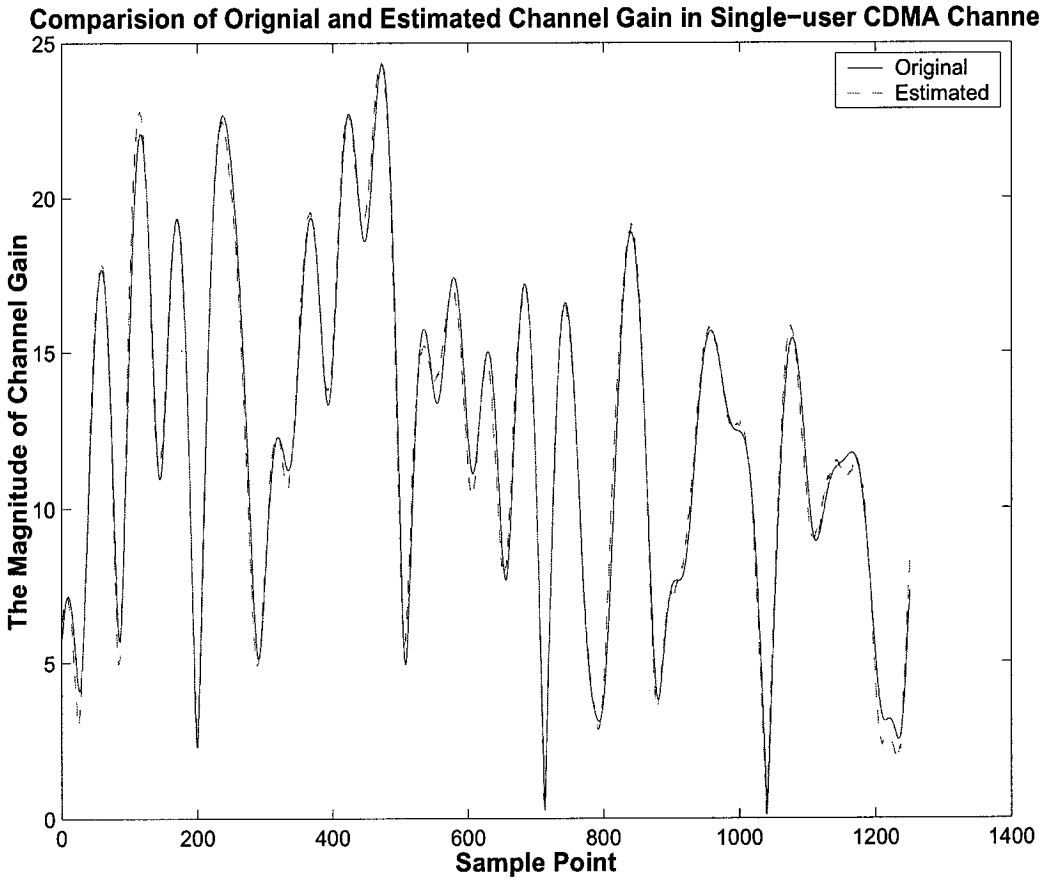

Figure 3.6: Comparison of Original and Estimated Envelope of the Channel Gain in a Single-user CDMA Channel System with a signal to noise ratio of 20dB (Frame size = 5, Interpolator size = 11 and Normalized Doppler Frequency = 0.01)

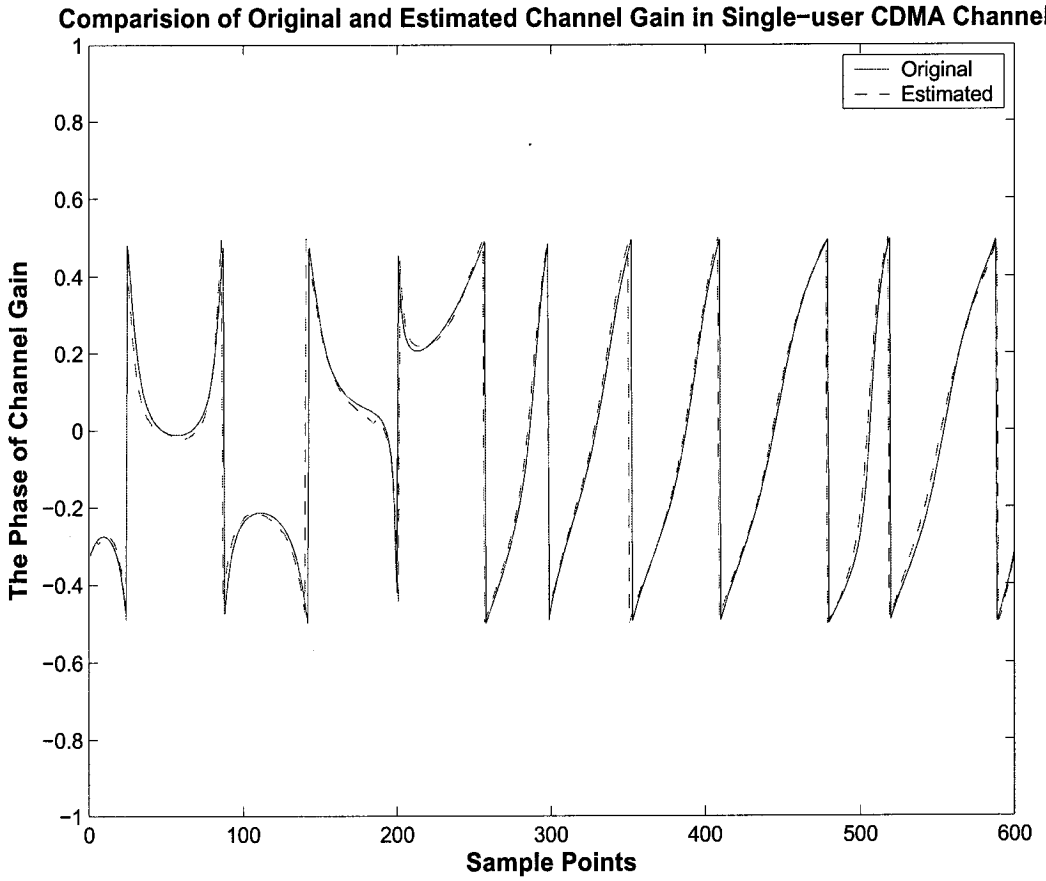

Figure 3.7: Comparison of Original and Estimated Phase of the Channel Gain in a Single-user CDMA System with a signal to noise ratio of 20dB (Frame size = 5, Interpolator size = 11 and Normalized Doppler Frequency = 0.01)

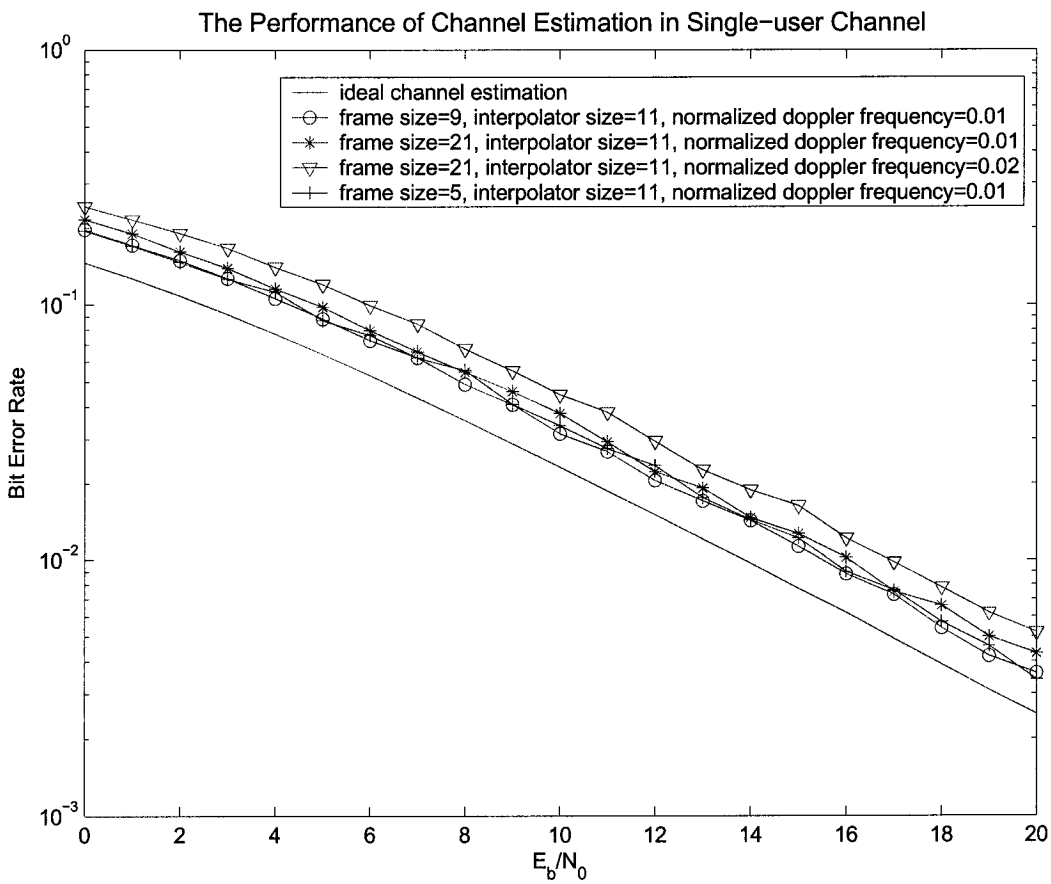

Figure 3.8: The BER Performance of Single-user CDMA Systems in Rayleigh Fading Channel with Estimated Channel Gains and a Spreading Gain of 60

figure, the circle line is the performance of Wiener interpolator filter with frame size 9 and normalized Doppler frequency 0.01, the star line is the performance of frame size 21 and normalized Doppler frequency 0.01, the triangle line is the performance of frame size 21 and normalized Doppler frequency 0.02. The cross line represents the performance of frame size of 5 and normalized Doppler frequency of 0.01. In the figure, the circle line is slightly better than star line because it uses a smaller frame size, which can track the channel gain more accurately. The reason why the triangle line performs worse than the star line is that its channel gain (normalized Doppler frequency is 0.01) varies faster than star line (Doppler frequency is 0.02). Therefore, the filter for the latter case has more difficults tracking the variation of channel.

3.3 PSAM for Multi-user Systems

In previous sections, we discussed PSAM in single user systems. In this section, we will extend it to the quasi-synchronous multi-user systems, whose delay is less than symbol period T. Although the frames are coarsely synchronized, the transmissions of different users are not symbol synchronized. This is shown in Figure 3.9.

According to last section's analysis, if the autocorrelation matrix $\mathbf{\Phi}_{yy}$ and cross-correlation $\mathbf{\Phi}_{gy}$ are known, the channel gain can be estimated in terms of Equation (3.14). The autocorrelation and crosscorrelation under the multi-user case is computed as follows based on Equation (2.4) in Chapter 2:

$$\begin{aligned} y_k(iM) &= A_k c_k(iM) b_k(iM) + \sum_{p=1}^{k-1} A_p c_p(iM) b_p(iM) \rho_{pk} \\ &\quad + \sum_{p=1}^{k-1} A_p c_p(iM+1) b_p(iM+1) \rho_{kp} + \sum_{p=k+1}^{K} A_p c_p iM b_p(iM) \rho_{kp} \end{aligned}$$

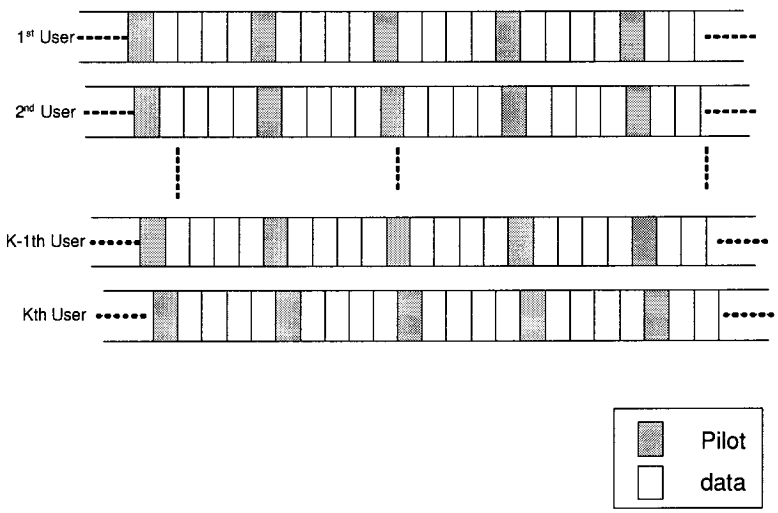

Figure 3.9: Pilot Insertion in Multiuser CDMA Systems

$$+\sum_{p=k+1}^{K} A_p c_p(iM-1)b_p(iM-1)\rho_{pk} + n_k(iM) \tag{3.16}$$

$$\begin{aligned} y_k(jM) &= A_k c_k(jM)b_k(jM) + \sum_{p=1}^{k-1} A_p c_p(jM)b_p(jM)\rho_{pk} \\ &+ \sum_{p=1}^{k-1} A_p c_p(jM+1)b_p(jM+1)\rho_{kp} + \sum_{p=k+1}^{K} A_p c_p jM b_p(jM)\rho_{kp} \\ &+ \sum_{p=k+1}^{K} A_p c_p(jM-1)b_p jM-1\rho_{pk} + n_k(jM) \end{aligned} \tag{3.17}$$

Therefore, the (i,j)-th component in autocorrelation matrix $\mathbf{\Phi}_{yy}$ is computed as follows:

$$\begin{aligned} E[y_k(iM)y_k(jM)] &= J_0(2\pi(i-j)T) + \sum_{p=1}^{k-1} J_0(2\pi(i-j)T)\rho_{pk}^2 \\ &+ \sum_{p=1}^{k-1} \delta_{i-j} J_0(2\pi(i-j)T)\rho_{kp}^2 + \sum_{p=k+1}^{K} J_0(2\pi(i-j)T)\rho_{kp}^2 \\ &+ \sum_{p=k+1}^{K} \delta i - j J_0(2\pi(i-j)T)\rho_{pk}^2 + N_0\delta(i-j) \end{aligned} \tag{3.18}$$

So,

$$E[y_k(iM)y_k(jM) = \begin{cases} J_0(2\pi(i-j)T)(1+\sum_{p=1}^{K}\rho_{pk}^2)+\sum_{p=1}^{K}\rho_{kp}^2] + N_0 & \text{if } i=j \\ J_0(2\pi(i-j)T)(1+\sum_{p=1}^{k-1}\rho_{pk}^2+\sum_{p=k+1}^{K}\rho_{kp}^2) & \text{if } i\neq j \end{cases} \tag{3.19}$$

The w-th component in $\mathbf{\Phi}_{gy}$ is same as in the single-user case.

Hence, the estimation can be made according to Equation (3.19) and (3.10).

However, in multi-user channel, since the received pilots and data have MAI components, it makes $\mathbf{\Phi}_{yy}$ and $\mathbf{\Phi}_{gy}$ complicated to calculate and the performance of estimation is not as accurate. To solve this problem, we decorrelate the pilots prior to doing the estimation [28, 29]:

To decorrelate the pilots and data, the output matrix of matched filters $\mathbf{Y}$ is multiplied by user's signature sequence autocorrelation matrix $\mathbf{R}^{-1}$. By doing this, the correlations between the users' pilots can be perfectly decoupled. As a result, the same algorithm of Wiener filter for single-user can be applied to every user. A better estimate performance is obtained.

3.4 The Performance of PSAM in Multi-user Systems

The simulation of the performance of Wiener interpolator filter in asychronous multi-user CDMA systems is carried out under the following conditions: spreading gain = 60, frame size=5, insertion rate = 0.8, interpolator filter size = 11 and the normalized Doppler frequency = 0.01. Also for the comparison purpose, the simulation is performed with decorrelator and without decorrelator respectively.

Figure 3.10 and 3.11 present the inphase and quadratre components respectively when the number of user is 3;

Figure 3.12 and 3.13 present the inphase and quadratre components respectively when the number of user is 10;

Figure 3.14 and 3.15 present the inphase and quadratre components respectively when the number of user is 20;

Figure 3.16 and 3.17 present the inphase and quadratre components respectively when the number of user is 30;

Figure 3.18 and 3.19 present the inphase and quadratre components respectively when the number of user is 40;

It is obvious from the figures that the simulation with decorrelator outperforms the simulation without decorrelator, which is referred to as"matched filter" in the legend. When the number of user is not too large, 3 users, for example, the performance of the system without decorrelator is similar to that with decorrelator, and both of them can obtain a very close channel gain estimate compared to the original values. As the number of user increases, the simulation with decorrelator can still reach a close performance to the theoretical values. However, the simulation without decorrelator starts deviating from the theoretical values.

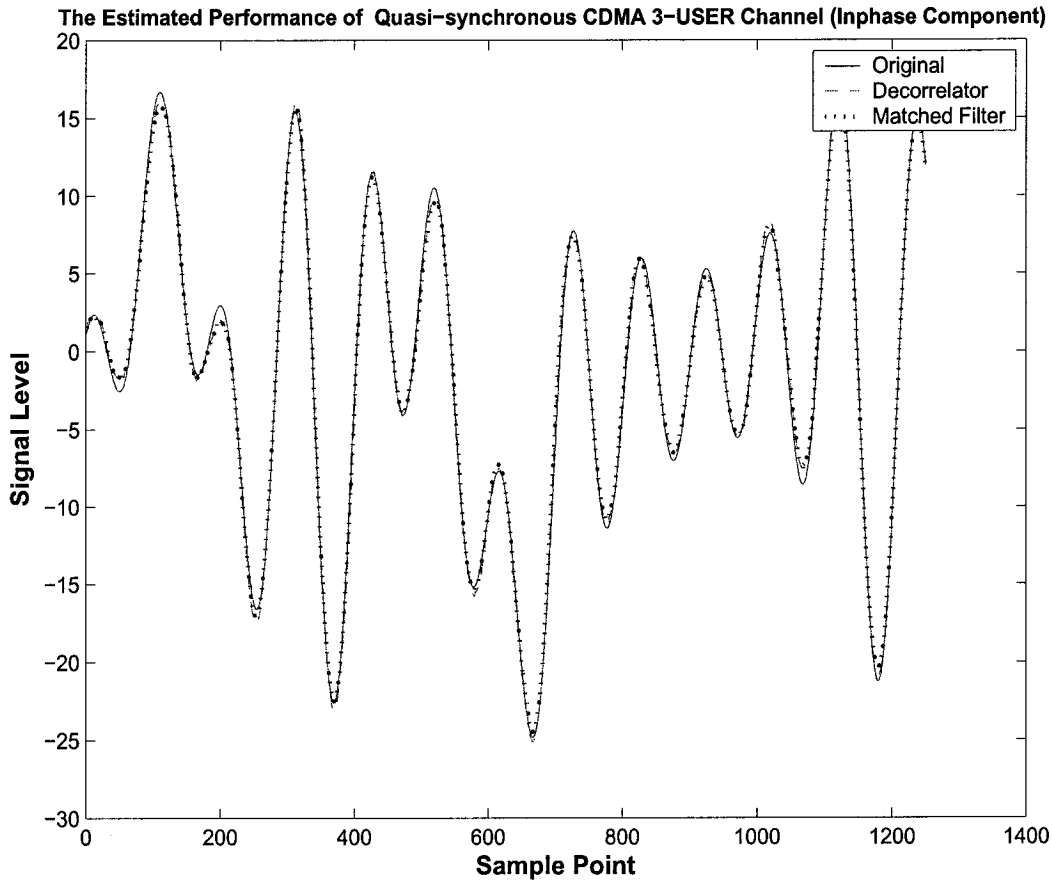

Figure 3.10: Inphase Component Estimation Performance for a 3-User quasi-synchronous CDMA System with a Spreading Gain of 60 (Frame size = 5, Interpolator size = 11 and Normalized Doppler Frequency = 0.01)

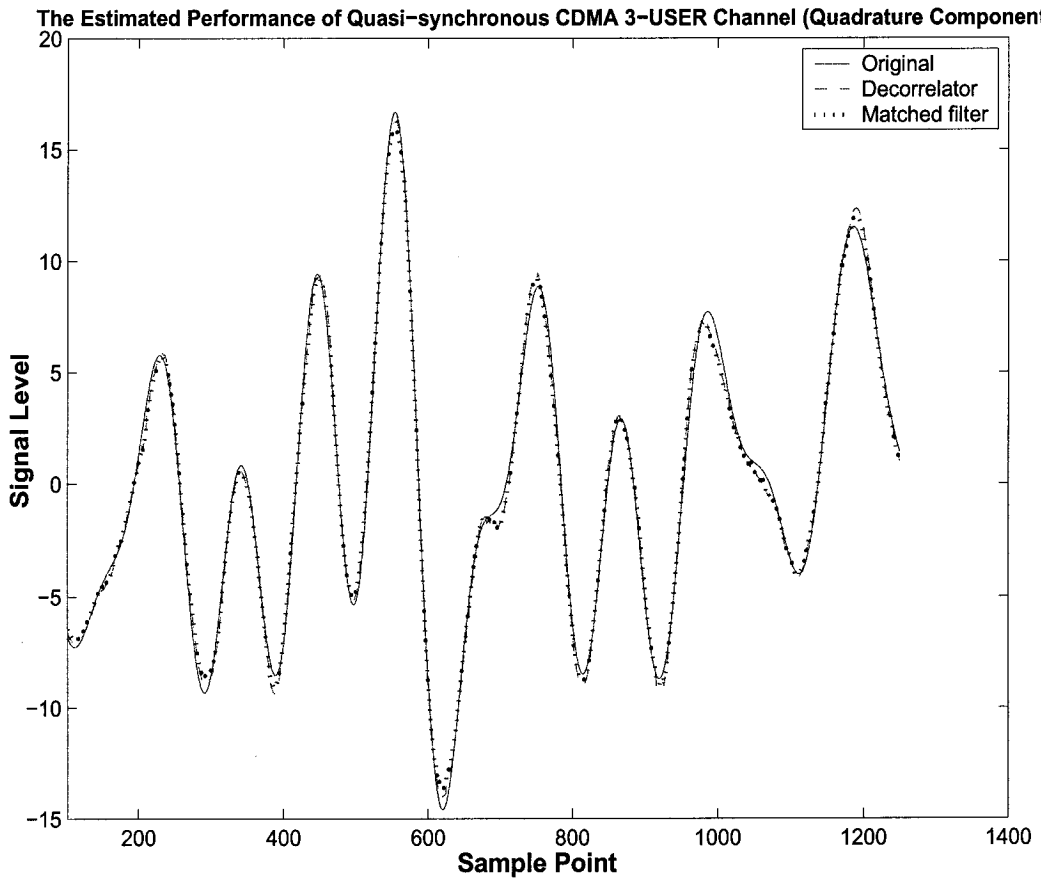

Figure 3.11: Quadrature Component Estimation Performance for a 3-User quasi-synchronous CDMA System with a Spreading Gain of 60 (Frame size = 5, Interpolator size = 11 and Normalized Doppler Frequency = 0.01)

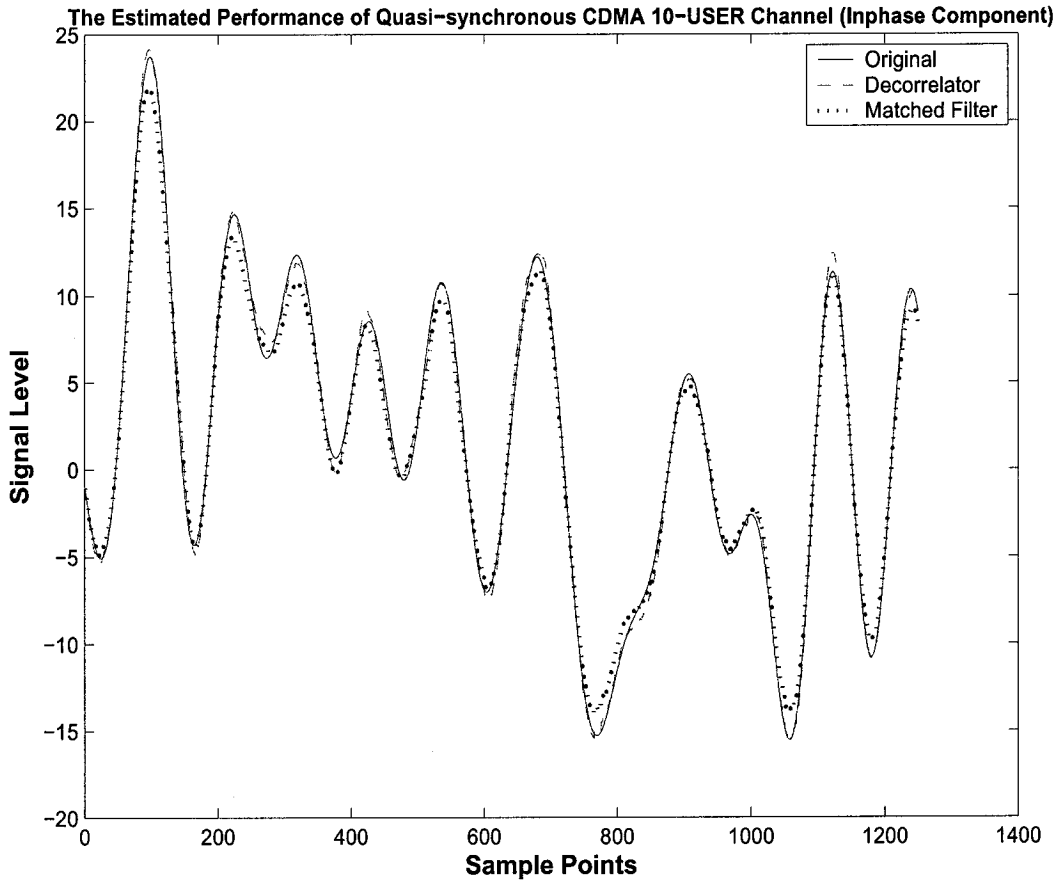

Figure 3.12: Inphase Component Estimation Performance for a 10-User quasi-synchronous CDMA System with a Spreading Gain of 60 (Frame size = 5, Interpolator size = 11 and Normalized Doppler Frequency = 0.01)

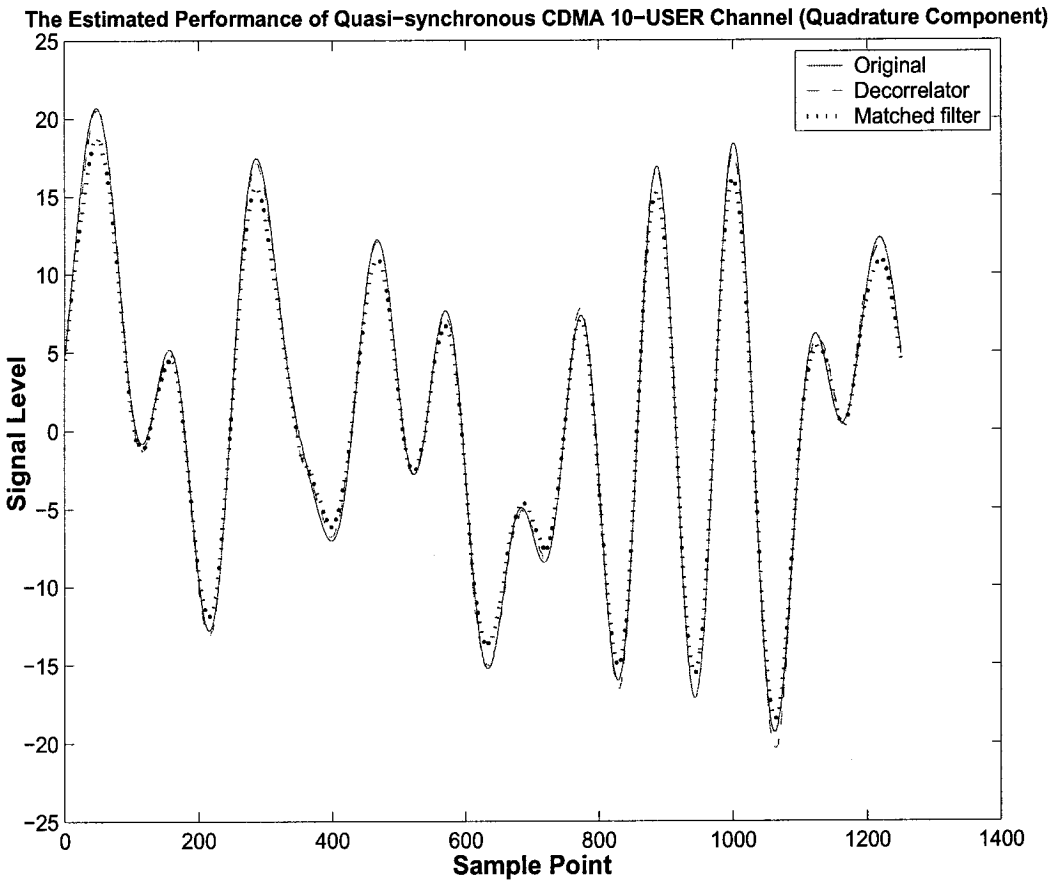

Figure 3.13: Quadrature Component Estimation Performance for a 10-User quasi-synchronous CDMA System with a Spreading Gain of 60 (Frame size = 5, Interpolator size = 11 and Normalized Doppler Frequency = 0.01)

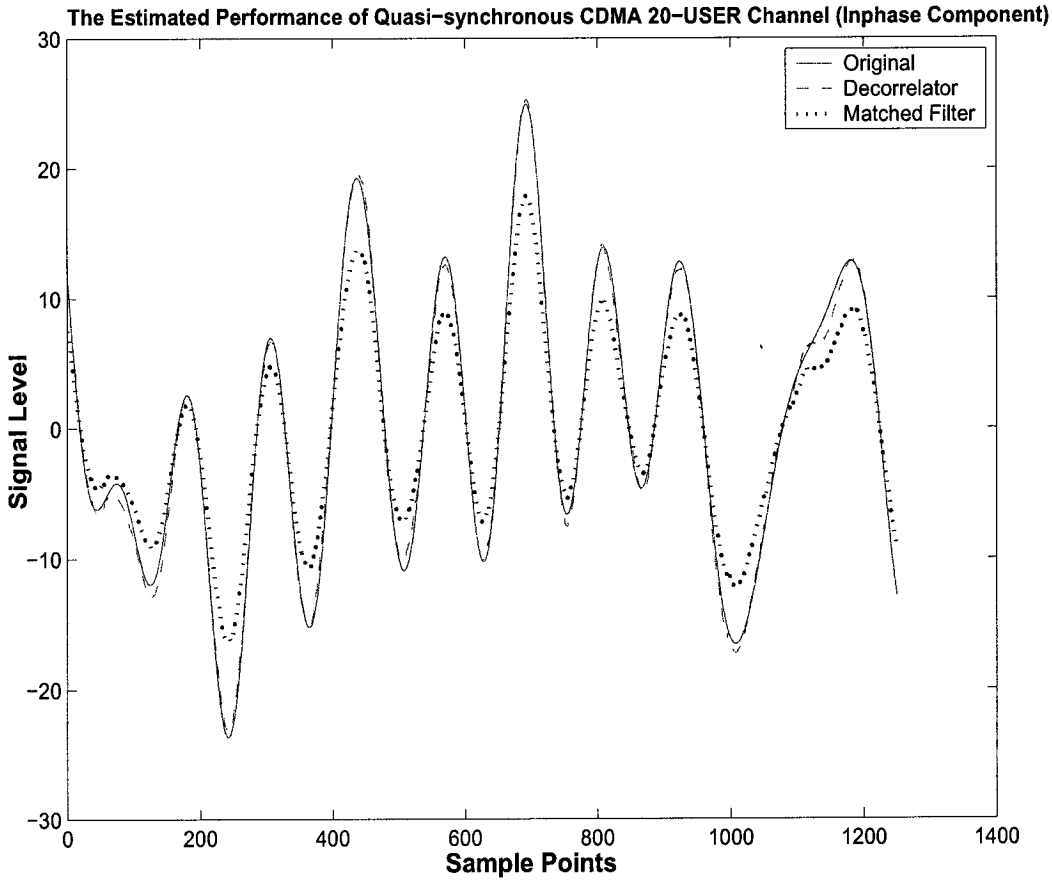

Figure 3.14: Inphase Component Estimation Performance for a 20-User quasi-synchronous CDMA System with a Spreading Gain of 60 (Frame size = 5, Interpolator size = 11 and Normalized Doppler Frequency = 0.01)

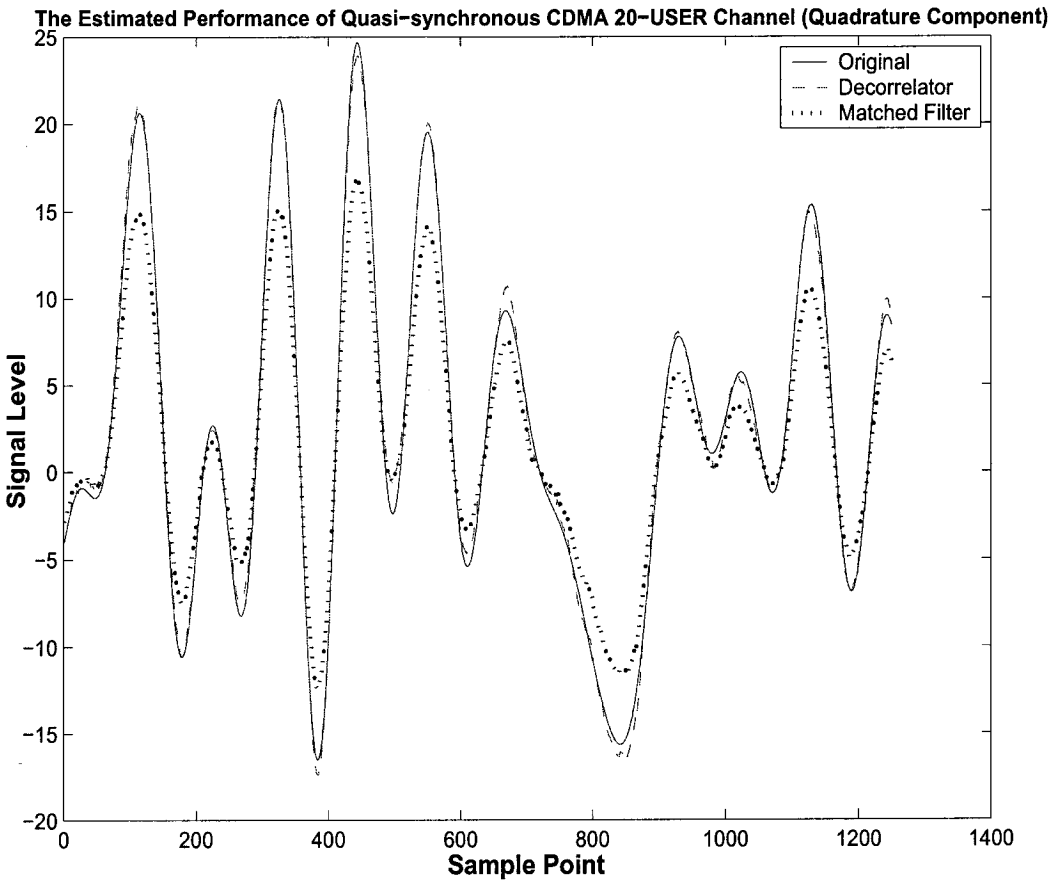

Figure 3.15: Quadrature Component Estimation Performance for a 20-User quasi-synchronous CDMA System with a Spreading Gain of 60 (Frame size = 5, Interpolator size = 11 and Normalized Doppler Frequency = 0.01)

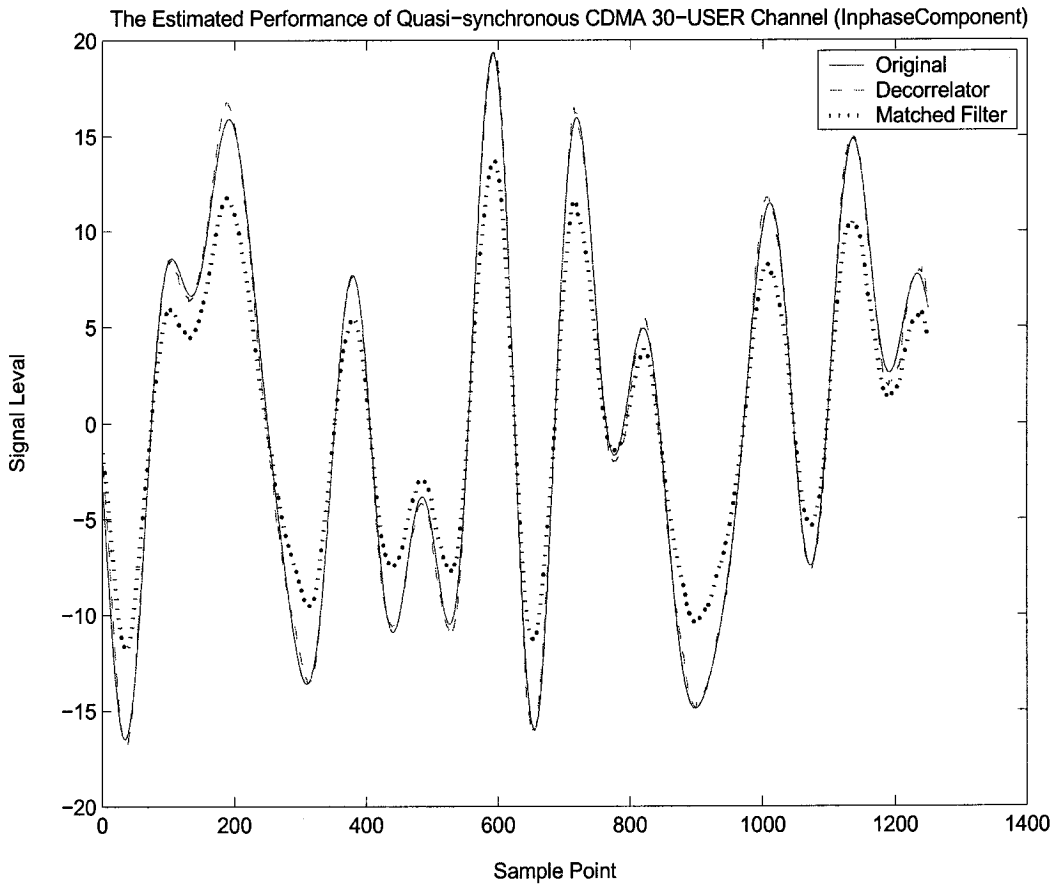

Figure 3.16: Inphase Component Estimation Performance for a 30-User quasi-synchronous CDMA System with a Spreading Gain of 60 (Frame size = 5, Interpolator size = 11 and Normalized Doppler Frequency = 0.01)

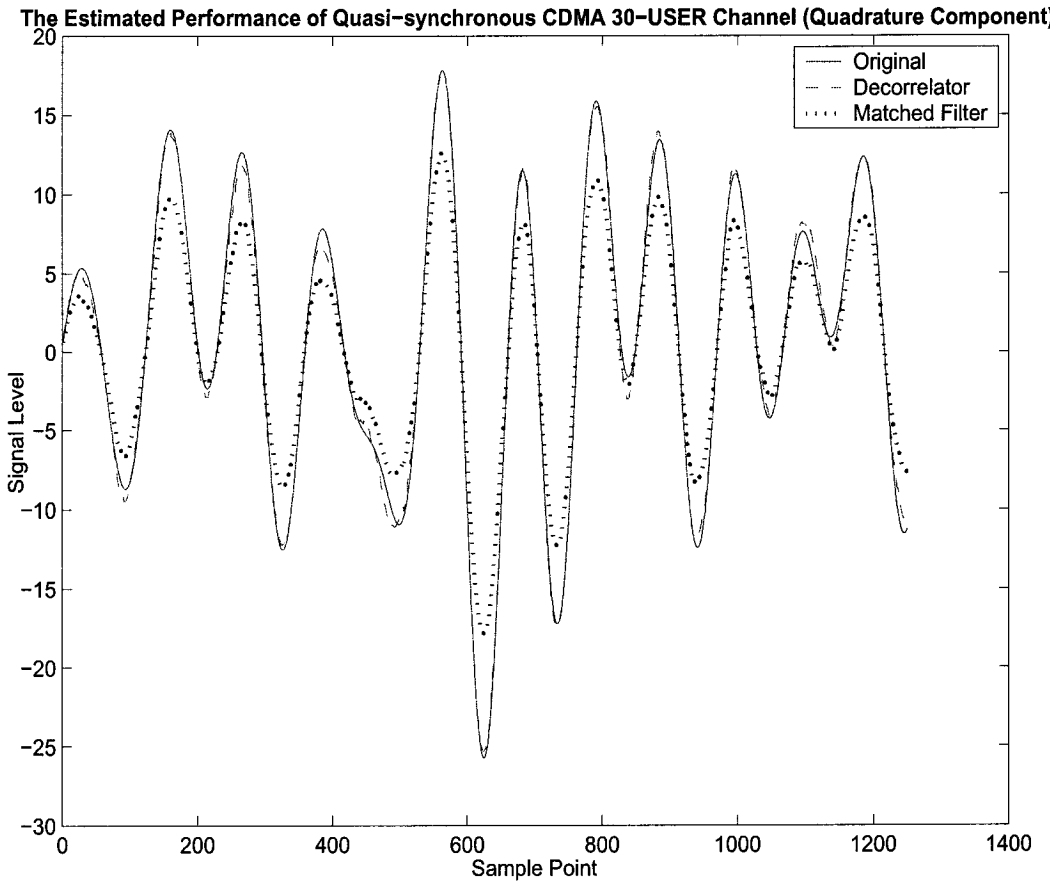

Figure 3.17: Quadrature Component Estimation Performance for a 30-User quasi-synchronous CDMA System with a Spreading Gain of 60 (Frame size = 5, Interpolator size = 11 and Normalized Doppler Frequency = 0.01)

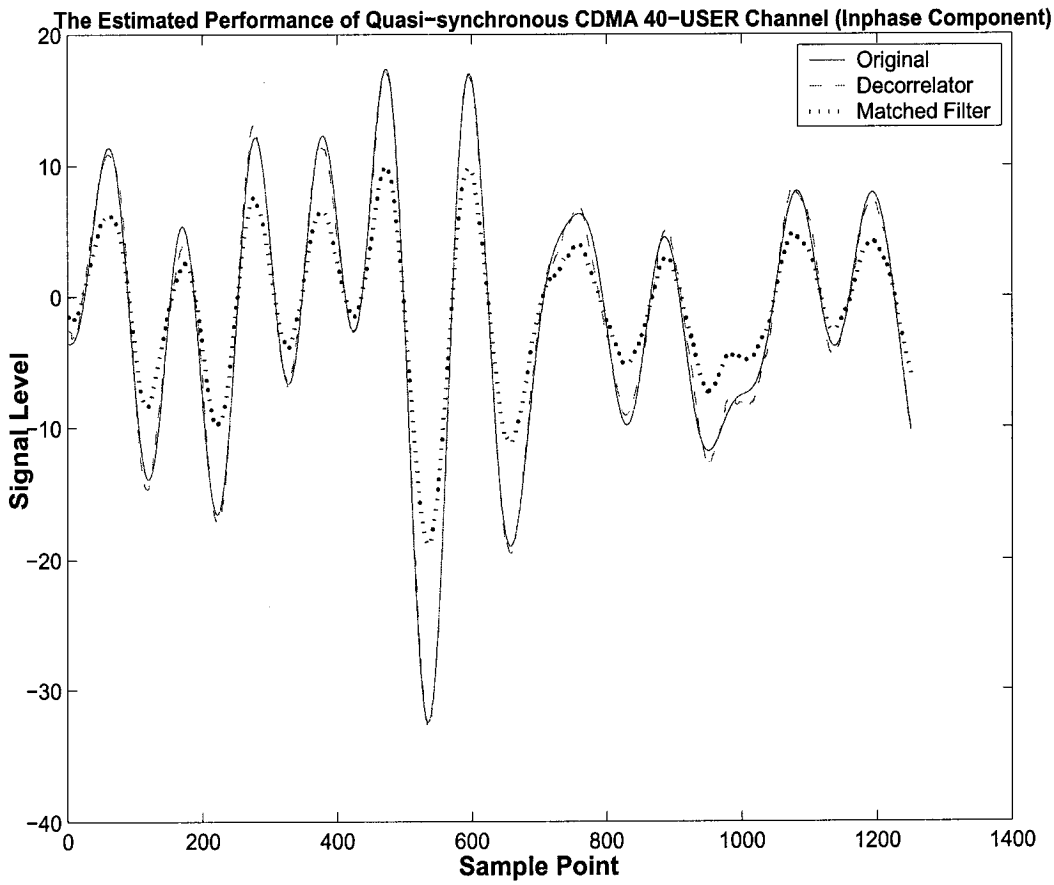

Figure 3.18: Inphase Component Estimation Performance for a 40-User quasi-synchronous CDMA System with a Spreading Gain of 60 (Frame size = 5, Interpolator size = 11 and Normalized Doppler Frequency = 0.01)

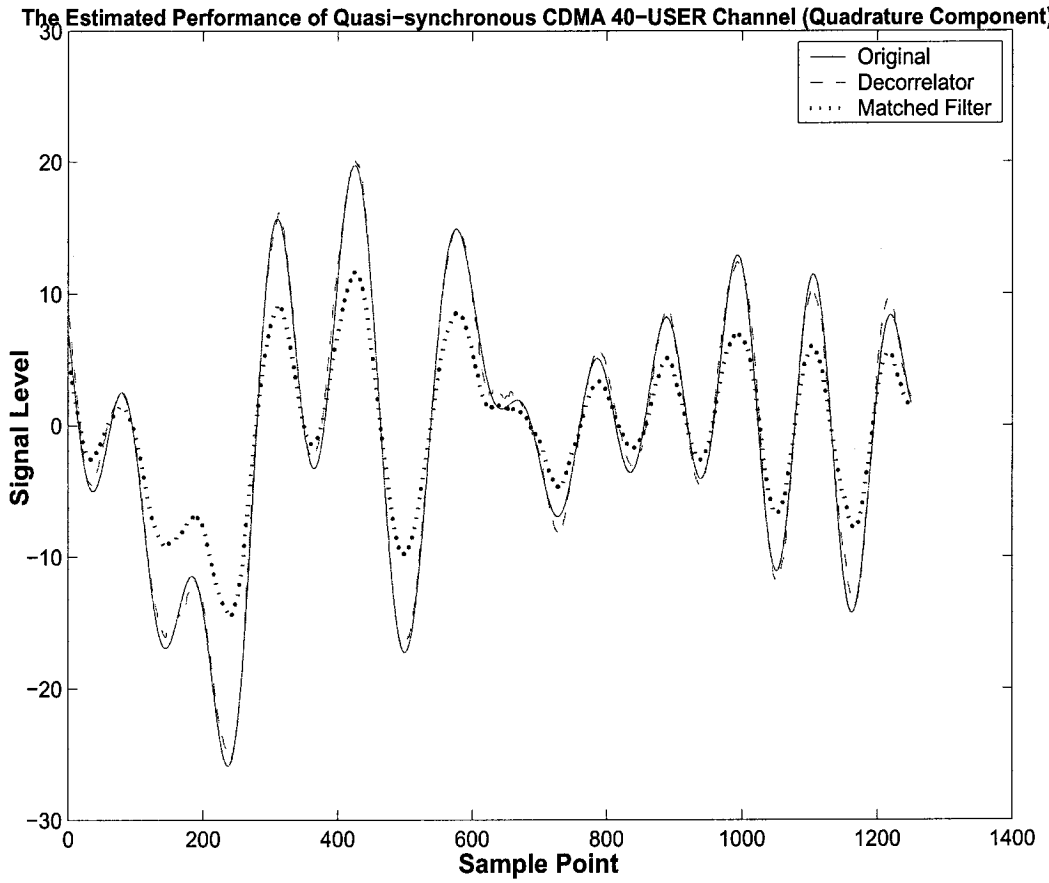

Figure 3.19: Quadrature Component Estimation Performance for a 40-User quasi-synchronous CDMA System with a Spreading Gain of 60 (Frame size = 5, Interpolator size = 11 and Normalized Doppler Frequency = 0.01)

Chapter 4

Selective Multistage Multi-user Detection

4.1 Selective Multistage Detection

Selective multistage algorithm is a modified multistage multi-user detection algorithm. This algorithm applied to a CDMA system in an AWGN channel is first proposed in [1]. In this thesis, we extend it to the flat Rayleigh fading channel, the computational efficiency and performance of this detection scheme is explored by computer simulation. The conclusion will be given based on the simulation result.

4.1.1 Brief Review for Multistage Detection Algorithm

Multistage detection algorithm is used to reduce the effect caused by MAI. Such detectors are often implemented with multiple stages, where the expectation is that the decisions will improve at the output of successive stages. In the first stage, the tentative hard decisions are formed based on the output of matched filters, and in the second stage, MAI is reconstructed for parallel interference cancellation. The final decision is made after subtracting the reconstructed MAI from the output of matched filters. Multistage structure is depicted in Figure 4.1.

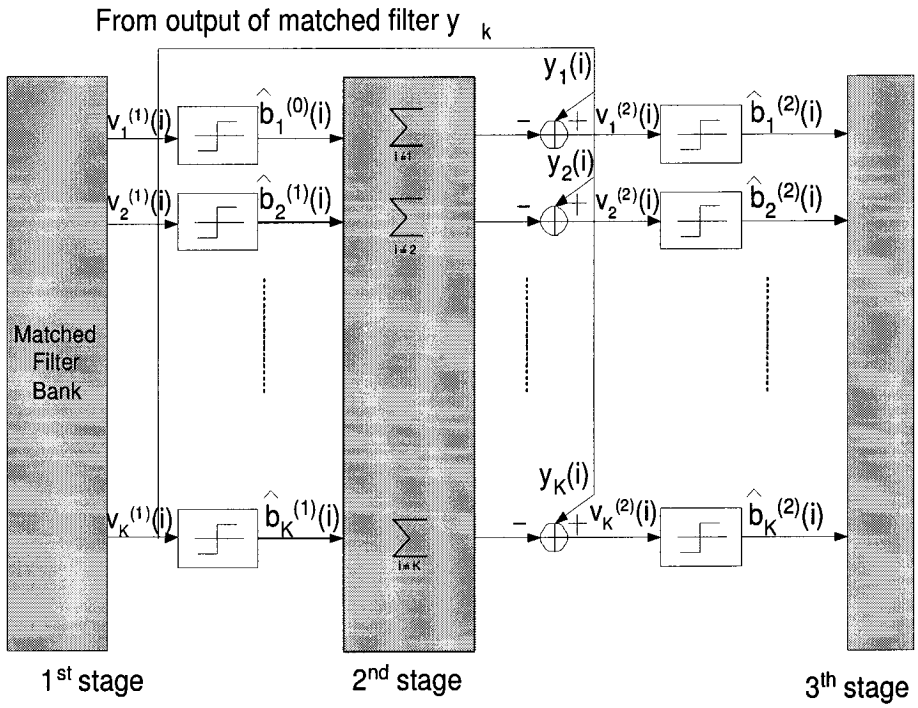

Figure 4.1: Structure of Multistage Detector

4.1.2 Selective Multistage Detection Algorithm in AWGN Channel

In selective multistage detection algorithm, the decision variables are first compared to a threshold level. If the magnitude of the decision variable falls below a threshold, it is considered to be an unreliable decision variable. Otherwise it is considered to be a reliable decision variable and probably would not benefit from MAI parallel interference cancellation. Thus, only the unreliable decision variables are subjected to MAI cancellation and computation is greatly reduced [1]. The algorithm is as follows, where only two stages processing is assumed. Matched filer is employed in the first stage.

1. The output of first stage $v_k^{(1)}(i)$ is equal to the output of matched filter, where $v_k^{(1)}(i)$ can be written as follows, where superscript of $v_k(i)$ represents the index of stage:

$$\begin{aligned} v_k^{(1)}(i) &= A_k b_k(i) + \sum_{j<k} A_j b_j(i+1)\rho_{kj} + \sum_{j<k} A_j b_j(i)\rho_{jk} \\ &\quad + \sum_{j>k} A_j b_j(i)\rho_{kj} + \sum_{j>k} A_j b_j(i-1)\rho_{jk} + n_k(i) \end{aligned}$$

2. Then the magnitude of $v_k^{(1)}(i)$ is compared with a threshold value $Th = \alpha A$, where α is greater than zero.

3. If $|v_k^{(1)}(i)| > Th$, it is considered as a reliable decision variable, then the output of 2nd stage $v_k^{(2)}(i) = v_k^{(1)}(i)$.

4. If $|v_k^{(1)}(i)| \leq Th$, it is considered to be a unreliable decision variable and MAI

parallel interference cancellation is applied, That is

$$\begin{aligned} v_k^{(2)}(i) &= v_k^{(1)}(i) - \sum_{j<k} v_j^{(1)}(i+1)\rho_{kj} - \sum_{j<k} v_j^{(1)}(i)\rho_{jk} \\ &\quad - \sum_{j>k} v_j^{(1)}(i)\rho_{kj} - \sum_{j>k} v_j^{(1)}(i-1)\rho_{jk} \end{aligned}$$

Here, the soft decision is used instead of hard decision.

5. The decision of second stage $\hat{b}_k^{(2)}(i)$ is made based on the sign of $v_k^{(2)}(i)$

4.1.3 Simulation Results for Selective Multistage Detection Algorithm in AWGN Channel

The BER performance of asynchronous CDMA employing the selective multistage detection algorithm in AWGN channel is compared to conventional multistage detection algorithm. The sytem are modeled in Matlab and the result are presented in Figure 4.2 and 4.3. The conditions and assumptions used in the simulation models are as follows:

1. All signals transmit at the same data bit rate, and all signals are received with the same power (perfect power control) and the relative delay between users is uniformly distributed between 0 and T.

2. The spreading gains used in the simulation are 15 and 30 individually. Spreading code are randomly generated.

3. The threshold value used in the system is $Th = \alpha A$, where α is chosen 0.4, 0.6 and 0.9.

4. The numbers of users are 5 and 7 respectively.

It is clearly shown from above figures that the performance of selective multistage algorithm outperforms conventional multistage algorithm in AWGN channel if the

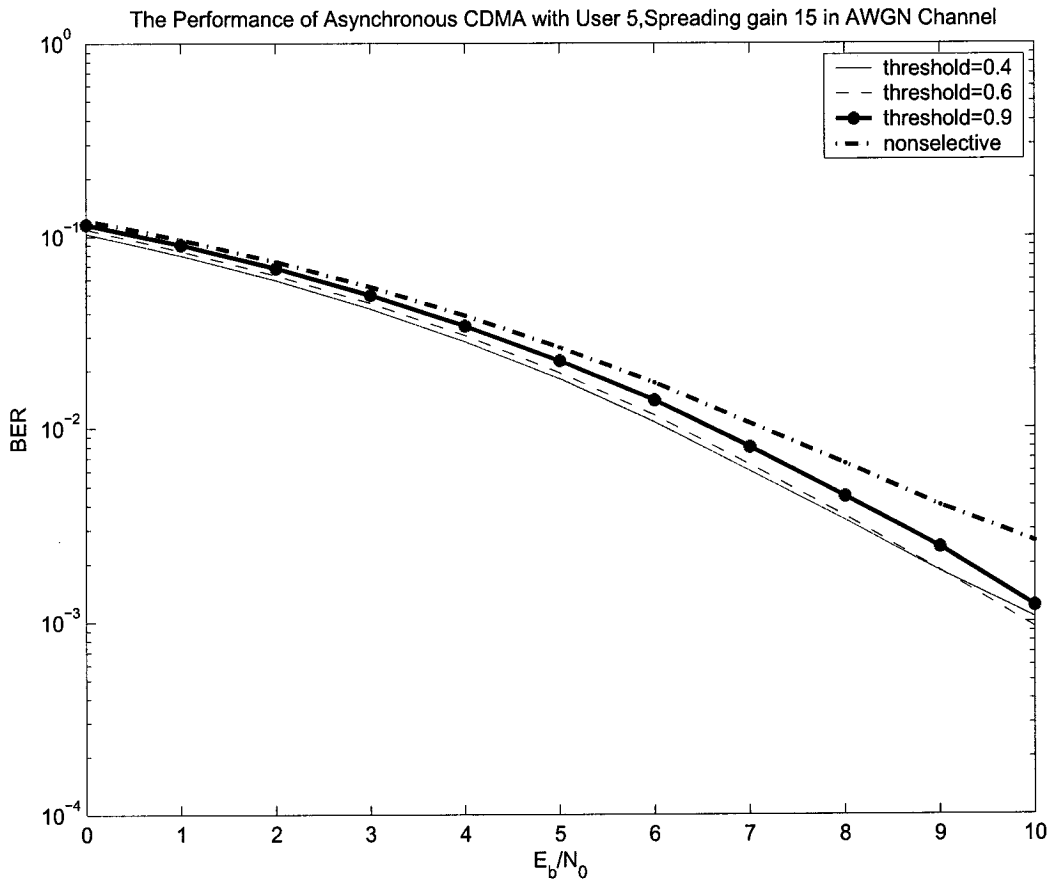

Figure 4.2: The Performance of an Asynchronous CDMA System for 5 Users with a Spreading Gain of 15

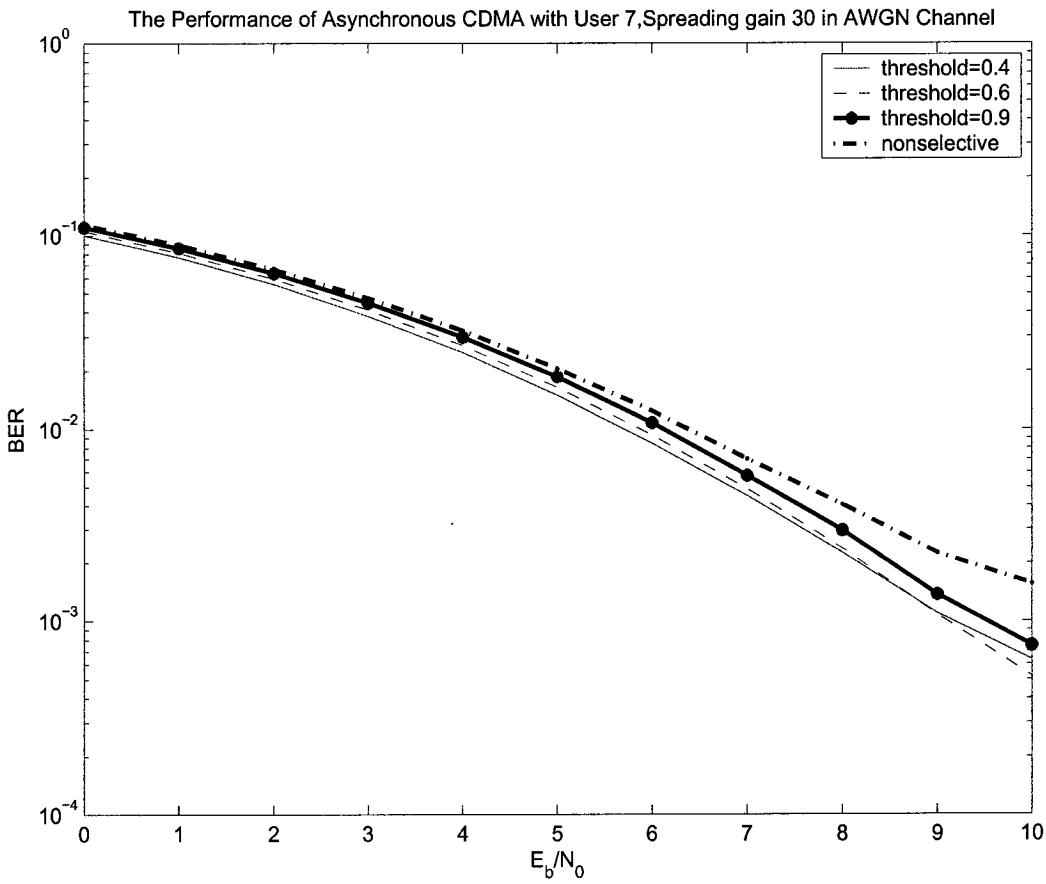

Figure 4.3: The Performance of an Asynchronous CDMA System for 7 Users with a Spreading Gain of 30

threshold value is properly selected.

Table 4.1 is the percentage of weak decision variables in selective multistage detection.

	E_b/N_o	$\alpha = 0.4$	$\alpha = 0.5$	$\alpha = 0.6$
3 users Spreading Factor =15	4dB	11.07%	15.43%	20.96%
	6dB	6.42%	10.18%	15.39%
	8dB	3.69%	6.64%	11.35%
3 users Spreading Factor =30	4dB	9.68%	14.03%	19.84%
	6dB	5.76%	9.32%	14.52%
	8dB	2.87%	5.65%	10.42%
5 users Spreading Factor =15	4dB	12.65%	17.21%	22.50%
	6dB	10.11%	13.51%	19.56%
	8dB	6.96%	11.03%	16.62%

Table 4.1: Probability of Weak Decision Variable in Selective Multistage Detection Algorithm

We can see from table that computation of selective algorithm has been greatly reduced. For example, when the number of users is 3, spreading gain is 15 and SNR is 6dB, 6.42% of all decision variables are weak decision variables, that is, only 6.42% of decision variables are selectived to MAI cancellation, the remaining 93.58% of decision variables don't require MAI cancellation.

4.1.4 Selective Multistage Detection Algorithm in Flat Rayleigh Fading Channel

The results in AWGN channel show that the selective multistage detection algorithm greatly reduces the number of computations while providing a slightly improvement in BER performance compared to the conventional multistage detection algorithm. Therefore, in this thesis, the selective multistage detection algorithm is applied to the slow flat Rayleigh fading channel which is typical of wireless world. The algorithm is presented as follows:

1. The output of first stage $v_k^{(1)}(i)$, is equal to the output of matched filter which is equal to

$$\begin{aligned} v_k^{(1)}(i) &= A_k b_k(i) c_k(i) + \sum_{j<k} A_j b_j(i+1) c_j(i+1) \rho_{kj} + \sum_{j<k} A_j b_j(i) c_j(i) \rho_{jk} \\ &\quad + \sum_{j>k} A_j b_j(i) c_j(i) \rho_{kj} + \sum_{j>k} A_j b_j(i-1) c_j(i-1) \rho_{jk} + n_k(i) \end{aligned}$$

2. The hard decision of first stage $\hat{b}_k^{(1)}(i)$ is made based on the sign of $Re\{v_k^{(1)}(i)\hat{g}_k^*(i)\}$. Where $\hat{g}_k^*(i)$ is the conjugate of estimated channel gain for k-th user on i-th signal interval.

3. The magnitude of $Re\{v_k^{(1)}(i)\hat{g}_k^*(i)\}$ is compared to a threshold βA, where $\beta > 0$

4. If $|Re\{v_k^{(1)}(i)\hat{g}_k^*(i)\}| > \beta A$, then $v_k^{(2)}(i) = v_k^{(1)}(i)$

5. If $|Re\{v_k^{(1)}(i)\hat{g}_k^*(i)\}| \leq \beta A$, it is considered to be an unreliable decision variable and cancellation is applied:

$$\begin{aligned} v_k^{(2)}(i) &= v_k^{(1)}(i) - \sum_{j=1}^{k-1} A_j \hat{c}_j(i) \hat{b}_j^{(1)}(i) \rho_{jk} - \sum_{j=1}^{k-1} A_j \hat{c}_j(i+1) \hat{b}_j^{(1)}(i+1) \rho_{kj} \\ &\quad - \sum_{j=k+1}^{K} A_j \hat{c}_j(i-1) \hat{b}_j^{(1)}(i-1) \rho_{jk} - \sum_{j=k+1}^{K} A_j \hat{c}_j(i) \hat{b}_j^{(1)}(i) \rho_{kj} \end{aligned}$$

6. The final decision of second stage is made based on the sign of $Re\{(v_k^{(2)}(i) \cdot \hat{g}_k^*(i))\}$

4.1.5 Some Simualtion Result for Selective Multistage Detection Algorithm in Flat Rayleigh Fading Channel

The simulation results for selective multistage algorithm are presented in Figure 4.4, 4.5, 4.6 and 4.7. Ideal channel estimation is assumed ($\hat{g}_k(i) = g_k(i)$).

From above figures, it is shown that selective multistage detection algorithm outperforms conventional multistage algorithm if the threshold value is properly choosen.

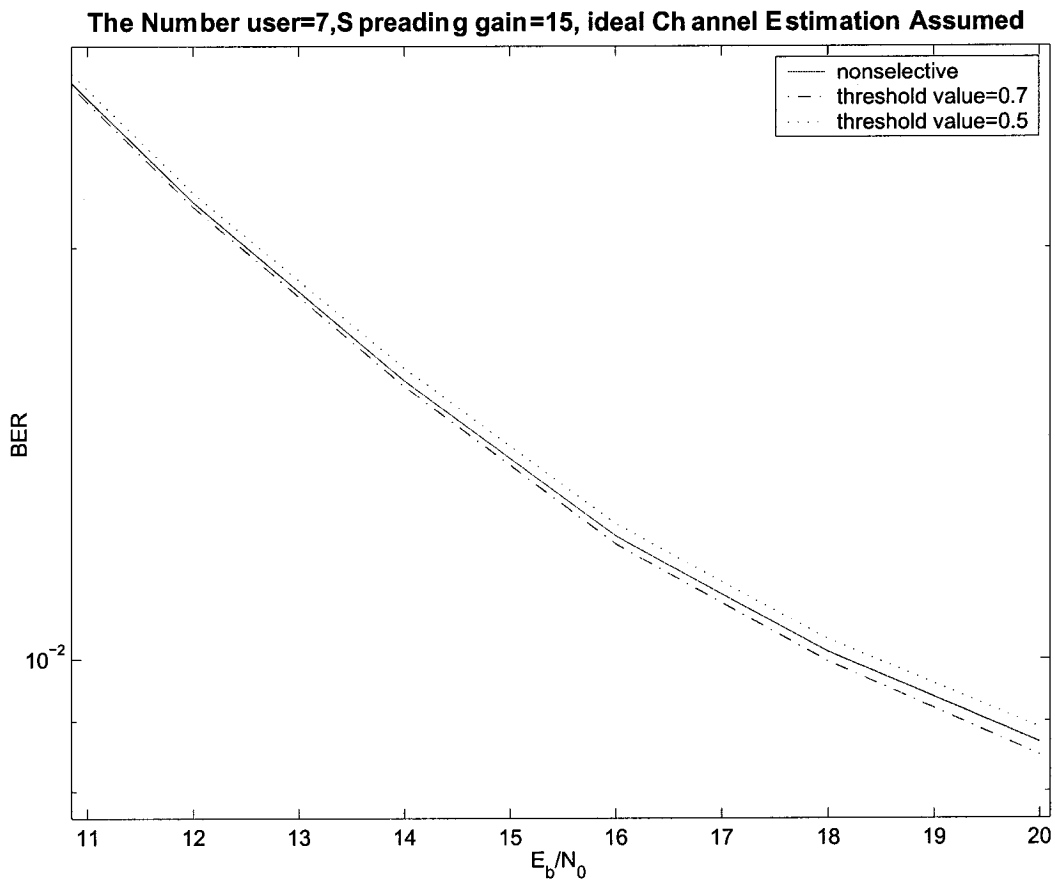

Figure 4.4: The Performance of an Asynchronous CDMA System for 7 Users with a Spreading Gain of 15 in Flat Rayleigh Fading Channel with Ideal Channel Estimation and Threshold Value is of $0.7\sqrt{E_b}$ and $0.5\sqrt{E_b}$.

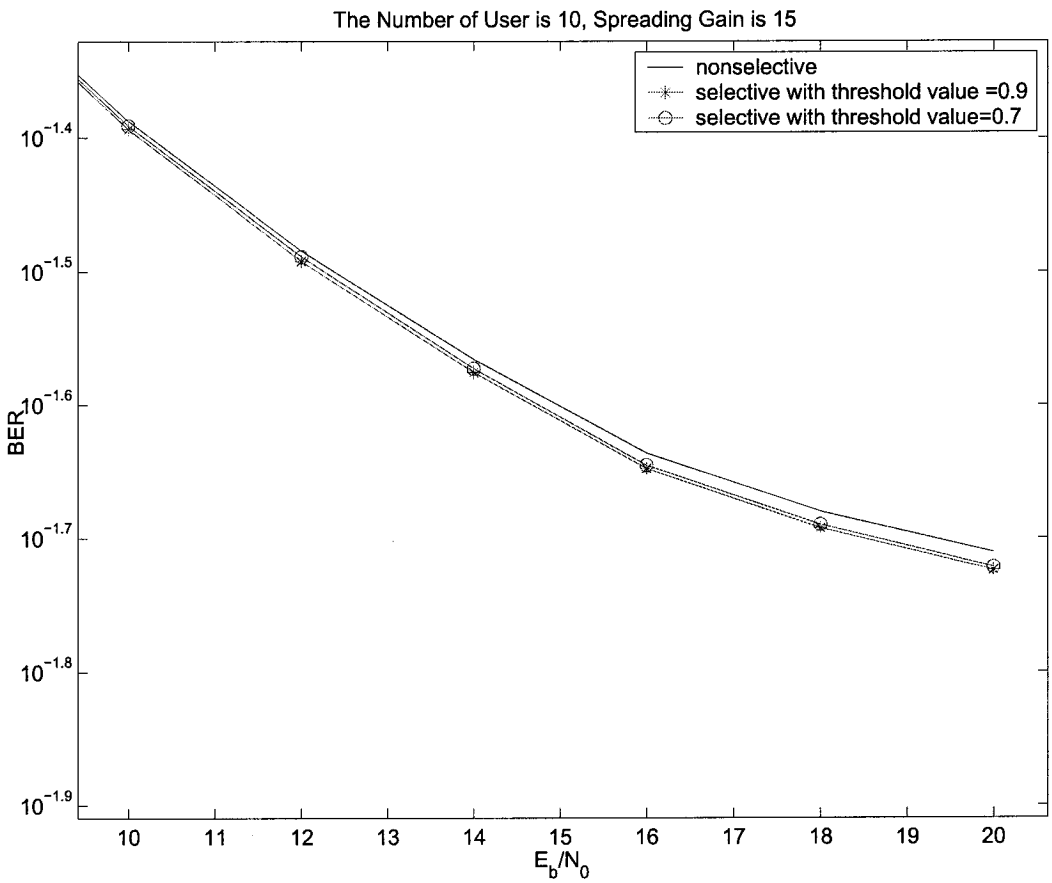

Figure 4.5: The Performance of an Asynchronous CDMA System for 10 Users with a Spreading Gain of 15 in Flat Rayleigh Fading Channel with Ideal Channel Estimation and Threshold Value is of $0.9\sqrt{E_b}$ and $0.7\sqrt{E_b}$.

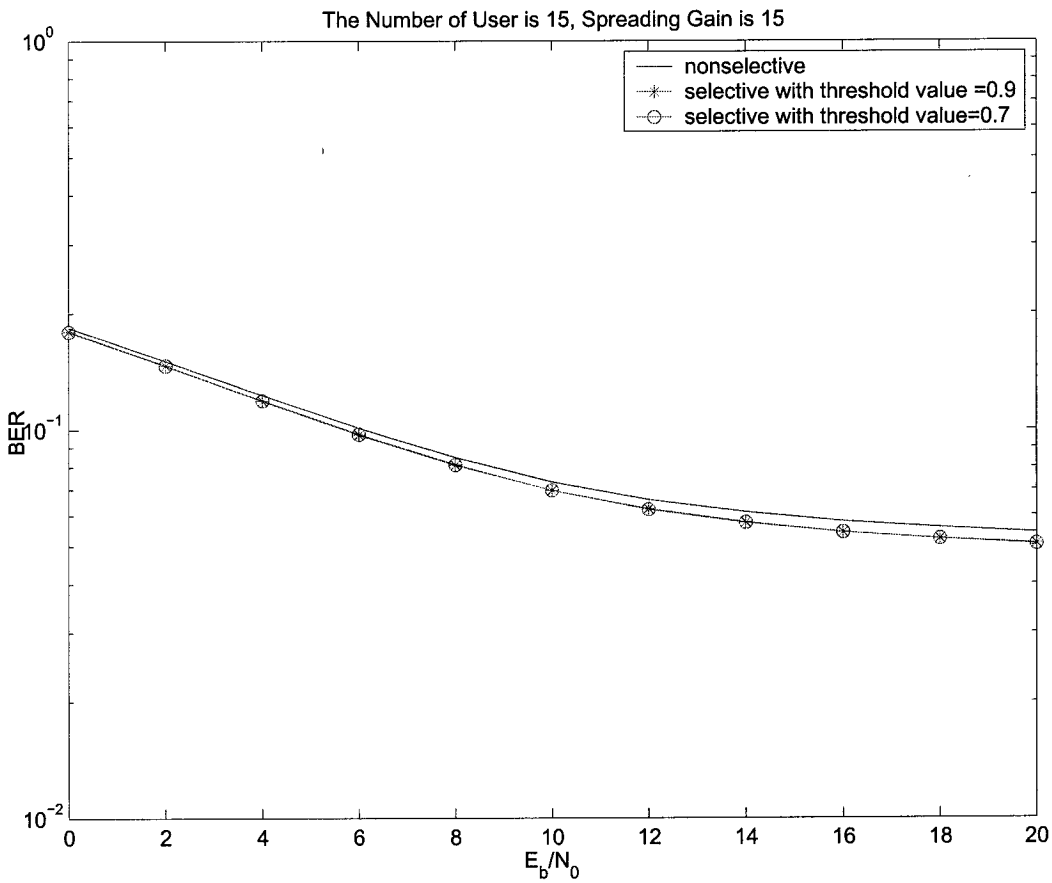

Figure 4.6: The Performance of an Asynchronous CDMA System for 15 Users with a Spreading Gain of 15 in Flat Rayleigh Fading Channel with Ideal Channel Estimation and Threshold Value is of $0.9\sqrt{E_b}$ and $0.7\sqrt{E_b}$.

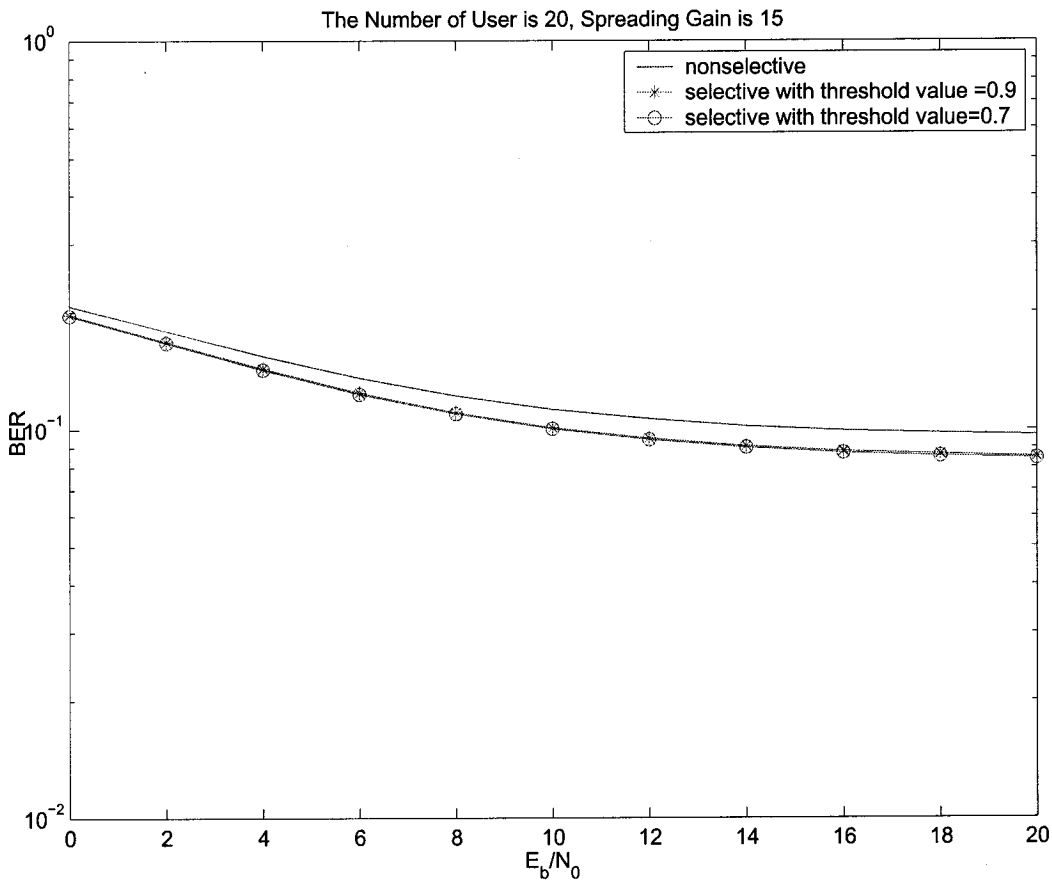

Figure 4.7: The Performance of an Asynchronous CDMA System for 20 Users with a Spreading Gain of 15 in Flat Rayleigh Fading Channel with Ideal Channel Estimation and Threshold Value is of $0.9\sqrt{E_b}$ and $0.7\sqrt{E_b}$.

As the number of users increases, the improvement becomes more pronounced.

4.2 Modified Selective Detection Algorithm in Flat Fading Channel

Although the selective multistage detection has some improvement in BER performance compared to the conventional multistage detection, the improvement is not great. In order to improve the BER performance further without increasing the computational complexity, a modified selective multistage detection algorithm is proposed based on work done in [30, 31, 32]. It is shown that the modified selective algorithm outperforms selective algorithm in BER performance, meanwhile, the number of computation is almost similar.

4.2.1 Modified Selective Multistage Detection Algorithm

The algorithm of modified selective multistage detection is depicted as follows:

1. The hard decision of first stage $\hat{b}_k^{(1)}(i)$ is made based on the sign of $Re\{v_k^{(1)}(i)\hat{g}_k^*(i)\}$.

2. The magnitude of $Re\{v_k^{(1)}(i)\hat{g}_k^*(i)\}$ is compared to a threshold βA, where $\beta > 0$

3. If $|Re\{v_k^{(1)}(i)\hat{g}_k^*(i)\}| > \beta A$, then $v_k^{(2)}(i) = v_k^{(1)}(i)$

4. If $|v_k^{(1)}(i)| \leq \beta A$, it is considered to be an unreliable decision variable and partial cancellation [33] is applied:

$$\begin{aligned} v_k^{(2)}(i) &= v_k^{(1)}(i) - \sum_{j=1}^{k-1} w_j(i) A_j \hat{c}_j(i) \hat{b}_j^{(1)}(i) \rho_{jk} - \sum_{j=1}^{k-1} w_j(i+1) A_j \hat{c}_j(i+1) \hat{b}_j^{(1)}(i+1) \rho_{kj} \\ &\quad - \sum_{j=k+1}^{K} w_j(i-1) A_j \hat{c}_j(i-1) \hat{b}_j^{(1)}(i-1) \rho_{jk} - \sum_{j=k+1}^{K} w_j(i) A_j \hat{c}_j(i) \hat{b}_j^{(1)}(i) \rho_{kj} \end{aligned}$$

Where $w_j(i)$ is the weighting coefficient for j-th user and i-th interval. If a decision variable is considered as a reliable variable, $w_j(i) = 1$, otherwise, $w_j(i)$ is less than 1, etc, 0.9 or 0.8. This takes into account the fact that the tentative hard decison made on the previous stage may be unreliable.

5. The final decision $b_k^{(2)}(i)$ is made based on the sign of $Re\{v_k^{(2)}(i) \cdot \hat{g}_k^*(i)\}$

4.2.2 Simulation Results for Modified Selective Multistage Detection Algorithm with Perfect Channel Estimation

The performance of modified selective multistage detection algorithm is compared with the selective multistage algorithm, presented in Figure 4.8, 4.9, 4.10 and 4.11, where ideal channel estimation is assumed.

It is clearly shown in these figures that the selective multistage algorithm outperform slightly the conventional multistage algorithm, while the modified selective multistage algorithm performs better than selective multistage algorithm and conventional multistage algorithm. For a very small increase in computation a better BER performance has been achieved.

4.2.3 Simulation Results for Modified Selective Multistage Detection Algorithm with Imperfect Channel Estimation

Using pilot symbols with imperfect channel estimation, the performance of modified selective multistage detection algorithm is compared with the selective multistage algorithm and conventional multistage algorithm. The results are presented in Figure 4.12, 4.13 and 4.14. Here, the simulation using the following parameters: insertion rate is 0.8, frame size is 5, interpolator size is 11 and normalized Doppler frequency

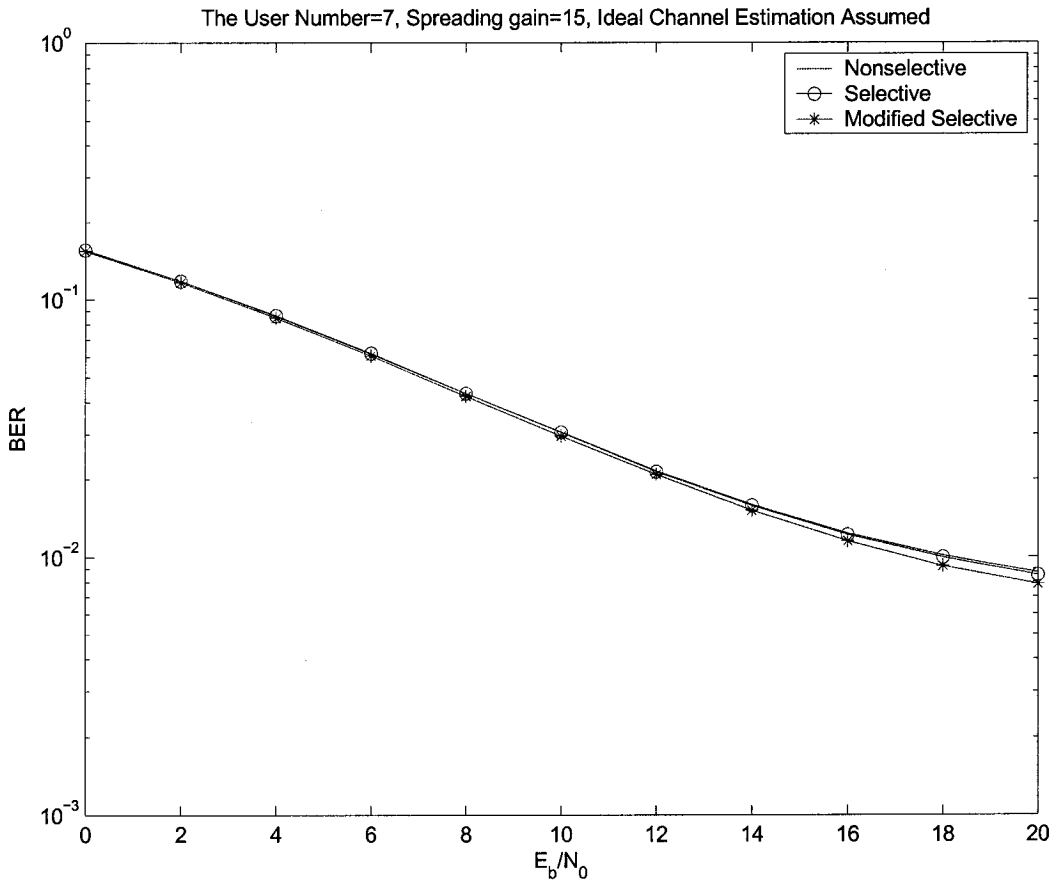

Figure 4.8: The Performance of Asynchronous CDMA Systems for 7 Users with a Spreading Gain of 15 in Flat Rayleigh Fading Channel with Ideal Channel Estimation (Normalized Doppler Frequency is 0.01)

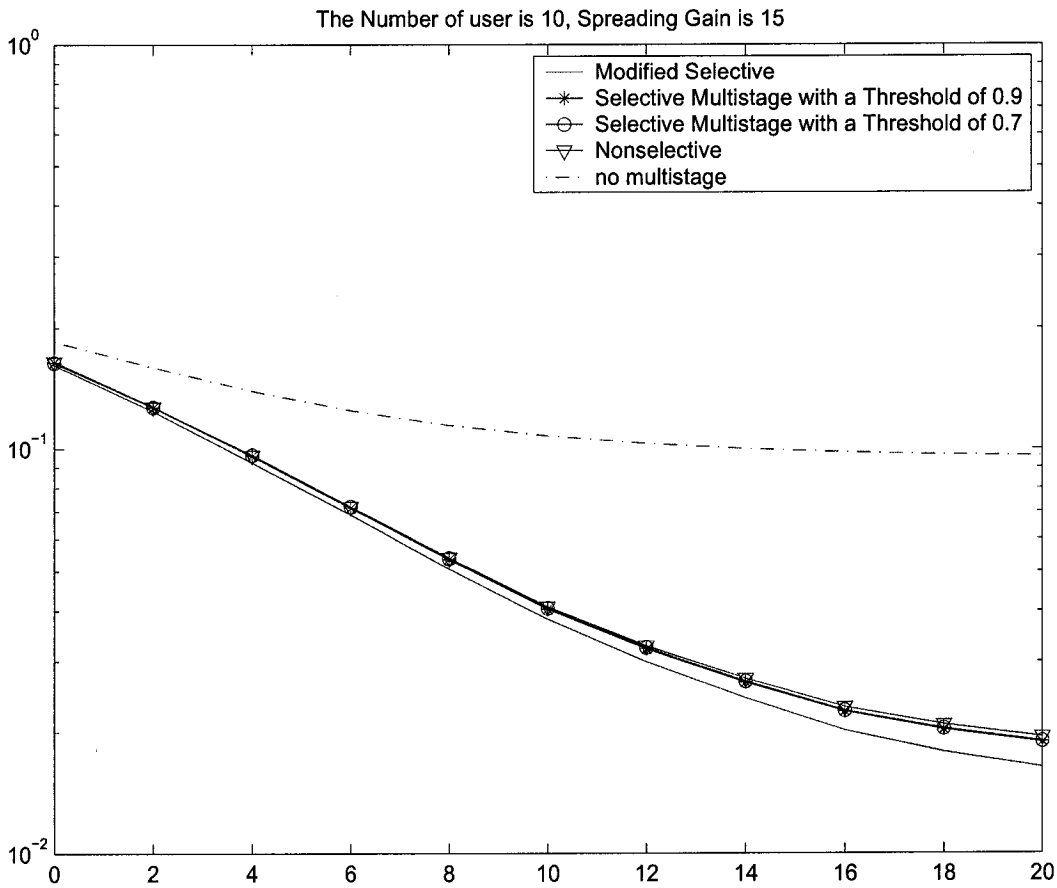

Figure 4.9: The Performance of Asynchronous CDMA Systems for 10 Users with a Spreading Gain of 15 in Flat Rayleigh Fading Channel with Ideal Channel Estimation (Normalized Doppler Frequency is 0.01)

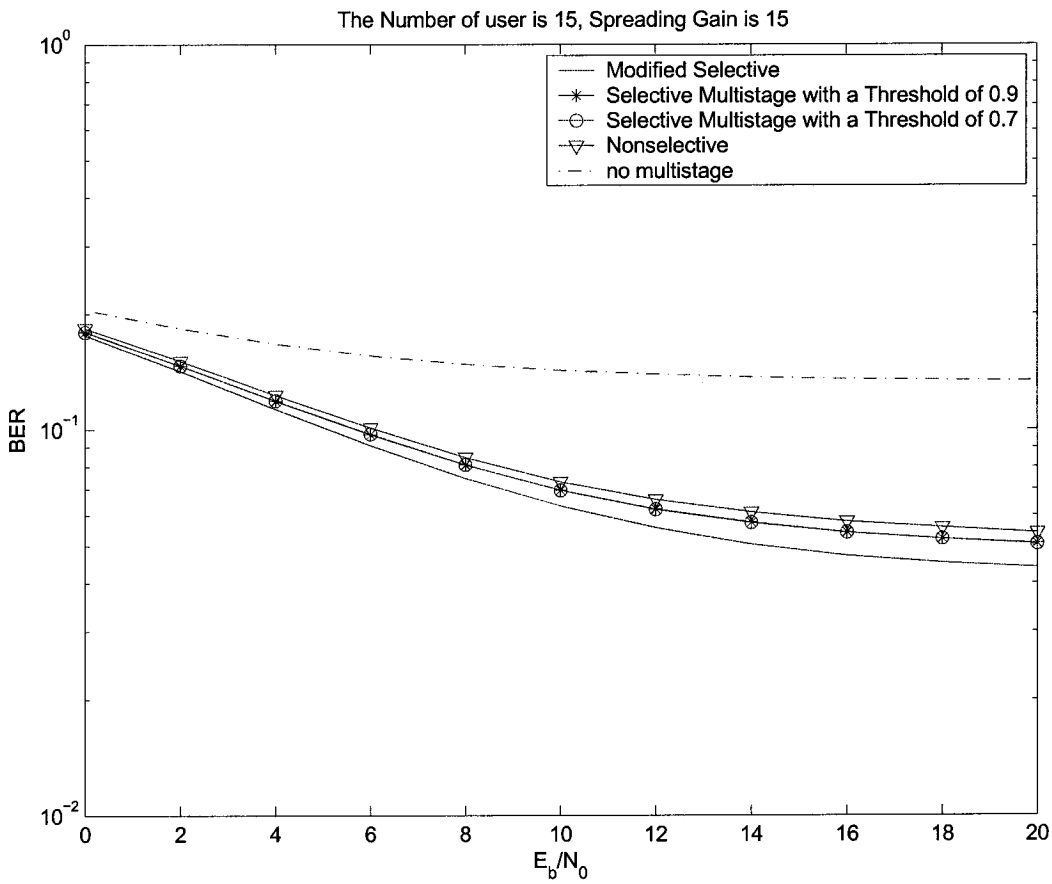

Figure 4.10: The Performance of Asynchronous CDMA systems for 15 Users with a Spreading Gain of 15 in Flat Rayleigh Fading Channel with Ideal Channel Estimation (Normalized Doppler Frequency is 0.01)

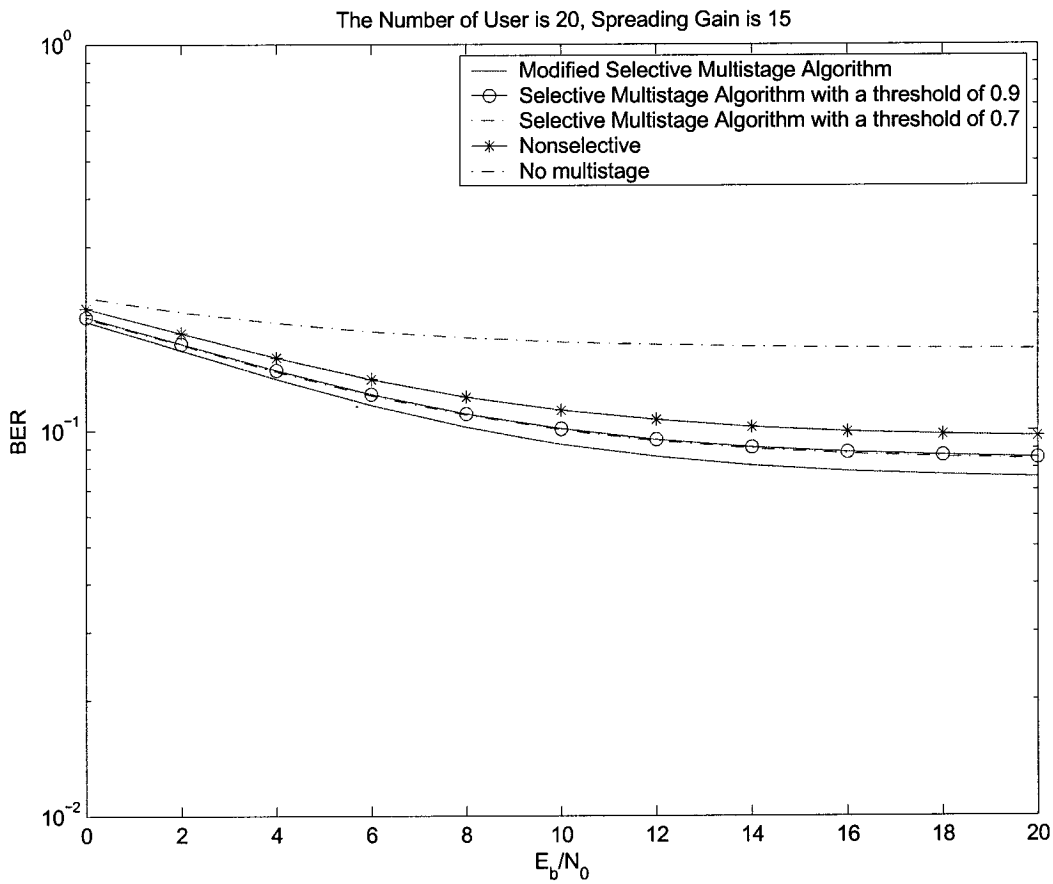

Figure 4.11: The Performance of Asynchronous CDMA systems for 20 Users with a Spreading Gain of 15 in Flat Rayleigh Fading Channel with Ideal Channel Estimation (Normalized Doppler Frequency is 0.01)

is 0.01.

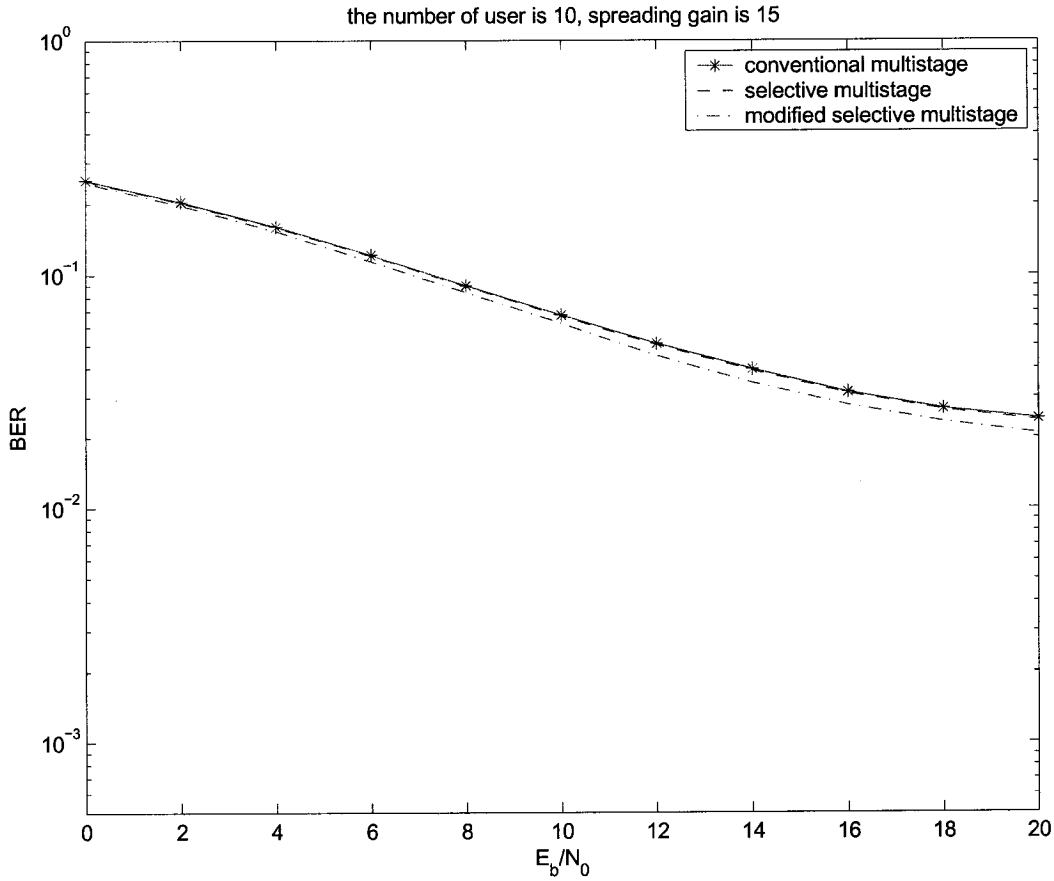

Figure 4.12: The Performance of an Asynchronous CDMA System in Flat Rayleigh Fading Channel for 10 Users with a Spreading Gain of 15 with Imperfect Channel Estimation

From above figures, we found that the modified selective multistage algorithm outperforms selective ones using PSAM system to estimate the channel gain. When BER increases, the performance of modified selective algorithm with imperfect channel estimation approaches to that of conventional multistage algorithm with perfect channel estimation case.

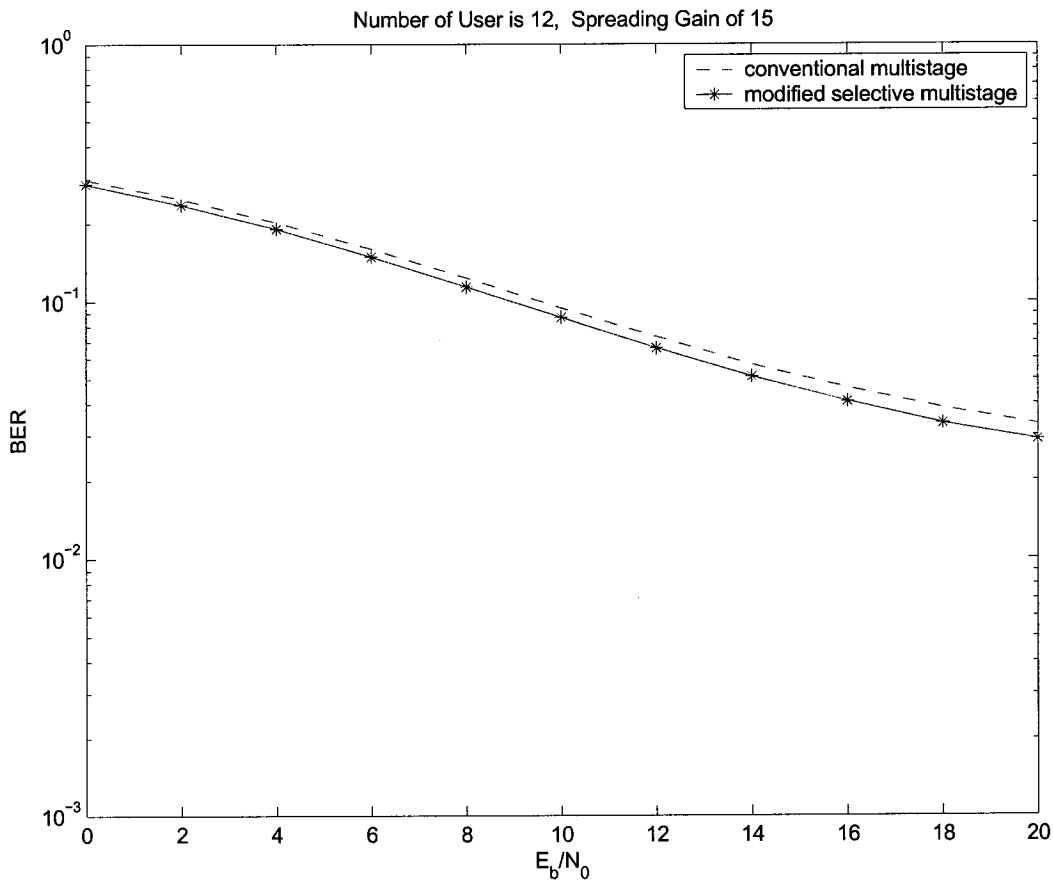

Figure 4.13: The Performance of an Asynchronous CDMA System in Flat Rayleigh Fading Channel for 12 Users with a Spreading Gain of 15 with Imperfect Channel Estimation

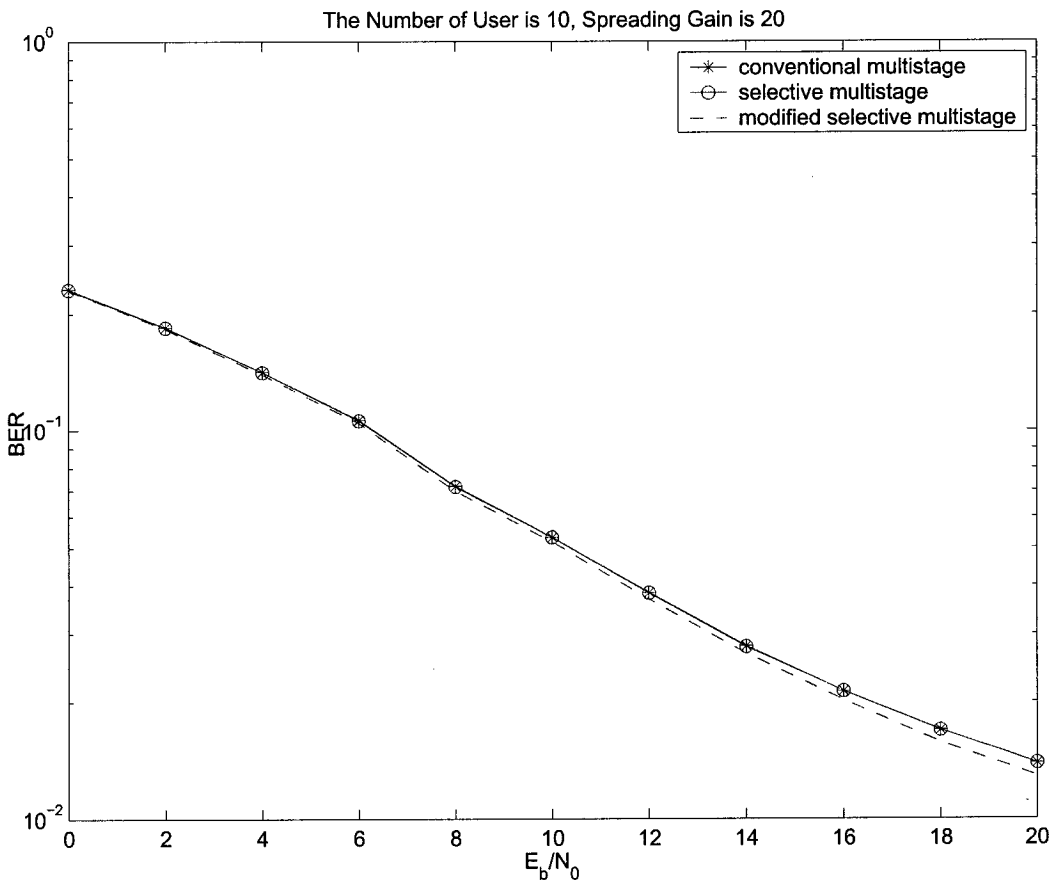

Figure 4.14: The Performance of an Asynchronous CDMA System in Flat Rayleigh Fading Channel for 10 Users with a Spreading Gain of 20 with Imperfect Channel Estimation

Chapter 5

Conclusion

5.1 Summary

In this thesis, we investigated the BER performance of asynchronous CDMA multi-user system employing selective multistage detection algorithm in the flat Rayleigh fading channel. The entire simulation system is made up of three main parts: channel modeling, channel estimation and selective multistage multi-user detection.

In channel modeling part, FFT Clarke model is employed to implement a slow flat Rayleigh fading channel. From the simulation results, it is shown that the statistical distribution of the simulated channel is consistent with that of an actual flat Rayleigh fading channel.

In channel estimation part, we used the pilot based optimum Wiener interpolator to estimate the fading channel coefficient of every user. For the single user case, it was shown that Wiener interpolator could estimate the channel coefficient very accurately if the interpolator size and frame size are properly chosen. Compared to the large frame size interpolator, the performance of small frame size interpolator is more accurate however more energy is allocated to pilots as well. Therefore, a tradeoff between estimation performance and energy loss exists. For multi-user case,

we estimate the channel coefficient by applying the principle of Wiener interpolator in single user case. However, we find that the estimation performance degrades especially when the number of users is large. The reason for degradation of performance is that the tracking pilots include the co-channel interference caused by other users. To solve this problem and improve the performance, we fed the tracking pilots into a decorrelator to decouple the cross-correlation of pilots and get rid of the co-channel interference. Then channel coefficients of every user are estimated separately based on decorrelated pilots. From the simulation result, it is shown that the latter method outperforms the previous one.

In selective multistage multi-user detection part, the selective multistage multi-user detection algorithm is employed to detect every user's data from the multi-user signals. By comparing the magnitude of the decision variable with a threshold value, selective algorithm determines which decision variables are more likely to produce errors. Only those unreliable decision variables are subjected to MAI cancellation, thus reducing the amount of computation performed by the receiver. At the same time, we find that the BER performance of selective algorithm is slightly better than conventional multistage ones if the threshold value is properly chosen. In order to improve the performance further without increasing the amount of computation, a modified selective multistage detection algorithm is proposed. This algorithm applies partial MAI cancellation instead of full MAI cancellation to the unreliable decision variable by multiplying the MAI estimate by a weight that is less than 1. The reason for doing partial MAI cancellation account for any unreliable decisions from the previous stage. We compare the performance of modified selective multistage detection algorithm with selective multistage algorithm under the condition of the perfect and imperfect estimated channel. For both cases, the modified algorithm performs

better than selective algorithm. For imperfect estimated channel, the performance of modified algorithm is close to that of conventional multistage algorithm in perfect estimated channel.

In this thesis, the performance of asynchronous DS-CDMA multi-user system is demonstrated by use of computer simulation. The simulation results prove that selective multistage multi-user detection algorithm is a more feasible multi-user scheme compared to the conventional multistage algorithm due to its reduced computation and slightly improved performance.

5.2 Future Work

Although this thesis awares many questions regarding selective multistage detection in Rayleigh fading channel, other aspects still need to be investigated. For example:

1. In this thesis, the optimum threshold value wasn't found. It is expected that it is a function of signal-to-noise ratio(SNR), spreading gain and number of users.

2. In this thesis, we only investigated single transmit antenna, single receive antenna system. In practice, multiple antennas (MIMO system) can also be considered as one option used to overcome the fading effect.

3. For multistage detection in this thesis, only two stages are considered. The performance of additional stages detection can be investigated. However, the relative performance of the different systems should still follow the trends shown in this thesis regardless of the number of stages.

4. The threshold value and partial cancellation weight used in this thesis is a constant. We can also use adaptive thresholds and weights in selective and modified selective multistage algorithm.

5. We only considered the case where all users' received power is the same. The near-far effect on the performance of the detection algorithm discussed in this thesis needs to be investigated.

Bibliography

[1] C. D'Amours, "A reduced-complexity multistage detection algorithm for DS-CDMA systems in AWGN channels," *Canadian Journal Electrical Computer Enginerring*, vol. 28, pp. 131–137, July/November 2003.

[2] S. Verdu, *Multiuser Detection.* Cambridge University Press, Cambridge, UK, 1998.

[3] S. Moshavi, "Multi-user detection for DS-CDMA communications," *IEEE Communication Magazine*, vol. 34, pp. 124–136, October 1996.

[4] Z. Xie, R. Short, and C. Rushforth, "A family of suboptimum detectors for coherent multiuser communications," *IEEE Journal on Selected Areas in Communications*, vol. 8, pp. 683–690, May 1990.

[5] R. Lupas and S. Verdu, "Near-far resistance of multiuser detectors in asynchronous channels," *IEEE Trans. on Communications*, vol. 38, pp. 496–508, April 1990.

[6] A. Duel-Hallen, "A family of multiuser decision-feedback detectors for asynchronous code-division multiple-access channels," *IEEE Trans. on Communications*, vol. 43, pp. 421–433, February/March/April 1995.

[7] D. Samardzija, N. Mandayam, and I. Seskar, "Blind successive interference cancellation for DS-CDMA systems," *IEEE Trans. on Communications*, vol. 50, pp. 276–289, February 2002.

[8] M. Varanasi and B. Aazhang, "Multistage detection in asynchronous code-division multiple-access communications," *IEEE Trans. on Communications*, vol. 38, pp. 509–519, April 1990.

[9] Z. Shi, W. Du, and P. Driessen, "Multistage detection in synchronous code-division multiple-access systems," in *Proc. of 3rd IEEE International Symposium on PIMRC, Boston, USA*, pp. 446–450, October 1992.

[10] A. Duel-Hallen, J. Holtzman, and Z. Zvonar, "Multiuser detection for CDMA systems," in *IEEE Personal Communications*, pp. 46–58, April 1995.

[11] L. Pan and C. D'Amours, "Selective multistage detection of DS-CDMA signals in the presence of slow frequency-nonselective Rayleigh fading," in *Proc. of 22nd Biennial Symposium on Communications (accepted), Kingston, Canada*, June 2004.

[12] Z. Zvonar and D. Brady, "On multiuser detection in asynchronous CDMA flat rayleigh fading channels," in *Proc. of 3rd IEEE International Symposium on PIMRC, Boston, USA*, pp. 123–127, October 1992.

[13] H. Wu and A. Duel-Hallen, "On the performance of coherent and noncoherent multiuser detectors for mobile radio CDMA channels," in *Proc. of 5th IEEE International Conference on Universal Personal Communications, Cambridge, USA*, vol. 1, pp. 76–80, September 1996.

[14] E. P. Lawrey, *Adaptive Techniques for multiuser OFDM.* PH.D Thesis, James Cook University, December 2001.

[15] T. Rappaport, *Wireless Communications : Principles and Practice.* Upper Saddle River, N.J. : Prentice Hall PTR, 2002.

[16] R. Clarke, "A statistical theory of mobile-radio reception," *Bell Systems Technical Journal*, vol. 47, pp. 957–1000, July-August 1968.

[17] J. Jakes, *Microwave Mobile Communication.* New York: John Wiley and Sons, 1974.

[18] K. Baddour and N. Beaulieu, "Autoregressive models for fading channel simulation," in *Proc. of GLOBECOM, Texas, USA*, vol. 2, pp. 1187–1192, November 2001.

[19] C. Xiao, Y. Zheng, and N. Beaulieu, "Second-order statistical properties of the WSS Jakes' fading channel simulator," *IEEE Trans. on Communications*, vol. 50, pp. 888–891, June 2002.

[20] G. Colman, S. Blostein, and N. Beaulieu, "An ARMA multipath fading simulator," in *Proc. of 7th Annual Virginia Tech Symposium on Wireless Personal Communications, Blacksburg, VA, USA*, vol. 5, pp. 1–12, June 1997.

[21] D. Young and N. Beaulieu, "On the generation of correlated Rayleigh random variates by inverse discrete fourier transform," in *Proc. of 5th IEEE International Conference on Universal Personal Communications, Cambridge, USA*, vol. 2, pp. 231–235, September 1996.

[22] J. Smith, "A computer generated multipath fading simulation for mobile radio," *IEEE Trans. on Vehicular Technology*, vol. VT-24, pp. 39–40, August 1975.

[23] C. D'Amours, M. Moher, and A. Yongacoglu, "Comparison of pilot symbol-assisted and differentially detected bpsk for DS-CDMA systems employing rake receivers in Rayleigh fading channels," *IEEE Trans. on Vehicular Technology*, vol. 47, pp. 1258–1267, November 1998.

[24] S. Sampei and T. Sunaga, "Rayleigh fading compensation method for 16QAM in digital land mobile radio channels," in *Proc. of 39th IEEE Vehicular Technology Conference, San Fransisco, USA*, vol. 2, pp. 640–646, May 1989.

[25] M. Moher and J. Lodge, "TCMP-A modulation and coding stragtegy for Rician fading channels," *IEEE Journal on Selected Areas in Communications*, vol. 7, pp. 1347–1355, December 1989.

[26] J. Cavers, "An analysis of pilot symbol assisted modulation for Rayleigh fading channels," *IEEE Trans. on Vehicular Technology*, vol. 40, pp. 686–692, November 1991.

[27] J. Torrance and L. Hanzo, "Comparative study of pilot symbol assisted modem schemes," in *Proc. of 6th International Conference on Radio Receivers and Associated Systems*, pp. 36–41, September 1995.

[28] Y. Ma, R. Schober, T. Lim, and S. Pasupathy, "Performance of multiuser detection with pilot-symbol-assisted channel estimation," in *Proc. of IEEE Vehicular Technology Conference, Orlando, Florida, USA*, October 2003.

[29] K. Yu, J. Evans, and I. Collings, "Pilot symbol aided adaptive receiver for Rayleigh faded CDMA channels," in *Global Telecommunications Conference, San Antonio, Texas, USA*, vol. 2, pp. 753–757, November 2001.

[30] S. Han and J. Lee, "Multi-stage partial parallel interference cancellation receivers for multi-rate DS-CDMA system," *IEICE Trans. Communictions*, vol. E86-B, pp. 170–180, January 2003.

[31] S. Han and J. Lee, "Multi-stage partial PIC receivers for multi-rate DS-CDMA system with multiple modulation," in *Proc. of Wireless Communications and Networking*, vol. 4, pp. 591–594, March 2003.

[32] J. Bae, I. Song, and D. Won, "A selective and adaptive interference cancellation scheme for code division multiple access systems," *Signal Processing*, vol. 83, pp. 259–273, February 2003.

[33] W. Tantiphaiboontana and S. Miller, "Performance analysis of partial parallel interference cancellation in synchronous DS-CDMA systems over frequency selective fading channels," in *Proc. of IEEE International Conference on Communications, Anchorage, Alaska, USA*, vol. 26, pp. 2557–2561, May 2003.